THE RELATIONSHIP BETWEEN OXIDATIVE STRESS, TRIGLYCERIDE ACCUMULATION AND MITOCHONDRIAL FUNCTION IN *IN VITRO* MODEL OF HEPATOCELLULAR STEATOSIS

DR. KHALIDA ANN LOCKMAN

MB Bch, MRCP

A THESIS PRESENTED FOR THE DEGREE OF DOCTOR OF MEDICINE

UNIVERSITY OF EDINBURGH

2013

DECLARATION

This thesis is submitted to the University of Edinburgh in Candidature for the Degree of Doctor of Medicine. It comprises original research carried out in the Department of Hepatology, University of Edinburgh, between September 2005 and July 2008. It has not been submitted, either as a whole or in part, in Candidature for any other Degree or Diploma. I have performed all the research myself under the supervision of Dr. Celine Filippi, Dr. John N Plevris. Dr. Alan J Jaap and Professor Peter C Hayes except for the following:

Mr. Robert Morris has kindly performed Oil red O and PAS staining

Dr. Forbes Howie has kindly performed LDH assays

Dr. Karl EV Burgess of Scottish Metabolomics Facility has kindly performed metabolomics analysis

Mr. Steve Mitchell has kindly prepared the pellets for electron microscopy

Dr. Nikolas Plevris-Papaiannou and Mrs. Shona McCall have kindly helped in BIODIPY staining confocal microscopy

Dr. James Baren and Dr. Christopher Pemberton have kindly assisted in superoxide FACS experiments

I designed these studies and analysed the data obtained. Quotations have been distinguished by quotation marks and sources of information acknowledged. All references cited have been reviewed by myself and are complete until July 2012.

Dr. Khalida Ann Lockman
MB Bch, MRCP
Department of Hepatology
University of Edinburgh
January 2013

TABLE OF CONTENTS

LIST OF FIGURES

LIST OF ABBREVIATIONS

AKT	Protein kinase B
AMPK	Adenine monophosphate kinase
ANOVA	Analysis of variance
ATP	Adenine triphosphate
ADP	Adenine diphosphate
ApoB	Apolipoprotein B 100
BSA	Bovine serum albumin
CPT	Carnitine palmitoyl transferase
COX	Cytochrome *c* oxidase
ChREBP	Carbohydrate response element-binding protein
CYP2E1	Cytochrome P450 2E1
DAG	Diacylglycerol
DAPI	Diamidino phenylindole
DGAT2	Diacylglycerol acyltransferase 2
DNP	2,4-Dinitrophenol
DMSO	Dimethyl sulphoxide
$\Delta\Psi$	Mitochondrial membrane potential
EDTA	Ethylenediaminetetraacetic acid
FFA	Free fatty acids
FBS	Fetal bovine serum
FAT/CD36	Fatty acid translocase/cluster differentiation 36
FOXO1	Forkhead box O transcription factor 1
GPX	Glutathione peroxidases

GSH	Glutathione (reduced form)
GLUT2	Glucose transporter 2
H_2O_2	Hydrogen peroxide
HOCl	Hydrochloric acid
4-HNE	4-hydroxynonenal
HBSS	Hank's balanced salt saline
IL	Interleukin
IRS	Insulin receptor substrates
IKKβ	Inhibitor of kappa B kinase-β
JNK	jun N-terminal kinase
LDH	Lactate dehydrogenase
LCFA	Long chain fatty acid
LP	Lactate and pyruvate
LPO	Lactate, pyruvate and octanoate
LPON	Lactate, pyruvate, octanoate and ammonia
mtDNA	Mitochondrial DNA
MnSOD	Mitochondrial superoxide dismutase
MDA	Malondialdehyde
MEME	Minimal essential medium Eagle
MAPK	Mitogen-activated protein kinase
MCD	Methionine choline deficient
MCFA	Medium chain free fatty acid
NAFLD	Nonalcoholic fatty liver disease
NASH	Nonalcoholic steatohepatitis
NAC	N-acetylcysteine

NAD	Nicotinamide adenine dinucleotide
NADH	Nicotinamide adenine dinucleotide reduced
NF-κB	Nuclear factor-κB
Prx	Peroxiredoxins
PBS	Phosphate-buffered saline
PPARγ	Peroxisome proliferator-activated receptor gamma
PPARα	Peroxisome proliferator-activated receptor alpha
PI3K	Phosphatidylinositol 3-kinase
PDH	Pyruvate dehydrogenase
PKC	Protein kinase C
PUFA	Polyunsaturated fatty acid
RET	Reverse electron transport
ROS	Reactive oxygen species
SREBP-1C	Sterol regulatory element-binding protein-1c
SEM	Standard error mean
SD	Standard deviation
SOD	Superoxide dismutase
TNF-α	Tumor necrosis factor-α
TOCO	α-Tocopherol
TGF-β	Transforming growth factor-β
TCA	Tricarboxylic acid
Trx	Thioredoxin-2
UCP	Uncoupling proteins
VLDL	Very-low density lipoprotein

ACKNOWLEDGMENTS

I would like to extend my appreciation and gratitude to my supervisors, Dr. John N. Plevris, Dr. Celine Filippi, Dr. Alan J. Jaap and Professor Peter C. Hayes.

I am deeply indebted to Dr. James P. Baren, Dr. Christopher J. Pemberton, Dr. Nikolas Plevris, Dr. Gail Masterton, Dr. Forbes Howie, Dr. Catherine Payne, Mrs. Anne Pryde, Mrs. Patricia Lee and Mrs. Pauline Cowan for their immeasurable support and assistance.

I would like to thank Mrs. Shona McCall and CALM facility for their guidance on confocal microscopy, Mr. Stephen Mitchell for his assistance on electron microscopy, Mr. Robert Morris for his expertise in Oil Red O and PAS staining, Ms. Kay Samuel for her guidance in FACS and Dr. Karl EV Burgess from Scottish Metabolomics facility, University of Glasgow for performing metabolomics analysis.

I would like to express my deepest gratitude to Mrs. Elaine Dowding and Mrs. Margaret Turnbull, from Department of Diabetes and Endocrinology, Royal Infirmary of Edinburgh for their unwavering support through thick and thin over the years.

SUMMARY

There is still debate about the relationship between fat accumulation and mitochondrial function in nonalcoholic fatty liver disease. It is a critical question since a proportion of individuals with steatosis progress to steatohepatitis. This thesis is focused on defining i) the effect of triglyceride accumulation and reactive oxygen species (ROS) on mitochondrial function ii) the contribution of triglyceride, ROS and subsequent mitochondrial impairment to the metabolism of energy substrates iii) the effect of the intracellular antioxidant, N-acetylcysteine, on hepatic mitochondrial function and metabolic alterations associated with human steatohepatitis iv) the effect of different free fatty acids species on ROS production and subsequent metabolic response in hepatocytes.

To address these questions, we designed *in vitro* models using human hepatoblastoma C3A cells treated with various combinations of oleate, octanoate (O), lactate (L), pyruvate (P) and ammonia (N) acutely or for 72 hours, before measurements of triglyceride concentration, cell respiration, ROS production, mitochondrial membrane potential, ketogenesis and gluconeogenesis, metabolomics analyses, confocal and electron microscopy.

Acutely, LPON treatment enhanced mitochondrial respiration and ROS formation. After 72 hours, despite the similarities in triglyceride accumulation, LPON treatment, but not oleate, dramatically affected mitochondrial function as evidenced by decreased respiration, increased mitochondrial membrane potential and enhanced ketogenesis.

Importantly, this was associated with increased markers of oxidative stress and enhanced gluconeogenesis. Furthermore, reduction in triglyceride with metformin did not improve mitochondrial function. By comparison, respiration and ROS formation remained unperturbed with oleate. The addition of the antioxidant N-acetylcysteine prevented mitochondrial dysfunction and reversed metabolic changes seen with LPON, strongly suggesting ROS involvement in mediating mitochondrial impairment.

Our data indicate that increased ROS formation, rather than cellular steatosis *per se*, impairs mitochondrial function. Thus, reduction in cellular steatosis may not always be the desired outcome without concomitant improvement in mitochondrial function and/or a decrease in ROS formation.

Dedicated to

Hajah Zawiyah Abu Bakar

and

Hajah Amiah Haji Daud

1. CHAPTER ONE

INTRODUCTION

1.1. Nonalcoholic fatty liver disease

Nonalcoholic fatty liver disease (NAFLD) has emerged as the most common liver disease in the developed world. It is a condition characterized by intracellular triglyceride accumulation within the liver that potentially, in the presence of inflammation, can progress to steatohepatitis (1-3). Similar to other chronic liver disorders, nonalcoholic steatohepatitis (NASH) can culminate in fibrosis or cirrhosis of the liver. Current estimates are that ~20% of the general United States population has NAFLD, with the prevalence in the morbidly obese population estimated as 75-92% (4-7). The true prevalence of NAFLD is likely to be higher, because most people in earlier stages of the disease are asymptomatic and remain undiagnosed. Importantly, this prevalence is expected to escalate mirroring the global epidemic of obesity and Type 2 diabetes.

The relationship between dietary fat, hepatic steatosis and/or cirrhosis has been recognised for ~60 years. For several decades, its clinical significance was uncertain; hepatic steatosis (in the absence of alcohol excess) was presumed to be a benign and inconsequential condition (8, 9). This long-held view was challenged when the concept of NAFLD came to fore in the 1980s. The term was coined by Ludwig *et al.* to denote

histological changes suggestive of steatohepatitis in liver biopsy specimens from 20 individuals who were mostly obese or with diabetes, and without significant alcohol intake (10). Similar to that seen with alcoholic hepatitis, these histological findings were characterized by the presence of striking fatty accumulation with concomitant lobular hepatitis, focal necrosis and inflammatory infiltrates. Importantly, these changes were accompanied by evidence of fibrosis and cirrhosis (10).

The findings by Ludwig *et al.* became the impetus to numerous studies, which now have firmly defined NAFLD as a continuum of histological changes encompassing simple steatosis in its most benign form to its most advanced form, cirrhosis. It is estimated that nearly 35% among those with steatosis would progress to steatohepatitis. Of these, a considerable proportion would develop fibrosis and cirrhosis (with its attendant complications such as hepatic failure and portal hypertension) (11, 12). More importantly, 4-27% of individuals with NASH-induced cirrhosis ultimately would progress to develop hepatocellular carcinoma (13).

Besides these liver complications, NAFLD is associated with insulin resistance and may be an independent risk factor for cardiovascular disease (14). Indeed, NAFLD has been proposed to be the hepatic component of metabolic syndrome. It is well established that insulin resistance is a prerequisite for its development (15). Thus, it is not surprising that diabetes is frequently encountered among individuals with NAFLD (16, 17). Conversely, the prevalence of NAFLD among individuals with Type 2 diabetes is estimated to be ~70% (18). In addition, the presence of diabetes is associated with more severe and rapidly progressing fibrosis (19, 20).

1.2. Pathogenesis of hepatic steatosis

The molecular events that lead to intrahepatic triglyceride accumulation are poorly understood but may involve interplay of a number of factors; 1) increased free fatty acid uptake, 2) elevated *de novo* synthesis of fatty acids, 3) impaired lipoprotein synthesis or secretion, and/or 4) reduced fatty acid oxidation. These factors result in an imbalance between triglyceride uptake and removal. Under physiological conditions, there are two potential sources of fat in the liver; first, hepatic fat may arise from uptake of free fatty acids (FFA) from the circulation. Circulating FFA can come from dietary derived chylomicron particles, lipoprotein remnants or from lipolysis of adipose tissue. Second, the liver has the capacity to synthesize fatty acids from other substrates (notably carbohydrates), in a process of *de novo* lipogenesis. Within the liver, FFA are esterified into triglycerides, which can then be stored as lipid droplets within hepatocytes or assembled with apolipoprotein B 100 (ApoB) to be secreted into the blood as very low density lipoprotein (VLDL). Additionally, triglycerides can be hydrolyzed into FFA, which can be channeled towards β-oxidation (Figure 1.2).

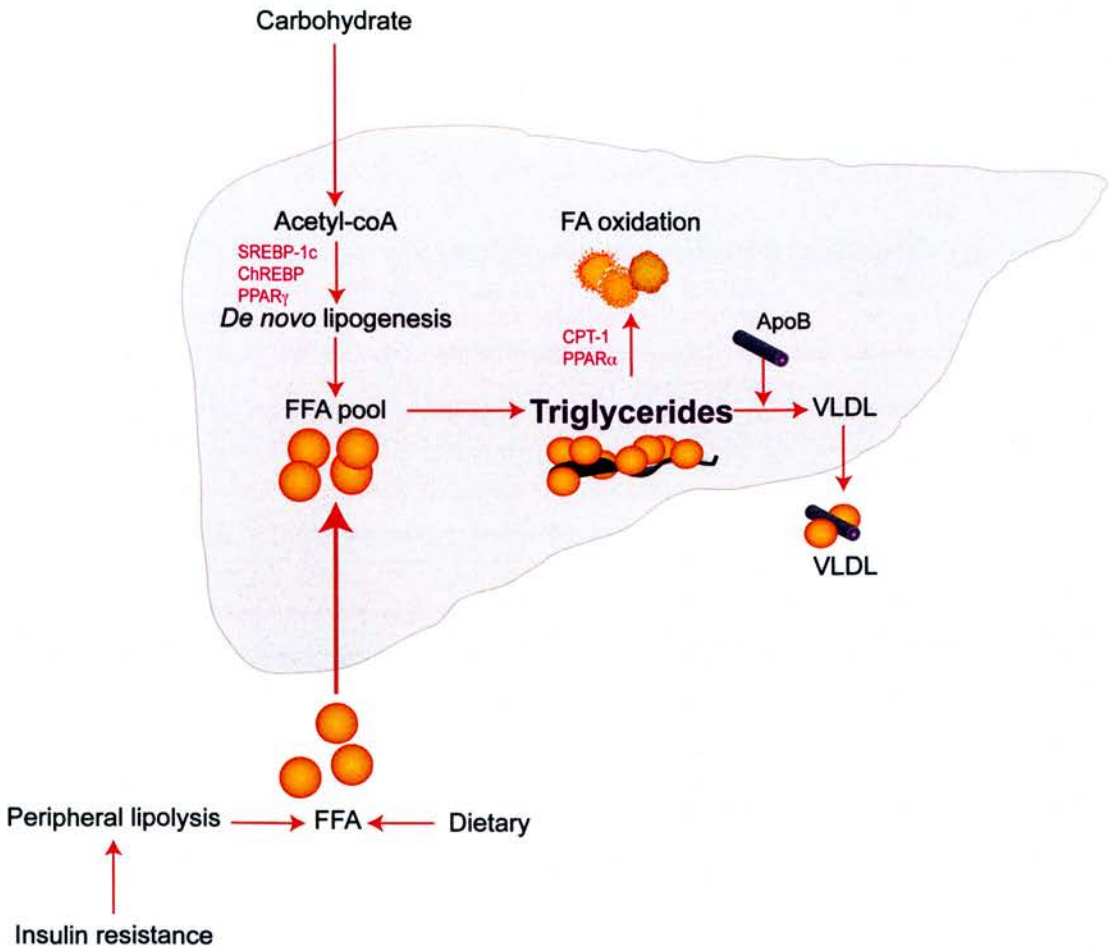

Figure 1.2. Intrahepatic triglyceride accumulation in NAFLD.

There are two potential sources of fat in the liver. First, hepatic fat may arise from uptake of free fatty acids (FFA) from the circulation. Circulating FFA can be derived from dietary chylomicron particles, lipoprotein remnants or from lipolysis of adipose tissue. Second, hepatic fat may also arise from *de novo* lipogenesis. Within the liver, FFA are esterified into triglycerides, which can then be stored as lipid droplets or secreted as very low density lipoprotein (VLDL). Triglycerides can be hydrolyzed into FFA, which can be channeled towards β-oxidation. Imbalances between uptake (increased FFA uptake or elevated *de novo* synthesis) and removal (impaired lipoprotein synthesis/secretion or reduced oxidation) lead to hepatic triglyceride accumulation. PPAR; peroxisome proliferator-activated receptor; ChREBP, carbohydrate response element-binding protein; CPT-1, carnitine palmitoyl transferase-1 and SREBP-1c, sterol regulatory element-binding protein-1c.

Liver fat accumulation in NAFLD is largely influenced by systemic availability of circulating FFA with minor contributions from *de novo* lipogenesis, FFA oxidation and lipoprotein secretions (21, 22). In an elegant study employing stable isotope tracers, Donnelly *et al.* demonstrated that ~60% of hepatic triglycerides resulted from FFA delivery to the liver (22). Peripheral insulin resistance is likely to enhance the portal concentration of FFA. Loss of insulin sensitivity in the adipose tissue results in failure to suppress lipolysis, liberating FFA into the circulation. Consequently, hepatic FFA uptake is increased, proportional to the portal concentration of FFA (23). The expression of genes involved in FFA uptake such as *Scarb*1 and *Cd*36 has been shown to be upregulated in NAFLD (24).

Increased peripheral insulin resistance is characterized by hyperinsulinaemia and hyperglycaemia. Insulin, a powerful instigator of *de novo* lipogenesis, acts by stimulating the activity of key lipogenic transcription factors, such as peroxisome proliferator-activated receptor gamma (PPARγ), carbohydrate response element-binding protein (ChREBP), and sterol regulatory element-binding protein-1c (SREBP-1c) (25-27). Similarly, hyperglycemia contributes to *de novo* lipogenesis through the formation of acetyl-coA, as well as through the activation of lipogenic transcription factors (28, 29). Indeed, individuals with NAFLD have an elevated *de novo* lipogenesis compared with healthy subjects (22, 30).

The capacity of lipid storage in the liver is limited. FFA oxidation and VLDL secretion serve as measures to remove excess FFA from the liver. The role of decreased β-oxidation or altered VLDL secretion in the pathogenesis of NAFLD remains uncertain. Diminished VLDL secretion is thought to be a feature of steatohepatitis rather than that

of simple steatosis (31). Similarly, steatosis is associated with increased β-oxidation but this remains unaltered with the onset of steatohepatitis (24, 32). In support of this, the expression of genes involved in mitochondrial β-oxidation is unchanged in NASH (21).

Hepatic lipid accumulation diminishes with the progression of steatohepatitis to cirrhosis, a phenomenon that has often been described as 'burnt-out NASH' (33). Thus, the appearance of an established nonalcoholic steatohepatitis/cirrhosis is largely indistinguishable from other causes of cirrhosis. The mechanism involved is yet to be delineated but is thought to be predominantly attributable to the downregulation of lipogenic transcription factor SREBP-1c, which diminishes the *de novo* lipogenesis (34). It has also been proposed that the overwhelming oxidative stress and the subsequent hepatocellular necrosis can promote the release of cellular lipid (35).

1.3. Progression to steatohepatitis and oxidative stress

As previously discussed, the progression to steatohepatitis occurs in approximately one third of individuals with steatosis (11). A considerable proportion of those with steatohepatitis would advance insidiously to fibrosis/cirrhosis. The presence of diabetes, metabolic syndrome, raised body mass index, older age and the presence of inflammation in the initial biopsy are among the risk factors identified for the progression to fibrosis (12, 19, 36). The prognosis of steatohepatitis-induced cirrhosis is poor; a third would develop significant liver related morbidity and mortality within a relatively short period (37).

Thus, dissecting the events involved is crucial. The 'two-hit' model proposed by Day and James provides a conceptual framework of the pathophysiology of steatohepatitis. According to this model, intracellular triglyceride accumulation is the first 'hit'. This increases the susceptibility of hepatocytes to an interplay between oxidative stress and cytokines or 'the second 'hit' (38).

Human and experimental NAFLD are characterized by chronic oxidative stress (39, 40). Oxidative stress is the result of an imbalance in the formation of prooxidant (reactive oxygen species (ROS)) and antioxidant (41). This disequilibrium is such that it favours the generation of prooxidants. ROS (superoxide, hydrogen peroxide and hydroxyl) are highly reactive molecules derived from oxygen formed mainly in the mitochondria as the byproduct of respiration. Although ROS have been implicated in many pathophysiological processes, they are also important signaling molecules (42-44). Under physiological condition, ROS formation is tightly regulated. Liver is endowed with antioxidants such as mitochondrial superoxide dismutase (MnSOD), glutathione peroxidases (GPX), catalase and peroxiredoxins, which are extremely efficient in counteracting the superfluous ROS (45).

Cellular damage can occur when ROS overwhelm the capabilities of antioxidants. In the liver, ROS can mediate hepatocyte injury by three potential mechanisms. First, ROS induce direct oxidative modification of macromolecular structures including lipid, protein and DNA (46). For example, ROS can instigate lipid peroxidation leading to the formation of reactive aldehydes such as 4-hydroxynonenal (4-HNE) and malondialdehyde (MDA). Second, ROS can initiate a cascade of proinflammatory cytokines such as tumor necrosis factor (TNF)-α, transforming growth factor (TGF)-β

and interleukin (IL)-8, which in turn, can promote the release of inflammatory mediators and activate the stellate cells (47). These cytokines in concert with the reactive aldehydes can generate further ROS thus perpetuating a vicious cycle (48). Third, ROS are known to induce stress pathways such as protein kinase C (PKC), mitogen-activated protein kinase (MAPK), jun N-terminal kinase (JNK), nuclear factor-κB (NF-κB)).

There is strong evidence to support increased prooxidant in steatohepatitis. For example, the expression of cytochrome P450 2E1 (CYP2E1), an enzyme with substantial prooxidant activity, has been shown to be upregulated in steatohepatitis (49). The activity of CYP2E1 is significantly higher in steatohepatitis than in simple steatosis (50). Similarly, the level of 8-hydroxydeoxyguanosine, a marker of DNA oxidative damage, is higher in NASH, but is rarely present in steatosis, and is undetectable in normal liver (51). Its expression correlates with hepatic necroinflammatory activity. The intermediates of lipid peroxidation are also increased in steatohepatitis suggesting heightened oxidative process (32, 51, 52). Similarly, pro-inflammatory pathways such as JNK and NF-κB are upregulated and can potentially trigger the release of cytokines (53, 54). Indeed, the levels of cytokines such as TNF-α, IL-6, and IL-8 are raised in individuals with steatohepatitis (55, 56). Diminished antioxidant activity coupled with glutathione depletion in human steatohepatitis can aggravate these inflammatory activities further (50, 57, 58). Importantly, mitochondrial alterations known to occur in steatohepatitis can perpetuate the release of ROS, thus bolstering the already enhanced proinflammatory activity (32, 46, 59).

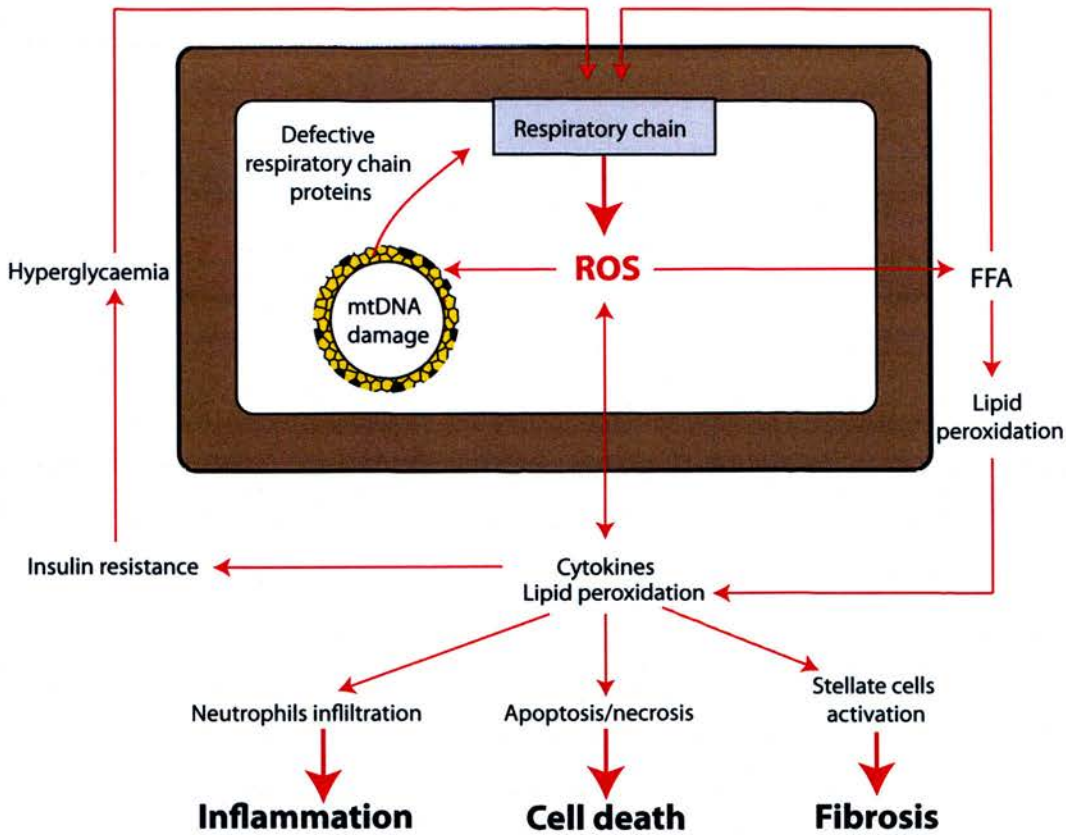

Figure 1.3. The mechanisms of reactive oxygen species mediated injury in the hepatocyte.

ROS are byproducts of normal respiration. An imbalance between ROS formation and antioxidant results in oxidative stress. Under this condition, ROS can alter macromolecular structures including mitochondrial DNA and mitochondrial respiratory chain. ROS can also induce lipid peroxidation as well as instigating the release of cytokines, which in turn can activate various pathways leading to fibrosis, cell death and inflammation.

1.4. Mitochondria and ROS formation

1.4.1. Mitochondrial structure

Mitochondria are cellular organelles responsible for ATP production in all eukaryotes. A double-layered membrane encloses each mitochondrion. The inner layer invaginates into the matrix to form a shelf-like structure known as cristae (Figure 1.4.1). Mitochondria do not exist as an individual organelle but comprise dynamic networks that constantly undergoing fission and fusion (60). Mitochondria are unique in that they possess a separate genome. Mitochondrial DNA (mtDNA), a circular double-stranded DNA molecule located in the matrix, encodes 13 of the respiratory chain polypeptides. The presence of mtDNA has become the crux of the endosymbionts hypothesis of its origin. This hypothesis posits that mitochondria are derived from α-proteobacteria that formed a symbiosis with archaebacteria ~2 billion years ago (61).

Aside from ATP formation, mitochondria regulate many crucial pathways including cell cycle, cell death and energy substrates oxidation. Metabolic pathways such as TCA cycle, urea cycle and β-oxidation occur in a close proximity to the respiratory chain within the mitochondria to allow a precise ATP regulation. However, the constant superoxide formation as the byproduct of respiration can predispose mitochondria to ROS mediated injury. Mitochondrial structural and functional abnormalities in steatohepatitis such as mtDNA depletion, decreased respiratory chain activity and diminished ATP are strongly linked to the oxidative stress (32, 62-64). Indeed, some have suggested that NAFLD might be a mitochondrial disease.

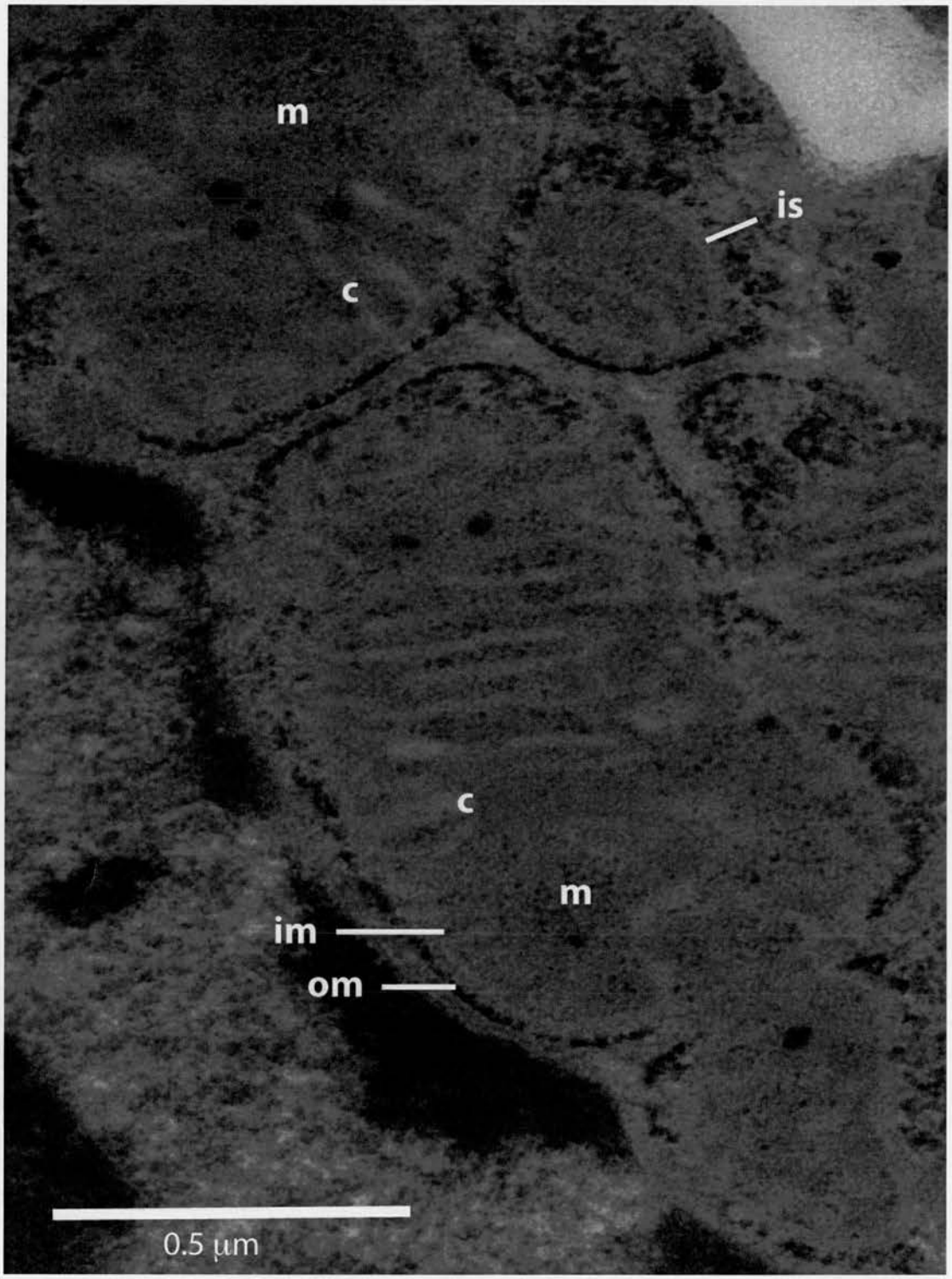

Figure 1.4.1. Mitochondrial structure viewed under electron microscopy.

Legends: im, inner membrane; om, outer membrane; m, matrix; c, cristae; is, intermembrane space.

1.4.2. Oxidative phosphorylation

Carbohydrates (glucose) and lipids (FFA) are the principal energy substrates in many living organisms. Amino acids are also an energy substrate, however, following deamination, they converge into the carbohydrate oxidative pathways. The coupling of substrate oxidation to the ATP formation by mitochondrial respiration i.e. oxidative phosphorylation, allows the fine-tuning to match the energy substrate oxidation to the ATP formation and energy demand.

The uptake of glucose into the hepatocytes occurs passively across the concentration gradient through a transmembrane carrier protein, glucose transporter 2 (GLUT2). Within the cytoplasm, glucose is phosphorylated by hexokinase to glucose 6-phosphate, which then enters glycolysis culminating in the formation of pyruvate. In turn, pyruvate is transported into the mitochondria and decarboxylated resulting in the formation of acetyl-coA.

Similarly, the uptake of FFA by fatty acid transporters such as fatty acid translocase (FAT/CD36) into the hepatocytes is proportional to its portal concentration. Fatty acid is activated by acyl-coA synthetase into fatty acyl-coA in the cytosol. Fatty acyl-coA is then transferred (for example, by carnitine palmitoyl transferase) into the mitochondria to undergo β-oxidation, leading to acetyl-coA formation. Thus, acetyl-coA is the point of convergence for both FFA and carbohydrates oxidation (Figure 1.4.2.1).

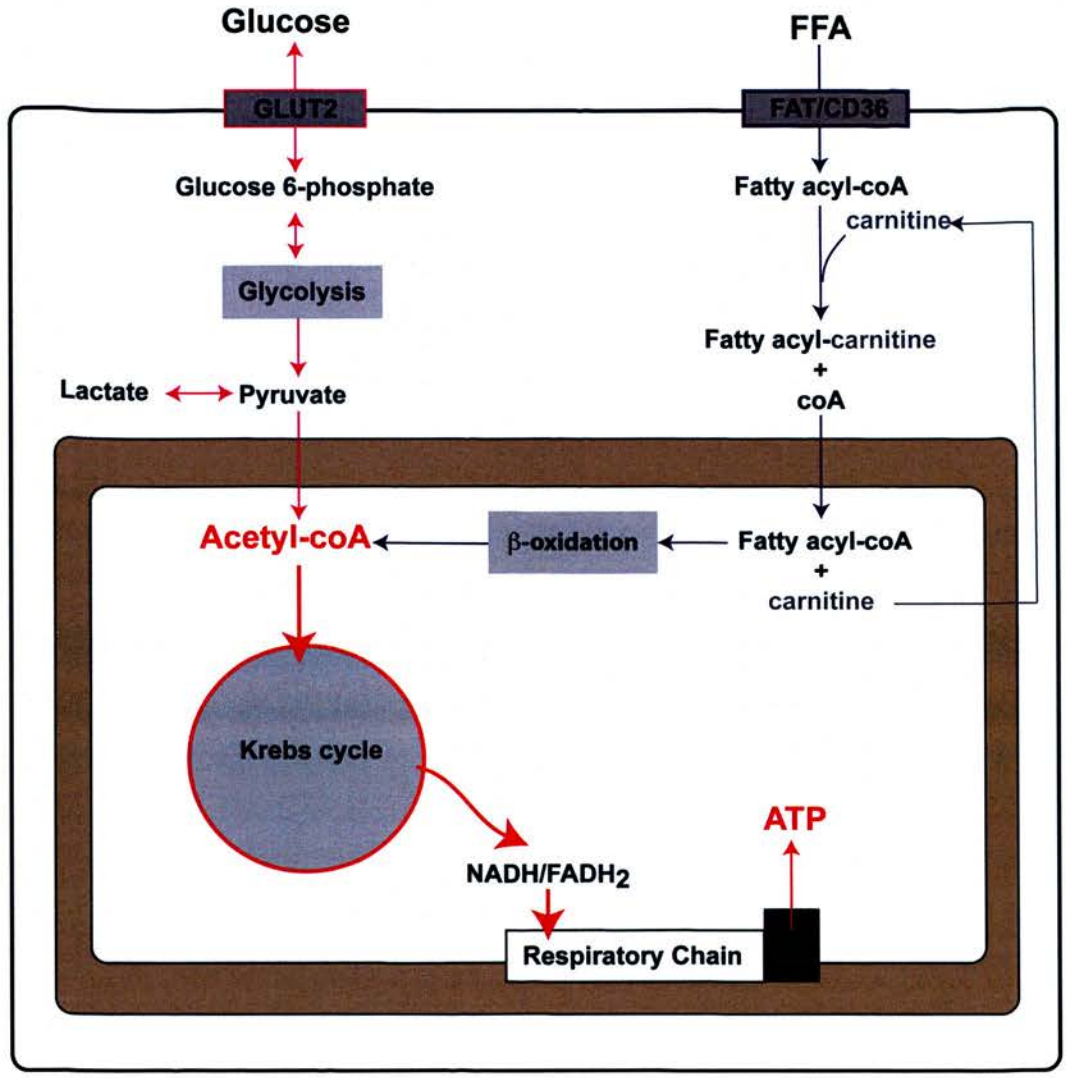

Figure 1.4.2.1. Glucose and free fatty acid metabolism.

Glucose transporter 2 (GLUT2) and fatty acid transporters such as fatty acid translocase (FAT/CD36) mediate glucose and FFA uptake into the hepatocytes respectively. Within cytoplasm, glucose enters glycolysis culminating in the formation of pyruvate, which is converted into acetyl-coA in the mitochondria. Similarly, FFA is activated in the cytoplasm into FFA acyl-coA, which is transported into the mitochondria for β-oxidation resulting in the formation of acetyl-coA. In turn, acetyl-coA enters the TCA cycle. The turnover of TCA cycle generates NADH and $FADH_2$ for mitochondrial respiratory chain.

The oxidation of acetyl-coA by the TCA cycle results in the formation of electron carriers, NADH and $FADH_2$, destined for the respiratory chain. The electrons from NADH are released to Complex I (or Complex II for $FADH_2$) of the respiratory chain and these electrons are subsequently transferred across a series of donors and acceptors. The passage of electrons continues until they are passed on to oxygen, the final electron acceptor (Figure 1.4.2.2).

The movement of electrons across the respiratory chain releases energy. This energy is harnessed by Complex I, III and IV and is utilized to extrude protons against the concentration gradient into the mitochondrial intramembrane space. This generates an electrochemical gradient across the inner mitochondrial membrane or proton motive force (65). Proton motive force is a major determinant of the mitochondrial membrane potential ($\Delta\Psi_m$) and is pivotal in ATP synthesis. It fuels the formation of ATP from ADP and inorganic phosphate using the energy released from the proton movement down the concentration gradient into the matrix through the ATP synthase (Figure 1.4.2.2). $FADH_2$ yields 40% less ATP than NADH. The reason is that NADH releases electron to Complex I thus the passage of electrons involves three proton-pumping complexes (complexes I, III and IV) whereas electrons from $FADH_2$ are released at Complex II and the subsequent forward movement of electrons only involves two sites for proton extrusion (complexes III and IV).

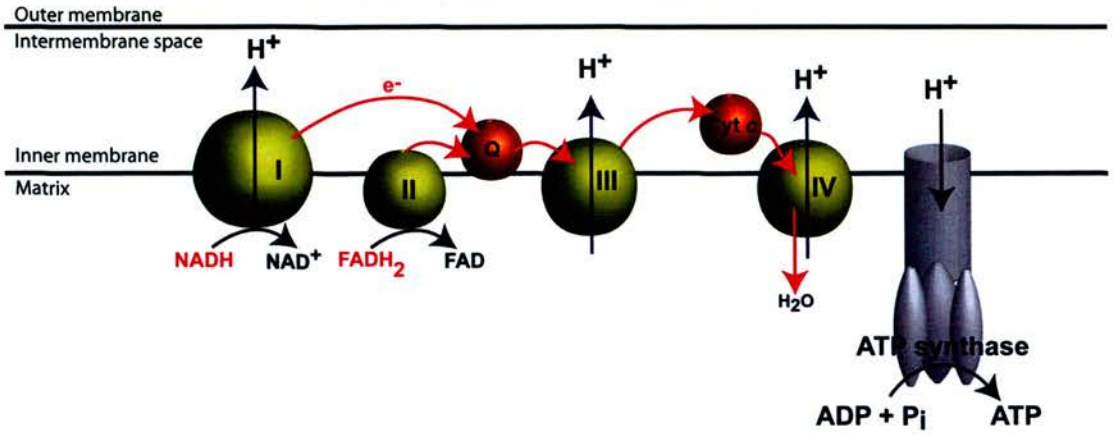

Figure 1.4.2.2. Oxidative phosphorylation.

Mitochondrial respiratory chain is a series of electron acceptors and donors. There are four transmembrane enzyme complexes embedded in the inner membrane (Complex I (NADH dehydrogenase), Complex II (succinate dehydrogenase), Complex III (cytochrome bc_1 complex) and Complex IV (cytochrome *c* oxidase) in addition to coenzyme Q (ubiquinone) and cytochrome *c*, which shuttle electrons to Complex III and IV, respectively. The movement of electrons (red arrows) is coupled with the extrusion of protons (purple arrows) from Complex I, III and IV into the intermembrane space. This generates proton gradient, which drives the ATP formation (brown arrow). The electrons are subsequently reduced by oxygen, the final electron acceptor, to form water. Q, coenzyme Q; Cyt *c*, cytochrome *c*.

1.4.3. ROS formation in the mitochondria

Electrons can escape from the carriers and interact with oxygen to generate superoxide (the progenitor of ROS) within the matrix. Under physiological condition, this process is both inevitable and essential; ROS are important signaling molecules. Thus, the concentration of electron carriers (in their reduced state i.e. NADH/$FADH_2$) and the rate of electrons released from the carriers are key determinants to the magnitude of superoxide formation. $\Delta\Psi_m$ also exerts a considerable influence on superoxide formation. In normal functioning mitochondria, an active ATP formation results in a relatively low $\Delta\Psi_m$. This allows a steady flow of electrons across the mitochondrial respiratory chain for constant NADH oxidation, thus minimizing the superoxide formation (Figure 1.4.3.1).

Diminished forward electron movement, for instance, in the presence of damaged mitochondrial respiratory chain, low ATP demand or with cytochrome *c* release during apoptosis, reduces NADH oxidation. Consequently, NADH concentration (and $NADH/NAD^+$ ratio) would rise, favouring the electron leaks to form superoxide. Under these circumstances, continuing NADH supply to Complex I could potentially augment superoxide formation (Figure 1.4.3.2). Similarly, increased $\Delta\Psi_m$ enhances mitochondrial superoxide formation. A significant rise in $\Delta\Psi_m$, for example, in the presence of diminished ATP formation, can inhibit proton extrusion and forward electron transfer. In these circumstances, the reverse movement of electrons (reverse electron transport (RET)) from Coenzyme Q (ubiquinone) to complex I can occur. This results in a reduction of NAD^+ to NADH in Complex I, thus increasing the NADH concentration and superoxide formation (Figure 1.4.3.3).

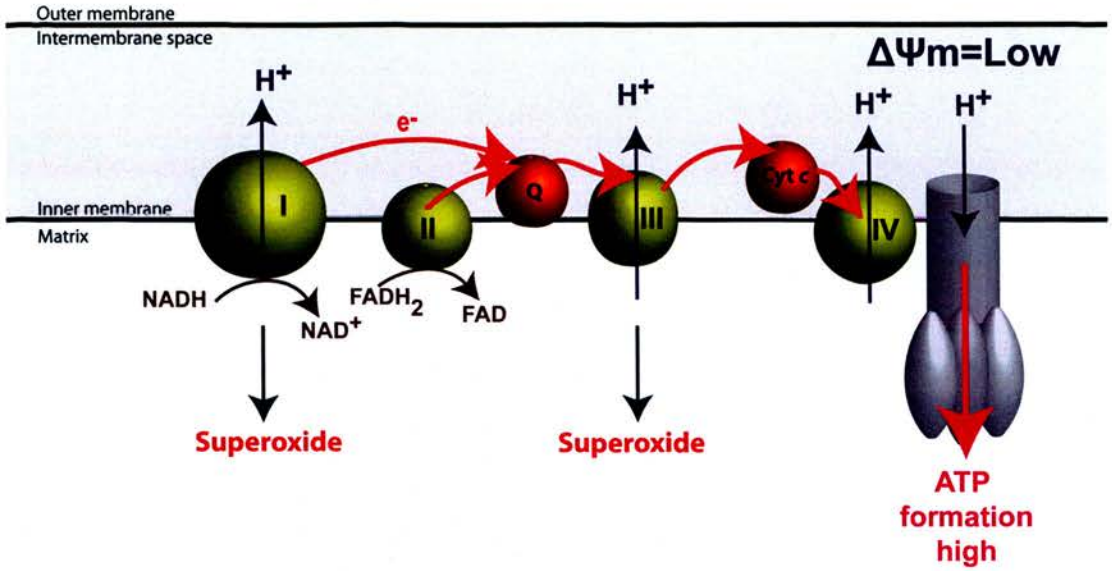

Figure 1.4.3.1. Superoxide formation in normal mitochondria.

In normal functioning mitochondria, an active ATP formation (pink arrow) results in a relatively low $\Delta\Psi_m$. Thus, a steady flow of electrons (red arrows) across the mitochondrial respiratory chain continues to maintain constant NADH oxidation to NAD^+ (brown arrow). Superoxide formation is kept to a minimum with mitochondrial antioxidant pathways countering any superfluous superoxide within the matrix. Q, Coenzyme Q (ubiquinone); Cyt *c*, cytochrome *c*.

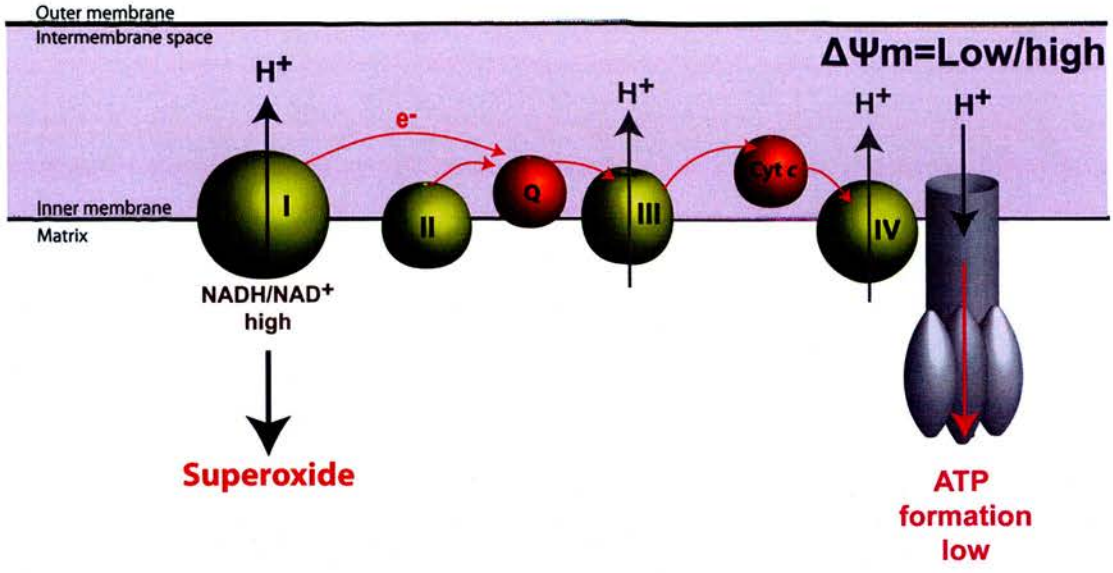

Figure 1.4.3.2. Mitochondrial superoxide formation in impaired respiration.

Impaired mitochondrial respiration results in decreased NADH oxidation to NAD^+. Similarly, any impediment to the release of electron from the carriers (red arrow) can increase the concentration of NADH (and the NADH/NAD^+ ratio) thus, enhancing electron untimely exit to form superoxide. Q, Coenzyme Q (ubiquinone); Cyt *c*, cytochrome *c*.

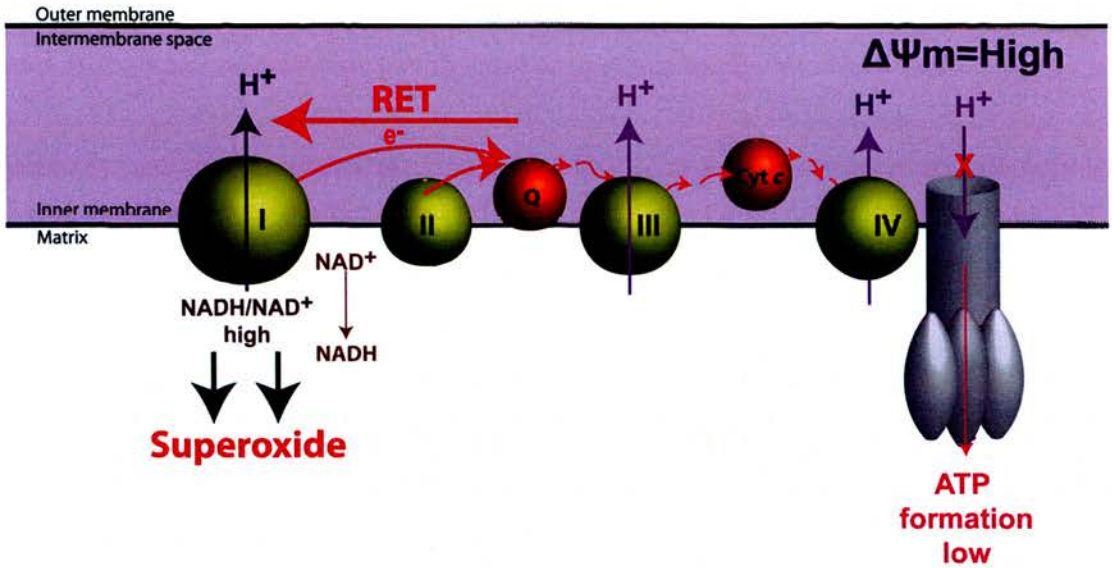

Figure 1.4.3.3. Mitochondrial superoxide formation and reverse electron transfer. Proton extrusion and forward electron transfer are inhibited when there is a significant rise in $\Delta\Psi_m$. In these circumstances, the reverse movement of electrons from Coenzyme Q (ubiquinone) to complex I, or reverse electron transport (RET), can occur. The reversed movement of electrons promotes NAD^+ reduction to NADH in Complex I. The concentration of NADH increases dramatically, thus enhancing superoxide formation. Q, Coenzyme Q (ubiquinone); Cyt *c*, cytochrome *c*.

1.4.4. Potential mechanisms for increased ROS formation in NAFLD

Increased energy substrate is central to the development of dietary NAFLD. Increased free fatty acid (FFA) flux, in tandem with hyperglycaemia that often characterized insulin resistance, can augment tricarboxylic acid (TCA) cycle resulting in the overproduction of electron donors NADH and $FADH_2$. Consequently, electron delivery to the respiratory chain is enhanced, paralleled by a rise in mitochondrial respiration. Under this circumstance, active ATP formation, which lowers the $\Delta\Psi_m$, is crucial in minimizing the inherent ROS production. However, if the electron supply exceeds the cellular ATP demand, $NADH/NAD^+$ ratio and ROS will rise. Decreased mitochondrial respiration and reduced ATP formation as often seen in steatohepatitis can potentially sustain the ROS formation (59, 62, 66, 67).

1.4.5. Uncoupling and ROS formation in NAFLD

As discussed above, superoxide formation is highly sensitive to the changes in $\Delta\Psi_m$; increased $\Delta\Psi_m$ promotes superoxide formation and conversely, a reduction in $\Delta\Psi_m$ (for example, during ATP formation) diminishes superoxide production (68). Decreased $\Delta\Psi_m$ can also occur when protons leak into the matrix independent of ATP synthase, therefore, uncoupling the ATP synthesis from substrate oxidation. Under physiological condition, basal proton leaks accounts for ~20–30% of the resting metabolic rate in active tissues such as hepatocytes and is thought to represent a protective mechanism to limit ROS production (69).

Proton leak is also inducible by uncoupling proteins (UCP). Superoxide, free fatty acids and lipid peroxidation products such as HNE, have been shown to induce UCP (70-73). UCP2 in particular, is strongly implicated in the pathophysiology of NAFLD. UCP2 has

been shown to be significantly upregulated in obesity, insulin resistance and fatty hepatocytes (74, 75). Although increased UCP2 attenuates superoxide formation, this can occur at the expense of ATP formation and thus, can potentially induce necrosis and increased susceptibility of hepatocytes to further injury (75, 76).

1.4.6. Oxidative stress and altered mitochondrial structure in NAFLD

Impaired mitochondrial function in NAFLD is often paralleled by alterations in mitochondrial structure, the most striking of which, is the development of enlarged mitochondria, collectively termed as megamitochondria (32, 77, 78). Their presence in experimental steatosis was initially described 50 years ago (79). It is estimated that megamitochondria occur in 5-15% of hepatocytes in steatohepatitis and are notably absent in cirrhosis (80).

Megamitochondria is thought to reflect hepatocellular injury. In steatohepatitis, megamitochondria are associated with oxidative stress, mitochondrial respiratory chain impairment and diminished ATP formation (32). The ability of ROS to induce similar alterations under experimental conditions suggests that these changes may represent either a degenerative or an adaptive response to oxidative stress (81, 82).

Mitochondria exist as a reticular network maintained by a dynamic balance of fusion and fission according to the cellular demand. A shift in balance towards fusion can result in enlarged or elongated mitochondria. Conversely, increased fission promotes smaller and fragmented mitochondria, as often seen during apoptosis (83). Interestingly, elongated mitochondria formed by decreased fission leads to diminished ROS

formation (84). This suggests that such alterations in mitochondrial structure may represent an adaptive response to minimize ROS formation in the presence of oxidative stress (82).

1.4.7. The relationship between ROS, mitochondrial function and insulin resistance

There is increasing evidence both from *in vivo* dietary models of NAFLD and *in vitro* hepatocyte lipid overload models, to suggest that hepatic lipid accumulation alters insulin signaling (85-87). Insulin is the principal hormone in glucose homeostasis. It acts by stimulating glucose influx and metabolism in muscle and adipocytes. In the liver, insulin inhibits gluconeogenesis and promotes glycogen synthesis. Insulin also modifies the expression and the activity of several enzymes including those involved in lipogenesis. Its action is mediated through the insulin receptor, a transmembrane glycoprotein with intrinsic protein tyrosine kinase activity. The binding of insulin to the receptor triggers tyrosine phosphorylation which cascades through insulin receptor substrates (IRS)/phosphatidylinositol 3-kinase (PI3K)/protein kinase B (AKT)/forkhead box O transcription factor (FOXO) 1. Additionally, there is a parallel pathway linking the insulin receptor to the lipogenic transcription factor SREBP1c (Figure 1.4.7.1). Several studies have documented defects in molecules involved in the IRS/PI3K/AKT/FOXO1 signaling pathway in NAFLD (85, 88). The alterations in insulin signaling are associated with increased endogenous glucose production (a marker of hepatic insulin resistance) (89, 90). However, it is thought that the activation of SREBP1c remains fully functional and continues to mediate lipogenesis (91).

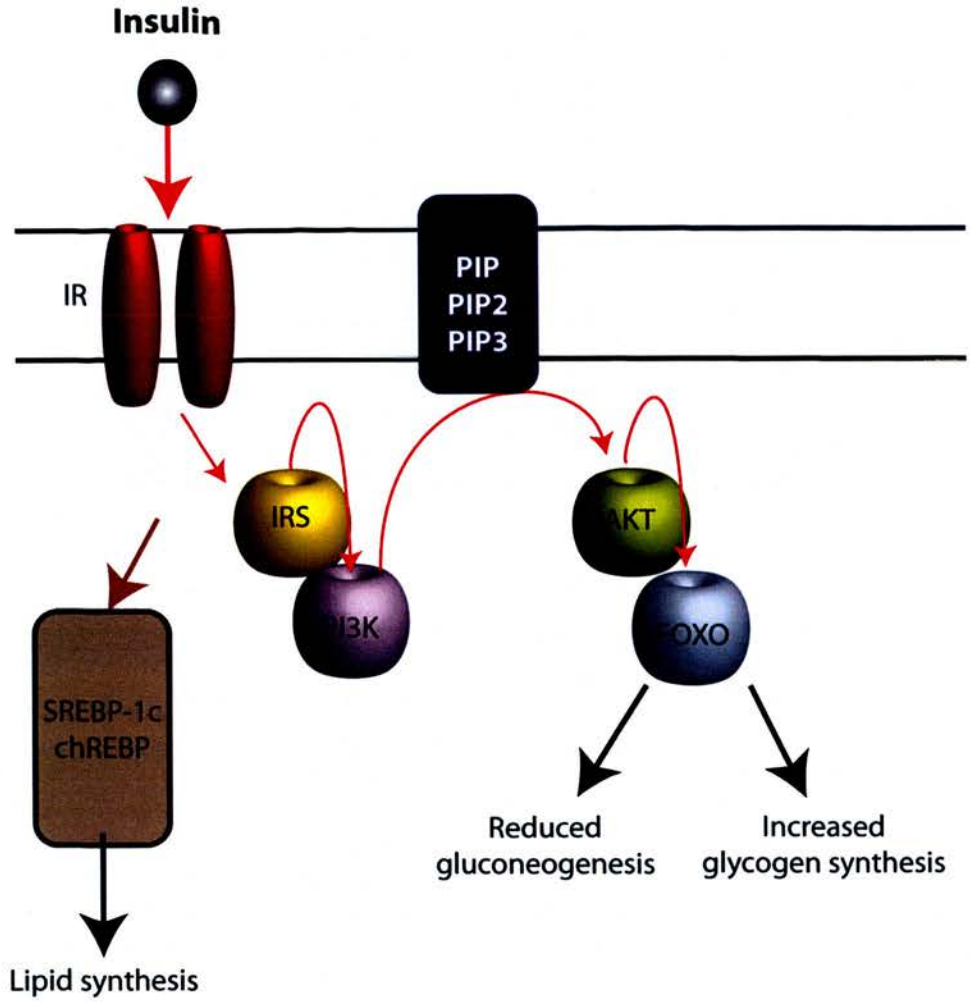

Figure 1.4.7.1. Insulin signaling.

The action of insulin is mediated by insulin receptor. The binding of insulin triggers tyrosine phosphorylation of the insulin receptor, which cascades through IRS/PI3K/AKT/FOXO1 (red arrow). This signaling pathway is thought to be selectively downregulated in hyperinsulinaemia. In contrast, a parallel pathway linking the activation of insulin receptor to the transcriptional upregulation of lipogenic transcription factor SREBP1c (brown arrow) remains fully functional and continues to mediate lipogenesis. IR, insulin receptor; IRS, insulin receptor substrate; PI3K, phosphatidylinositol 3-kinase; AKT, protein kinase B; FOXO1, forkhead box O transcription factor 1; PIP, phosphatidylinositol phosphate; PIP2, phosphatidylinositol 4,5-bisphosphate; PIP3, phosphatidylinositol 3,4,5-trisphosphate; SREBP-1c, sterol regulatory element binding protein-1c; ChREBP; carbohydrate responsive element binding protein.

Oxidative stress has been strongly implicated in the development of insulin resistance (92). Increased expression of pro-oxidant CYP2E1 in steatohepatitis leads to the development of insulin resistance (49). In a cellular model of steatosis, palmitate-induced insulin resistance has been shown to be mediated by mitochondrial ROS (85). Furthermore, activation of pro-inflammatory cytokines (e.g. TNF-α, IL-1β, and IL-6) by ROS interferes with insulin signaling through activation of the kinases and transcription factors such as JNK, NFκB, inhibitor of kappa B kinase-β (IKKβ) (93).

However, the relationship between ROS and insulin resistance is undergoing reexamination. For example, a recent study has shown that depending on the concentrations, H_2O_2 can either enhance or attenuate insulin signaling (94). The finding of enhanced PI3K/Akt signaling hence insulin sensitivity in mice with Gpx1 deficiency further supports this contention (95). Indeed, it has been proposed that ROS-mediated insulin resistance is a cellular adaptive response to oxidative stress (96).

Similarly, it is unclear if triglyceride accumulation *per se* modulates insulin sensitivity. Reduction in triglyceride accumulation does not necessarily improve insulin sensitivity or prevent the progression to steatohepatitis. For example, inactivation of diacylglycerol acyltransferase 2 (DGAT2), the enzyme that catalyses the final step of triglyceride biosynthesis, dramatically reduces hepatic fat accumulation in a mouse model of methionine choline deficient (MCD) but this is associated with exacerbation of necroinflammatory activity and fibrotic response in the liver (97).

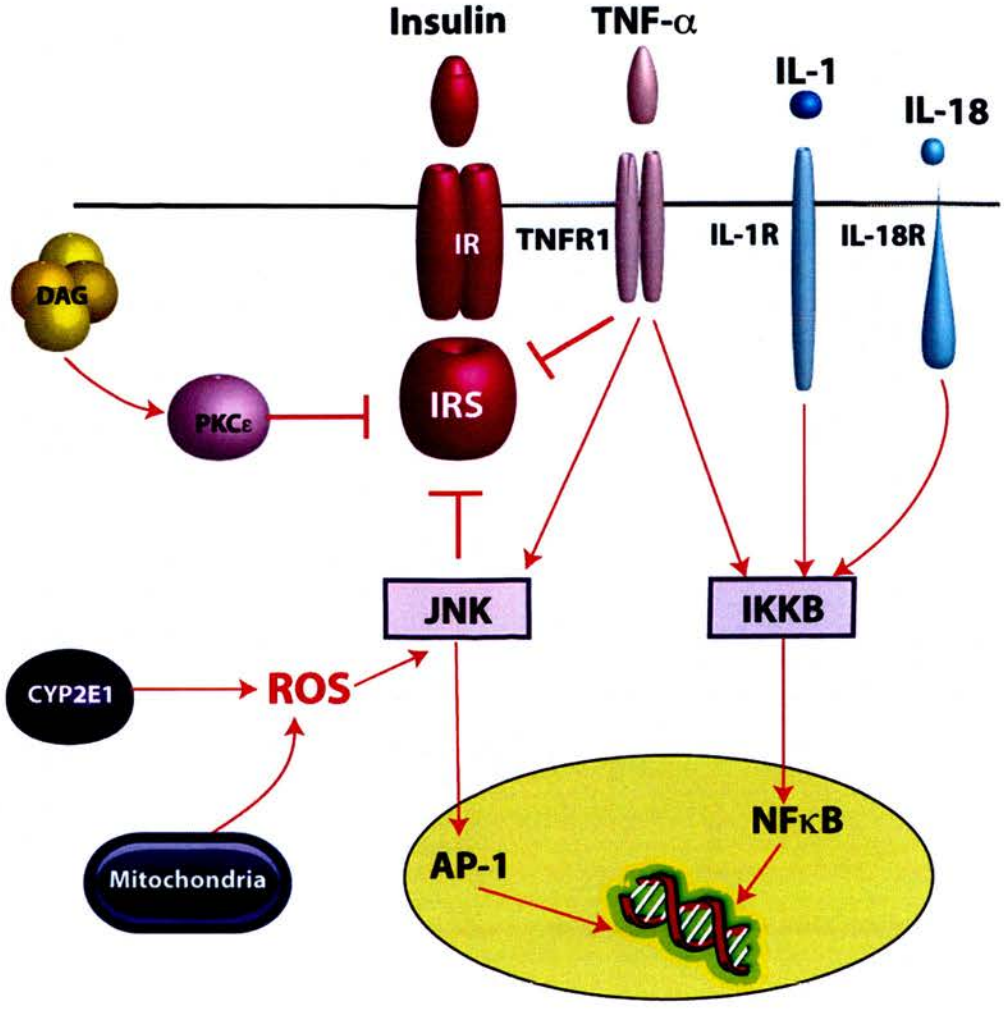

Figure 1.4.7.2. The proposed mechanisms of insulin resistance.

ROS play an integral role in promoting insulin resistance in steatohepatitis. Potential mechanism includes ROS activation of pro-inflammatory cytokines, which interferes with insulin signaling through activation of JNK and IKKβ. A number of recent studies have proposed that DAG activation of PKCε attenuates insulin signaling by promoting serine (instead of tyrosine) phosphorylation of the insulin receptor. AP-1, activator protein-1; DAG, diacylglycerol; IR, insulin receptor; IRS; insulin receptor substrate; IL, interleukin; IL-1R, interleukin-1 receptor; IL-18R, interleukin-18 receptor; IKKβ, inhibitor of kappa B kinase-β; JNK, jun N-terminal kinase; NF-κB, nuclear factor-κB; PKC, protein kinase C; TNF-α, tumor necrosis factor-α; TNFR1, tumour necrosis factor receptor 1.

1.5. Project aims

Our study sought to address several fundamental questions on hepatic mitochondrial impairment in the presence of increased energy substrates.

1. *Does steatosis exert deleterious effects on mitochondrial function in the absence of ROS?*

This is a critical question since a proportion of individuals with steatosis progress to steatohepatitis. Evidence to support the role of mitochondrial dysfunction in NAFLD is almost always associated with steatohepatitis and is inevitably characterized by increased oxidative stress. The impact of cellular steatosis *per se* on mitochondrial function remains uncertain. Yet, the reduction in intracellular triglyceride accumulation is often construed as a marker of improvement in NAFLD.

2. *What are the individual contributions from ROS, mitochondrial dysfunction and steatosis towards the metabolic derangements associated with NAFLD?*

Chief among the metabolic derangements in NAFLD is the development of insulin resistance, which can lead to hyperglycaemia and hyperinsulinaemia. The contributions of steatosis *per se* towards these metabolic derangements have not been determined. Similarly, the relationship between mitochondrial dysfunction and the development of hyperglycaemia remains unclear; does altered glucose metabolism precede, parallel, or simply a consequence of impaired mitochondrial function?

3. *What are the effects of the intracellular antioxidant N-acetylcysteine on hepatic mitochondrial function and metabolic alterations associated with cellular steatosis?*

N-acetylcysteine, an antioxidant known to reduce cellular ROS, has been shown to enhance mitochondrial function in adipocytes, cardiac and skeletal muscle (98-100).

However, the effects of NAC on hepatic mitochondrial function and metabolic alterations associated with human steatohepatitis are yet to be established (32).

4. *Does medium chain fatty acid invoke different metabolic responses in hepatocytes when compared with long chain fatty acid?*

The ability of medium chain free fatty acids (MCFA) such as octanoate, to diffuse into the mitochondria independent of carnitine palmitoyl transferase (CPT) allows a more efficient β-oxidation than long chain fatty acids (LCFA) (101). Indeed, increased basal lipolysis with octanoate in adipocytes has prompted interest in the use of MCFA to induce weight loss (102, 103). The effect of MCFA including octanoate on hepatic mitochondrial function and ROS formation particularly in a milieu that is already burdened by enhanced respiration have not been previously examined.

1.6. *In vitro* model

Dissecting the pathophysiology of NAFLD is often hampered by the relative inaccessibility of the liver. Although liver biopsy remains as the gold standard in diagnosing steatohepatitis clinically, it is invasive and prone to sampling error. Thus, repeat biopsies to demonstrate the continuum of the pathophysiology involved in NAFLD is not feasible.

Many of the animal models of NAFLD have provided vital insights into the pathophysiology involved but are yet to recapitulate the entire phenotype as encountered in clinical practice. More important, many differ from the metabolic aspects of the human disease despite the similarities in gross histological appearance

(104). Furthermore, dissecting the contribution of steatosis, ROS and mitochondrial function in the liver is difficult to achieve *in vivo* owing to the confounding factors such as peripheral insulin resistance and adipocytokines. By comparison, *in vitro* studies provide a controlled environment, independent of the influence exerted by adipocytokines and peripheral hyperinsulinaemia thus focusing on events that occur specifically in the liver.

The most important prerequisite of an *in vitro* model of NAFLD is cellular steatosis. Most of the existing *in vitro* models are based on lipid loading where hepatocytes are incubated with optimal concentrations of free fatty acids to induce steatosis. Free fatty acid such as oleate, alone or in combination with palmitate are most commonly used. This is largely based on studies suggesting that triglyceride accumulation in NAFLD is largely driven by an increase in palmitate and oleate (105, 106).

However, achieving similar triglyceride composition does not necessarily recapitulate human NAFLD. For example, oleate promotes triglyceride accumulation but without excessive ROS formation or insulin resistance (107). Palmitate is poorly incorporated into triglyceride and its use is limited by its propensity to induce apoptosis (108). More important, both are long chain free fatty acids rendering them relatively unsuitable for examining the impact of accelerated mitochondrial superoxide formation. The underlying reason is that their entry into the mitochondria has to be regulated by carnitine palmitoyl transferase (CPT), a rate-limiting enzyme for β-oxidation. Thus, the production of mitochondrial ROS with long chain fatty acids can be unpredictable.

1.7. LPON as an *in vitro* model of cellular steatosis

One of the main objectives of the present study was to examine *in vitro* the relationship between energy substrates, mitochondrial reactive oxygen species (ROS) formation and mitochondrial function in the presence of hepatic steatosis. In dietary-induced NAFLD, the sequence of events is almost always instigated by increased energy substrate, which promotes hepatic steatosis as well as enhances cell respiration and hence ROS formation. In order to recapitulate this sequence of events, we designed an *in vitro* model using energy substrates that can enhance respiration. The prerequisites of the substrates chosen are their ability to induce adequate steatosis in addition to their capacity in promoting tricarboxylic acid cycle (TCA) to generate NADH for mitochondrial respiratory chain. Being a medium chain free fatty acid (MCFA), octanoate, enters mitochondria independent of carnitine palmitoyl transferase (CPT) leading to an efficient β-oxidation. Acetyl-coA generated from complete and exclusive β-oxidation can be incorporated into triglyceride through *de novo* lipogenesis. Indeed, the acyl chains of triglyceride formed by octanoate through *de novo* lipogenesis are palmitate and palmitoleate (101).

Acetyl-coA can also enter the TCA cycle culminating in the formation of reducing equivalents ($NADH/FADH_2$) destined for mitochondrial respiratory chain. Thus, we chose octanoate due its ability to induce adequate steatosis in addition to its immediate availability as an energy substrate to the TCA cycle. In stark contrast to octanoate, the entry of long chain fatty acid (LCFA), oleate, into the mitochondria has to be regulated by CPT, a rate-limiting enzyme for β-oxidation. Direct esterification of oleate allows significant triglyceride accumulation but without excessive ROS species formation.

We used C3A cells, a clonal derivative of human hepatoblastoma HepG2, treated with either oleate or octanoate to induce triglyceride accumulation. These FFA were chosen due to their contrasting effects on β-oxidation and ROS production. The rate of mitochondrial respiration was further manipulated by adding the end products of glycolysis, lactate (L) and pyruvate (P) to octanoate (O). The reasoning was that these energy substrates would synergistically enhance mitochondrial respiration and promote significant intracellular lipid accumulation through *de novo* lipogenesis. To augment the endogenous ROS synthesis further, we added ammonia to the LPO combination with the hypothesis that the metabolism of ammonia by the urea cycle or the glutamine pathways (in the presence of suboptimal urea cycle, for example, in progressive hepatic dysfunction as well as in HepG2/C3A cells) would promote NADH formation and further enhance mitochondrial respiration (109, 110).

The focus was then to observe the events that occurred as consequences of enhanced TCA activity similar to what potentially may occur with nutrient excess.

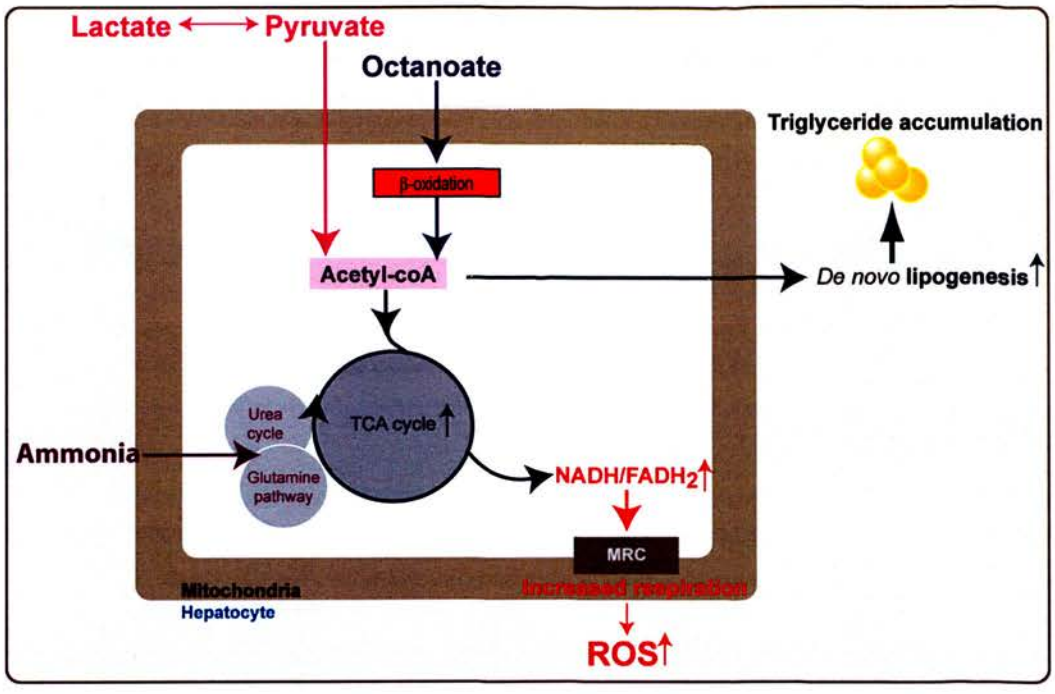

Figure 1.7. *In vitro* model of cellular steatosis using LPON.

LPON were chosen for their swift ability to form acetyl-coA for TCA cycle. Acetyl-coA is formed by the recurring sequence of β-oxidation and from pyruvate by pyruvate dehydrogenase. Acetyl-coA enters the TCA cycle with resultant NADH formation for mitochondrial respiratory chain. Additionally, it can contribute towards *de novo* lipogenesis. We hypothesized that the combination of the substrates would increase the turnover of the TCA cycle resulting in enhanced NADH formation. Consequently, mitochondrial respiration is augmented and ROS formation is increased. MRC, mitochondrial respiratory chain; TCA, tricarboxylic acid cycle.

1.8. C3A cells

C3A cells, a derivative of human hepatoblastoma cell line HepG2, is selected for its enhanced hepatic phenotype (111, 112). C3A cells retain most of the primary hepatocyte functions including albumin synthesis, alpha-fetoprotein formation, GSH synthesis and to a certain extent, cytochrome P450 for detoxification (113, 114). Indeed, these characteristics support their use in bioartificial liver devices (111). When cultured in three-dimensional spheroids, C3A cells demonstrate typical morphology of the primary hepatocyte i.e. tight junctions, polar cells, the presence of bile canaliculi and enhanced cytochrome P450 expression (115). Importantly, C3A cells are able to accumulate triglyceride when exposed to free fatty acids and have been previously used as an experimental model of cellular steatosis (116).

Although primary hepatocytes have superior metabolic and synthetic function than C3A cells, these characteristics diminish within 72 hours. By comparison, gluconeogenesis, galactose elimination and β-oxidation are sustained in C3A cells even after 10 days of preconditioning with the metabolic substrates; lactate, pyruvate, octanoate and ammonia.

2. CHAPTER TWO

GENERAL MATERIALS AND METHODS

2.1. Material

2.1.1. Cell culture

The C3A cell line (CRL-10741) was obtained from American Type Culture Collection, Manassas, VA, USA. Minimal essential medium Eagle (MEME), Hank's balanced salt saline (HBSS), phosphate-buffered saline (PBS), sodium pyruvate, penicillin/streptomycin solution, trypsin, fetal bovine serum (FBS) were purchased from Sigma, Poole, UK. 75cm^2, 25cm^2 flasks and 6-well plates were resourced from Corning, NY, USA.

2.1.2. Other chemicals

Bovine serum albumin powder (BSA), insulin, sodium azide, 4% paraformaldehyde, 2,4-dinitrophenol (DNP), oligomycin, N-acetylcysteine, dimethyl sulphoxide (DMSO), NAD^+, glycine, hydrate hydrazine, β-hydroxybutyrate dehydrogenase, NADH, and metformin (Sigma Aldrich, Poole, UK); ProLong® gold antifade reagent (Invitrogen, NY, USA); lactate dehydrogenase (LDH) and triglyceride assays (Alpha Laboratories, Eastleigh, Hampshire, UK); BCA protein assay reagent (Pierce Biotechnology, Rockford, IL, USA).

2.2. General methods

2.2.1. Cell culture and maintenance

C3A cells were cultured in 75 cm^2 tissue culture flasks in minimal essential medium Eagle (MEME) with 10% fetal calf serum (FCS) and antibiotics (100IU/ml penicillin, 100mg/ml streptomycin) at 37°C and 5% CO_2 until 70% confluent. The medium was changed every 48 hour after the initial plating. Cells were passaged every 7-10 days.

2.2.2. Cell culture preparation for experimentation

When C3A cells reached 70% confluence, culture medium was aspirated and the attached cells were washed twice with HBSS. Cells were then incubated for 10 minutes at 37°C with 5ml trypsin/EDTA. After 10 minutes, 5ml MEME with FCS was added to each flask and the contents were centrifuged (600 rpm for 2 minutes). The supernatant was discarded, resuspended in MEME with FCS and cells were aliquoted to experimental plates.

2.2.3. Treatment with energy substrates

MEME with FBS in the experimental plates was supplemented with combinations of octanoate (O) (2mM) or oleic acid (Ol) (0.25mM) (complexed with bovine serum albumin (BSA)), lactate (L) (10mM), pyruvate (P) (1mM), with or without ammonia (N) (4mM). Cells were cultured in the supplemented media for 72 hours (unless specified) prior to experimentation. Unless stated otherwise, cells were cultured in triplicates.

2.2.4. Supernatant and cell collection

Supernatant from each treatment group was aspirated, aliquoted into 750µl tubes and kept on ice for immediate analyses. Cell monolayer was rinsed twice with 2ml of PBS (with added calcium chloride and magnesium chloride). Further PBS (500µl) was added to each well and cells were then gently harvested mechanically using a soft spatula. The pellets were kept frozen at -80°C.

2.2.5. Total protein assay

Cell pellets were thawed, lysed by sonication (three pulses of 10 seconds using a Soniprep 150 Sonicator, Wolf Laboratories Ltd., York, UK). Protein measurements were determined using the standard BCA Protein Assay. Briefly, BCA working reagent was prepared as specified by the manufacturer. An aliquot of 10µl from the sample were placed in 96-well plate. The reagent (20µl) was added to each sample. After a 30 minute incubation at 37°C, readings were made on a spectrophotometer set to an absorbance of 562nm. Protein concentrations were obtained from standard curves prepared as specified by the manufacturer.

2.2.6. Cell viability

Cell viability was assessed as the percentage retention of lactate dehydrogenase (LDH) in the cell monolayer as originally described by Gay *et al.* (117). Briefly, intracellular and extracellular LDH activities of the cell lysates and culture medium respectively, were determined by the rate of NAD^+ reduction to NADH. This reaction corresponds to a decrease in absorbance at 340nm, which in turn, is directly proportional to LDH activity. LDH was detected using a commercial LDH assay (Alpha Laboratories,

Hampshire, UK) modified for use on the Cobas-Fara centrifugal analyser (Roche Diagnostics Ltd., Welwyn Garden City, UK). The results were expressed as % LDH activity retained, calculated from: intracellular LDH activity/(extracellular LDH activity + intracellular LDH activity) x 100.

2.3. Statistical analyses

Statistical analyses were performed using GraphPad Prism® (GraphPad Software, CA, USA). Results are expressed as mean ± standard error of the mean (SEM) except for data obtained from metabolomics profiling, which are presented as mean ± standard deviation (SD). Unless stated otherwise, differences between groups were compared with one-way ANOVA with Newman-Keuls multiple comparison analysis to determine the strength of statistical significance between groups.

3. CHAPTER THREE

INDUCTION OF CELLULAR STEATOSIS *IN VITRO*

3.1. Introduction

Triglyceride accumulation is the hallmark of NAFLD. Triacylglycerol or triglyceride is a major neutral lipid, which comprises three fatty acids attached by ester bonds to a glycerol backbone. Stored within the lipid droplets in cytoplasm, triglyceride is an efficient fatty acid storage molecule, not only crucial for energy homeostasis but is also vital for maintaining cell membrane composition and lipoprotein secretion. Lipid droplets are highly dynamic, which in response to the appropriate signals, can be esterified, hydrolyzed or reesterified to meet cellular demand (118). Importantly, triglyceride is fundamental in protecting cells against the deleterious effects of free fatty acids (108).

The association between triglyceride accumulation and deranged metabolic states is well established. However, the relationship is complex. In essence, it is unclear whether triglyceride accumulation is the cause or simply a marker of the deranged metabolic milieu.

The presence of intracellular triglyceride accumulation is a cardinal feature of any *in vitro* model aiming to dissect the pathogenesis of NAFLD. We chose a long chain fatty acid,

oleate, or a medium chain fatty acid, octanoate, to induce triglyceride accumulation in C3A cells. Additionally, lactate and pyruvate were added to octanoate to synergistically promote significant intracellular lipid accumulation through *de novo* lipogenesis.

The aims of this chapter are:

1. To confirm that the energy substrates would induce intracellular lipid accumulation *in vitro*.
2. To quantify and examine the pattern of triglyceride accumulation induced by the specified combination of energy substrates.

3.2. Methods

3.2.1. Oil red O staining

Cells were plated on chamber slides and treated for 72 hours. Treated cells were fixed with 10% formaldehyde at room temperature for 10 minutes and washed in 60% isopropanol for 30 seconds. Oil red O staining was conducted by Mr. Robert Morris, Queens Medical Research Institute, using method previously described by Green and Kehinde (119). Briefly, Oil red O (0.2g) was dissolved in 200ml of isopropanol. The solution was warmed to 56°C for at least one hour and then cooled at room temperature. Working solution was prepared immediately before use by adding 4 parts of distilled water to 6 parts stock solution. This solution was then vortexed and left for 10 minutes before filtering it through a fine filter paper (No. 42 Whatman). Slides were stained with Oil red O for 10 minutes and washed in 60% isopropanol for 5 seconds. Mayer's haematoxylin solution (1 ml) was added. After 30 seconds, slides were rinsed with distilled water, counterstained with sodium phosphate for 5 minutes and air-dried before being mounted using a water-based preservative. Slides were viewed using Olympus BH-2 light microscope (Olympus America Inc., NY, USA), and digital images were captured using attached camera (Leica, Solms, Germany) at the magnification of 10, 20 and 40x.

3.2.2. BODIPY 493/503 staining

BODIPY® 493/503 (4,4-difluoro-3a, 4a- diaza-s-indacene) (Invitrogen, NY, USA) is a non-polar, lipophilic fluorescent dye that stains neutral lipid intense green. Cells were treated on chamber slides for 72 hours and fixed with 4% paraformaldehyde for 30 minutes before staining with 200µl of BODIPY 493/503 for 10 minutes. Diamidino

phenylindole (DAPI) was used to stain the nuclei where appropriate. Cells were mounted in coverslips using ProLong® gold antifade reagent and were left for 24 hours at 4°C before viewed using confocal laser microscope (LSM510; Carl Zeiss MicroImaging, Inc., Cambridge, UK). Fluorescent intensity from at least 50 cells per image was analyzed using ImageJ software (National Institutes of Health, Bethesda, MD, USA). To determine the number of lipid droplets, the stack of 3D BODIPY confocal images were analysed using Volocity 3D image analysis software (Perkin Elmer, Waltham, MA, USA).

3.2.3. Triglyceride concentration

Oil red O and BODIPY 493/503 stainings are useful to demonstrate neutral lipids within cells but they are not without pitfalls. Variations in the dye penetration can affect the intensity of the staining and sampling bias during image acquisition can often occur. These factors render them relatively inaccurate for quantitative analyses. Thus, if possible, they should be complemented with direct measurements of cellular triglyceride levels.

To determine triglyceride concentrations, cells were treated with the specified combination of energy substrates in 6-well plates (in triplicates) for 24, 72 and 120 hours. Cell pellets were prepared as described in section 2.2.4. Cells were then thawed and lysed by sonication (three pulses of 10 seconds) (Soniprep 150 Sonicator, Wolf Laboratories Ltd., York, UK).

Intracellular triglyceride concentrations were measured using a commercial kit adapted

for the Cobas-Fara centrifugal analyzer (Roche Diagnostics Ltd., Welwyn Garden City, UK). The assay was based on the following reactions:

- Triglycerides hydrolysis by lipoprotein lipase results in the formation of glycerol and fatty acids.
- Glycerol kinase phosphorylates glycerol to form glycerol 3-phosphate (in the presence of ATP).
- Glycerol 3-phosphate is subsequently oxidised by glycerol-3-phosphate oxidase to produce dihydroxyacetone phosphate and hydrogen peroxide.
- The enzyme peroxidase catalyses the reactions between hydrogen peroxide, 4-aminoantipyrine and 3,5-dichloro-2-hydroxybenzene sulfonate resulting in the formation of a red compound, the intensity of which is proportional to the concentration of triglyceride.

Cell pellets were microcentrifuged at 11,000*g* for 10 minutes prior to the triglyceride measurement. Precinorm® U was used for quality control. The reagent (300µl) and the sample (3µl) were incubated at 37°C for 5 minutes before spectrophotometer analysis (500nm). Triglyceride concentration is normalized to the total protein and expressed as µg per gram of total protein.

3.2.4. Electron microscopy

Cells were centrifuged to form pellets in the fixative (3% glutaraldehyde in 0.1M sodium cacodylate buffer, pH 7.3) then washed in three 10-minute changes of 0.1M sodium cacodylate. Specimens were then post-fixed in 1% osmium tetroxide in 0.1M sodium cacodylate for 45 minutes, and washed in three 10-minute changes of 0.1M sodium cacodylate buffer. Samples were dehydrated in 50%, 70%, 90% and 100% normal grade

acetones for 10 minutes each, then for a further two 10-minute changes in analar acetone. Samples were embedded in Araldite resin. Sections, 1μm thick, were cut on a Reichert OMU4 ultramicrotome (Leica Microsystems Ltd., Milton Keynes, UK), stained with toluidine Blue and viewed in a light microscope. Ultrathin sections of 60nm were cut from selected areas, stained in uranyl acetate and lead citrate before viewed in Phillips CM120 Transmission electron microscope (FEI UK Ltd., Cambridge, UK). Images were taken using Gatan Orius CCD camera (Gatan UK, Oxford, UK).

3.3. Results

3.3.1. Lipid droplets are visible under electron microscopy

First, we confirmed the presence of lipid droplets in cells treated for 72 hours using the electron microscopy. Figure 3.3.1.1 (Panel A-D) are representative images from electron microscopy demonstrating the presence of intracellular lipid vacuoles in all treatment groups. Lipid droplets were present in the cytoplasm juxtaposed among the mitochondria (Figure 3.3.1.1).

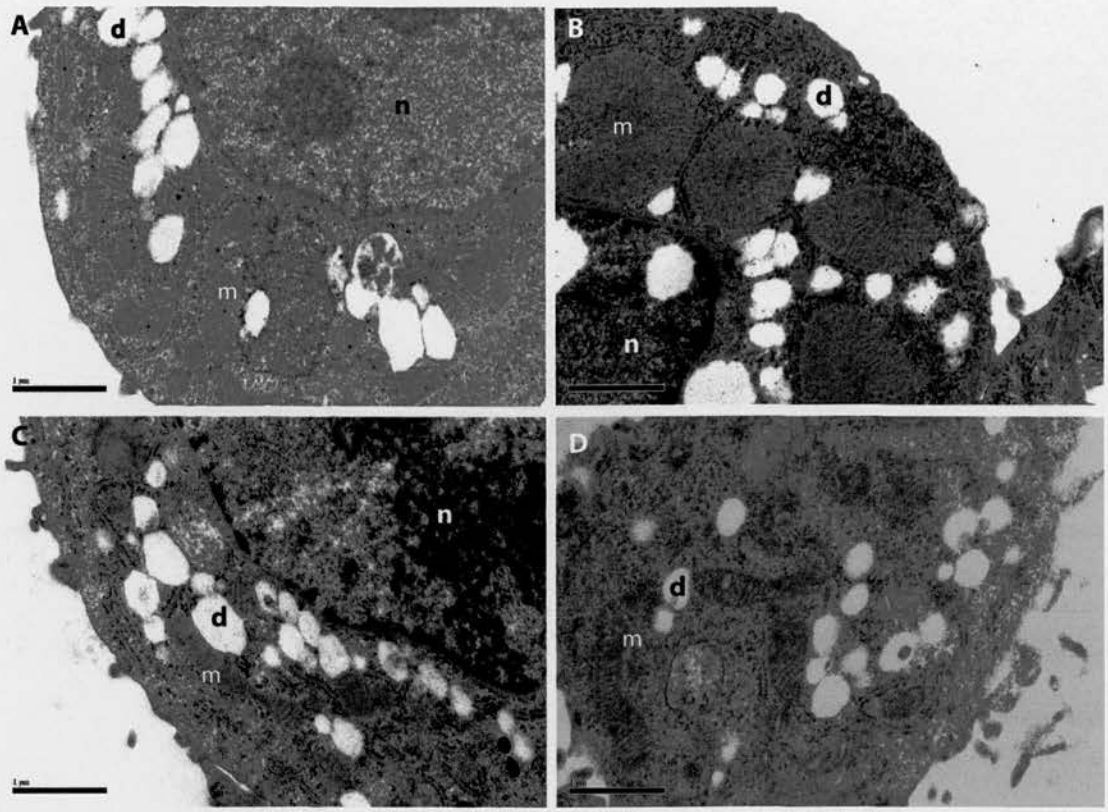

Figure 3.3.1.1. Lipid droplets in treated cells viewed under electron microscopy.

A, Untreated; B, Octanoate; C, LPON and D, Oleate treated cells. Cells were treated for 72 hours and centrifuged to form pellets described in section 3.2.4 for electron microscopy. d, droplets; m, mitochondria, n, nucleus (scale bar represents 1μm, magnification x4800).

3.3.2. Oil red O and BODIPY 493/503 confirm the presence of triglyceride

Oil red O staining (Figure 3.3.2.1) and BODIPY 493/503 staining (Figure 3.3.2.2 and 3.3.2.3) confirmed the presence of triglyceride. As demonstrated in Figure 3.3.2.1, lipid droplets were stained red with Oil red O. Similarly, Figure 3.3.2.2 Panel A and B are representative images of treated C3A cells stained with BODIPY 493/503. BODIPY 493/503 stained lipid droplets fluorescent green whilst DAPI blue fluorescent staining highlighted the nuclei. Panel C demonstrates the number of lipid droplets accumulated after 24 hours of treatment with specified energy substrates.

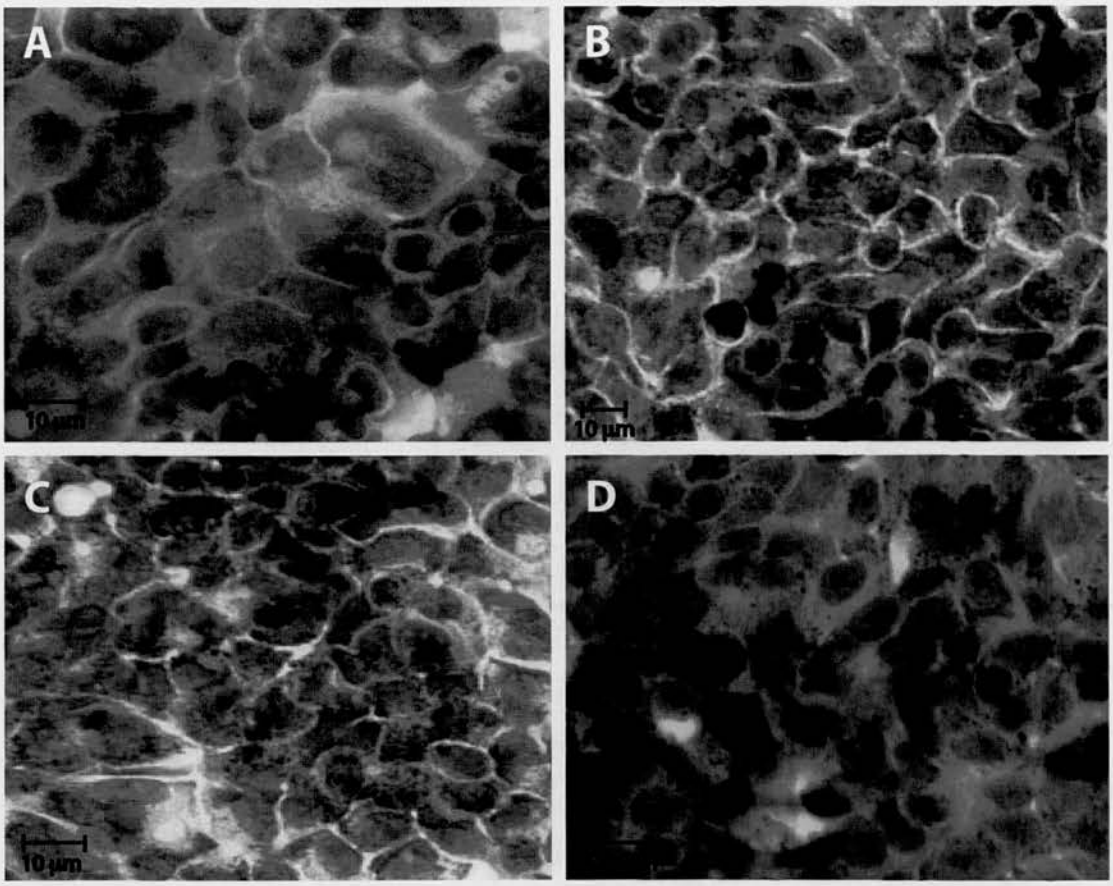

Figure 3.3.2.1. Oil red O staining in treated C3A cells.

Cells were grown and treated in two chamber slides. After a 72-hour treatment, cells were fixed and Oil red O staining was performed as described in section 3.2.1. The area with triglyceride accumulation was stained bright red. Images were viewed under light microscopy (magnification x40). A, Untreated; B, Oleate; C, Octanoate; D, LPON.

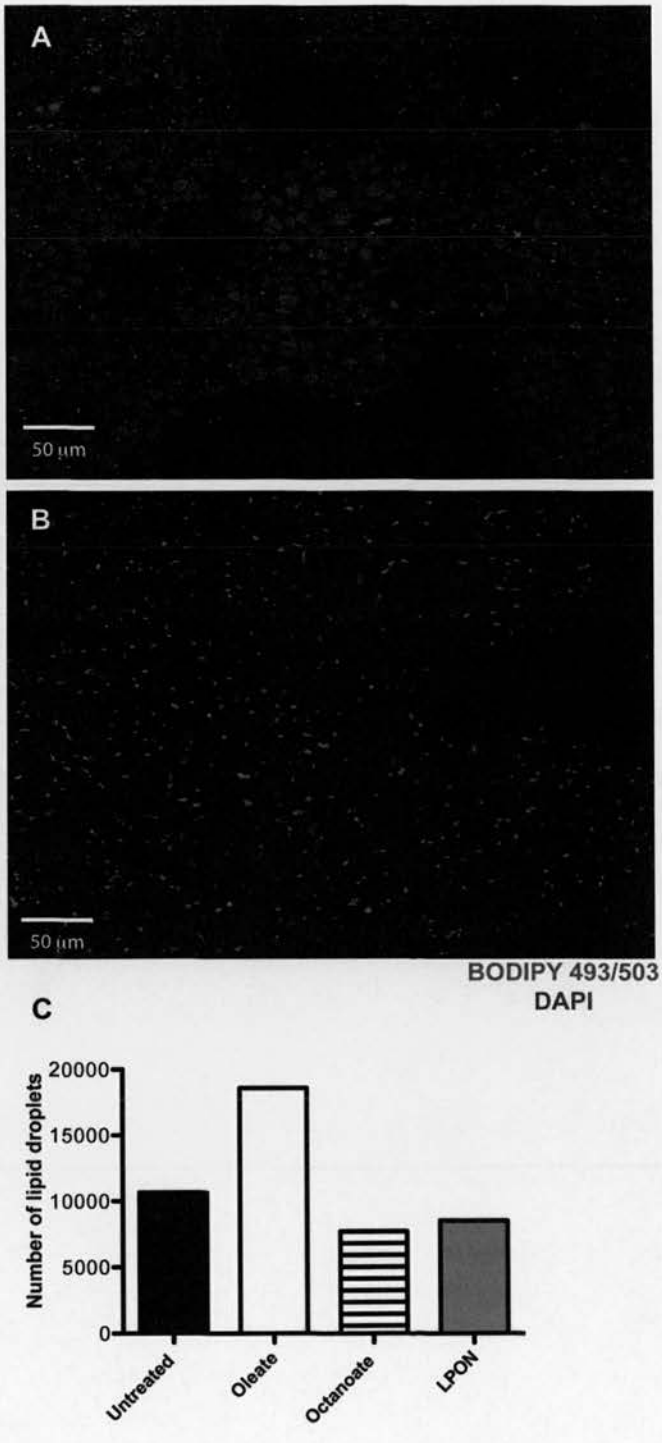

Figure 3.3.2.2. BODIPY 493/503 staining in treated C3A cells.

Cells were treated in two-chamber slides for 24 hours before BODIPY 493/503 and DAPI staining (described in section 3.2.2). A, LPON; B, Oleate; C, The number of lipid droplets accumulated after a 24-hour treatment with specified energy substrates quantified by 3D image processing software, Volocity.

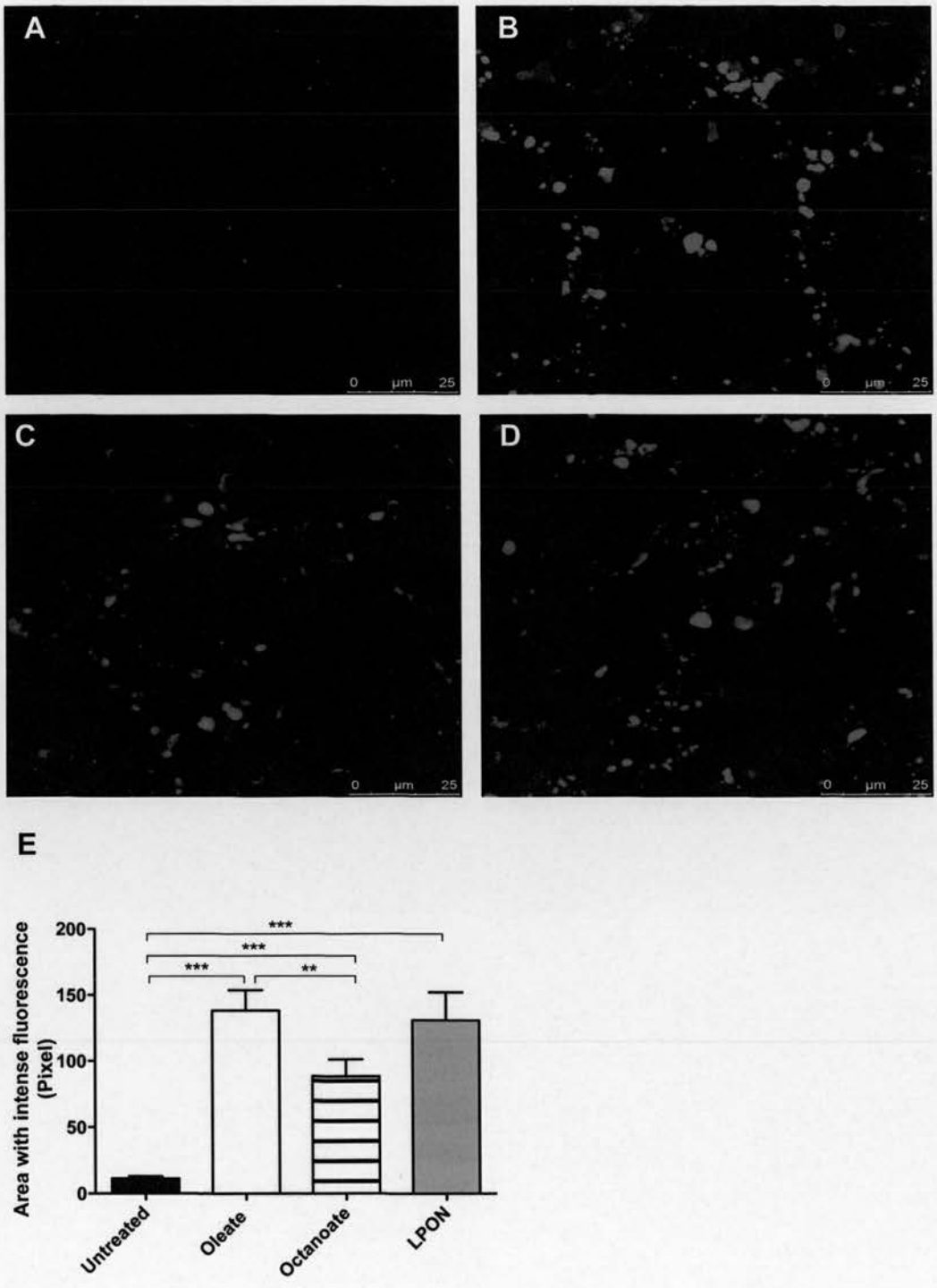

Figure 3.3.2.3. BODIPY 493/503 staining in treated C3A cells.

Cells were treated in two-chamber slides for 72 hours before BODIPY 493/503 staining (described in section 3.2.2). A, Untreated; B, LPON; C, Octanoate; D, Oleate; E, Area with intense fluorescence from BODIPY staining quantified using ImageJ. Data are presented as mean ± SEM; $P<0.0001$; *** $P<0.001$, ** $P<0.01$.

3.3.3. Triglyceride concentration in treated cells

Next, we quantified and examined the pattern of intracellular lipid accumulation. Cells were treated with specified combinations of energy substrates over 24, 72 and 120 hours. Intracellular triglyceride concentrations were measured at each time point. With the exception of ammonia, all groups showed significantly higher lipid accumulation than the untreated cells at 72 and 120 hours (Figure 3.3.3). However, the pattern of accumulation differed over time, notably, the contrasting pattern of triglyceride accumulation between oleate and octanoate. Oleate induced higher triglyceride concentrations in the first 24 hours but this subsequently plateaued. In contrast, triglyceride concentration with octanoate increased with time potentially reflecting *de novo* lipogenesis from acetyl-coA rather than direct esterification. The synergistic effect of lactate, pyruvate and octanoate (LPO) resulted in higher triglyceride accumulation than that seen with either LP ($P<0.001$) or octanoate alone ($P<0.001$). Triglyceride concentrations with LPON after 72 hours were 40% lower than seen with LPO ($P<0.001$) but were similar to that accrued with oleate.

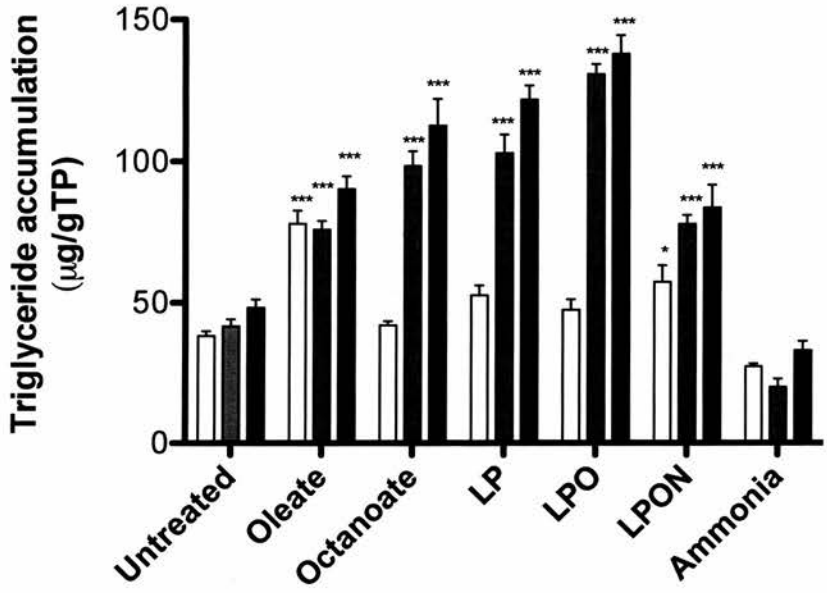

Figure 3.3.3. Triglyceride concentrations in treated C3A cells.

Triglyceride concentrations were measured after a 24, 72 or 120-hour treatment. $P<0.0001$ for interaction between treatment and duration of treatment (determined using two-way ANOVA). $^{***}P<0.001$ and $^{*}P<0.05$ when compared to the untreated cells of the same treatment duration; $n=3$ in triplicates. Data are presented as mean ± SEM.

3.4. Discussion and conclusion

This chapter is focused on confirming the presence of intracellular triglyceride accumulation, an important prerequisite for an *in vitro* model designed to dissect the pathophysiology of NAFLD.

The main findings from this chapter are:

1. The combination of energy substrates, LPON, induced significant triglyceride accumulation *in vitro.*
2. The addition of lactate and pyruvate synergized with octanoate to promote significant triglyceride accumulation.

These findings highlight two main observations. First, the pattern of lipid accumulation differs between oleate and octanoate. Oleate led to a dramatic rise in triglyceride accumulation within 24 hours, but plateaued thereafter consistent with direct esterification that parallels its concentration (120). In contrast, the incorporation of octanoate into triglyceride followed a steady time-dependent course, which reflects *de novo* lipogenesis from the acetyl-coA. This disparity stems from their differences in β-oxidation. The recurring sequence of efficient β-oxidation with octanoate accelerates the formation of acetyl-coA, which serves as the foundation for fatty acid synthesis (101) (Figure 3.4.1).

Acetyl-coA is the crossroad between glucose and lipid metabolism. The conversion of pyruvate, the end product of glycolysis, into acetyl-coA is a crucial step in partitioning

excess carbohydrate into fat for storage. Indeed, the synergistic effect of lactate, pyruvate and octanoate in promoting a time-dependent rise in triglyceride most likely through *de novo* lipogenesis highlights the importance of carbohydrate, for instance, in hyperglycaemic conditions, in the formation of hepatic steatosis. Interestingly, we have demonstrated that triglyceride concentration decreased with ammonia. The mechanism involved is yet to be delineated. In astrocytes, ammonia has been demonstrated to accrue diacylglycerol, instead of triacylglycerol (121).

Second, the co-localization between lipid droplets and mitochondria supports the contention that dynamic metabolic and physical interactions exist between these organelles. This has been previously observed in adipocytes and skeletal muscle, and is thought to promote efficient FFA delivery for ATP formation.

In conclusion, LPON induces a significant triglyceride accumulation fundamental for an *in vitro* model of cellular steatosis.

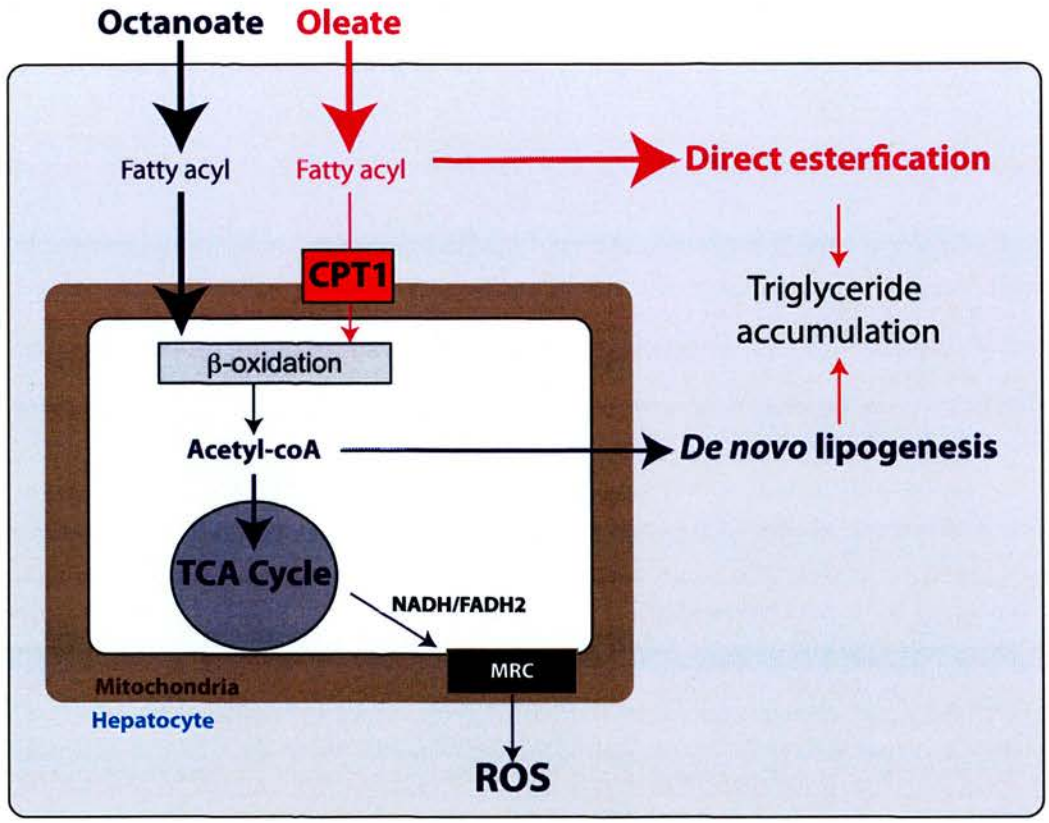

Figure 3.4.1. The patterns of lipid accumulation in cells treated with oleate or octanoate.

Both oleate and octanoate can lead to a significant triglyceride accumulation. However, triglyceride accumulation with octanoate follows a steady time-dependent course through *de novo* lipogenesis whilst oleate is directly esterified. The differences reflect the variation in β-oxidation. Octanoate has an efficient β-oxidation resulting in acetyl-coA formation, which can be diverted towards the *de novo* lipogenesis. In contrast, the entry of oleate into the mitochondria hence its β-oxidation is regulated by CPT1. MRC, mitochondrial respiratory chain; CPT1, carnitine palmitoyl transferase 1; ROS, reactive oxygen species.

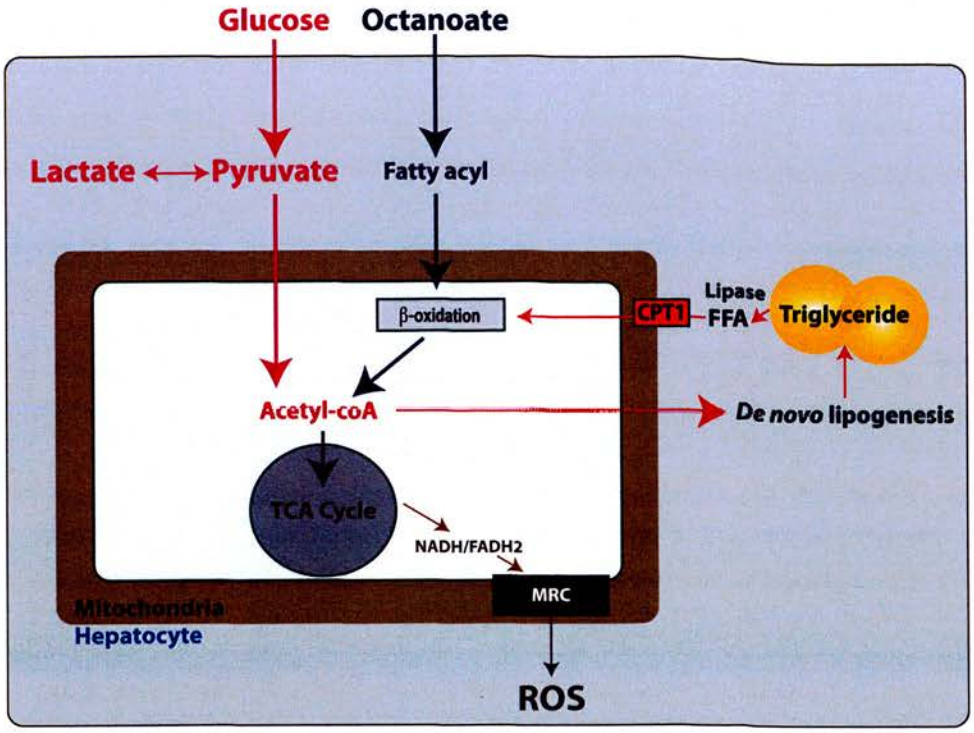

Figure 3.4.2. Lactate, pyruvate and octanoate synergize to promote *de novo* lipogenesis.

The synergistic effect of pyruvate and octanoate leads to enhanced acetyl-coA formation. Acetyl-coA can be diverted towards the *de novo* lipogenesis. The close proximity between mitochondria and lipid droplets allows FFA released from triglyceride hydrolysis to enter mitochondria for β-oxidation. FFA, free fatty acids; MRC, mitochondrial respiratory chain; CPT1, carnitine palmitoyl transferase 1; ROS, reactive oxygen species.

4. CHAPTER FOUR

LPON ENHANCES ACUTE RESPIRATION AND REACTIVE OXYGEN SPECIES FORMATION

4.1. Introduction

Central to the development of dietary-induced NAFLD is enhanced energy substrate availability to the hepatocytes. This is often compounded by increased free fatty acids in tandem with hyperglycemia that characterizes insulin resistance. The surge in energy substrates can culminate in the overproduction of electron donors $NADH/FADH_2$, thus enhancing mitochondrial respiration and the formation of its byproduct, superoxide.

Our aim was to recapitulate this sequence of events *in vitro* using C3A cells treated with a combination of energy substrates, lactate, pyruvate, octanoate and ammonia (LPON). We postulated that LPON could swiftly maximize the TCA cycle turnover and enhance the formation of reducing equivalents ($NADH/FADH_2$) with resultant rise in mitochondrial respiration and superoxide formation.

Having shown that LPON induced triglyceride accumulation, in this chapter, we examine the impact of LPON on acute mitochondrial respiration and ROS formation.

The aims of this chapter are:

1. To determine whether the combination of energy substrates lactate, pyruvate, octanoate and ammonia would acutely increase cell respiration.
2. To examine whether the potential rise in respiration with LPON would enhance superoxide formation.
3. To determine the impact of LPON on cell viability.

4.2. Methods

4.2.1. Mitochondrial respiration

C3A cells were grown in 25cm^2 flasks until 70% confluent. Naïve cells were rinsed with HBSS (10ml) before trypsinization (trypsin (5ml) with EDTA) for 5 minutes. Trypsinized cells were centrifuged for 2 minutes and resuspended in MEME (with FBS) (2ml). Cells were subsequently counted to obtain 0.5x10^6 cells in single suspension, which were then added to each well of the BD™ Oxygen Biosensor 96-well plate (BD Biosciences, CA, USA) containing the specified media; oleate or octanoate with/without the combination of lactate and pyruvate with/without ammonia. The BD™ Oxygen Biosensor System is a 96-well plate-based sensor containing a ruthenium based-dye incorporated into the silicon rubber matrix. The matrix and the dye are impermeable to liquid but are freely permeable to oxygen. The fluorescent change with oxygen consumed during respiration allows the determination of respiration rate. The fluorescent plates were read in CytoFluor Reader Series 4000 (Applied Biosystems, NY, USA) for 40 cycles, for 40 minutes. The respiration rates were measured from the linear portion of the slope of fluorescence rise. Data are presented as fold of change from the untreated cells.

4.2.2. Mitochondrial superoxide formation

Mitochondrial superoxide is generated within the mitochondria from the reduction of O_2 by an electron during oxidative phosphorylation. Mitochondrial superoxide production was measured using the live-cell permeable fluorescent probe MitoSOX™ (Invitrogen, NY, USA). Once in the mitochondria, MitoSOX™ is oxidized by

superoxide and exhibits red fluorescence. Briefly, MitoSOX™ stock solution was prepared according to protocol specified by the manufacturer. For fluorescent microscopy, naïve C3A cells grown in two-chamber slides were incubated with MitoSOX™ for 60 minutes at 37°C. The supernatant was then removed and cells were rinsed, before the addition of 500µl of HBSS with or without specified combination of the energy substrates into each chamber. The slides were kept at 37°C and viewed under fluorescent microscopy. Images of phase contrast and fluorescent field were obtained using fluorescent microscopy (LSM510; Carl Zeiss MicroImaging, Inc., Cambridge, UK). These images were then merged using image editor software, Photoshop CS4, (Adobe Systems Incorporated, San Jose, CA, USA). Fluorescence intensity from each image was analysed using ImageJ (National Institute of Health, Bethesda, MD, USA).

4.2.3. Cell viability

Cell viability was assessed as the percentage retention of lactate dehydrogenase (LDH) as previously described in the section 2.1.6.

4.3. Results

4.3.1. Acute LPON treatment enhances respiration in C3A cells

We postulated that the combination of lactate, pyruvate, and ammonia would act synergistically with octanoate to enhance mitochondrial respiration thus increasing superoxide formation in a mechanism akin to that proposed in human NAFLD. To test this hypothesis, treatment media were added to naïve C3A cells before the measurements of cell respiration. As shown in Figure 4.3.1, LPO resulted in a 2.5-fold rise in respiration whereas LPON resulted in a 3-fold increment when compared with the untreated groups.

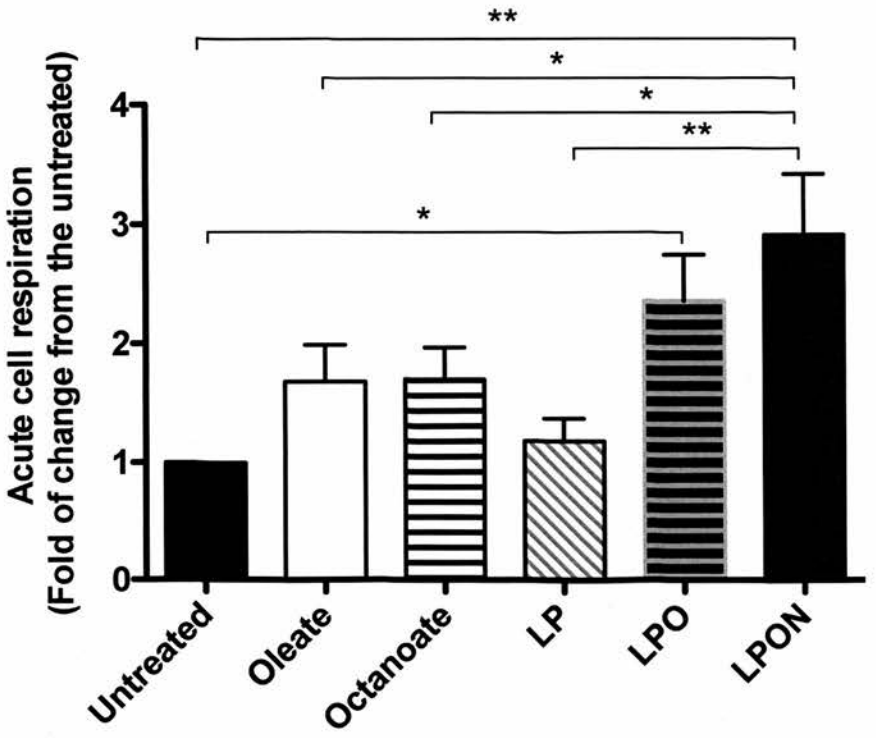

Figure 4.3.1. Acute respiration in C3A cells exposed to the specified energy substrates.

Naïve C3A cells in single suspension were used for each well of the BD™ Biosensor fluorescent plate containing one of the following media: HBSS with oleate (0.25mM) or specified combinations of lactate (L) (10mM), pyruvate (P) (1mM), octanoate (O) (2mM) and ammonia (N) (4mM). Cell respiration was calculated from the slope of the linear section of the curve representing the fluorescence rise. Data are presented as mean ± SEM; P=0.0008; $^{**}P<0.01$, $^{*}P<0.05$.

4.3.2. Mitochondrial superoxide formation

4.3.2.1. MitoSOX™ as an indicator of superoxide formation

Next, we investigated whether the acute rise in respiration with LPON is paralleled by enhanced ROS formation. The formation of mitochondrial superoxide, the progenitor of ROS, is examined using MitoSOX™ as described in section 4.2.2. MitoSOX™ emits red fluorescence when oxidized by superoxide. Panel A of Figure 4.3.2.1 is a representative image of mitochondrial superoxide fluoresced bright red in the naïve cells after a 60-minute labeling with MitoSOX™. Panel B shows the corresponding phase contrast image (Panel C). These images were merged to juxtapose superoxide with the cells (Panel D).

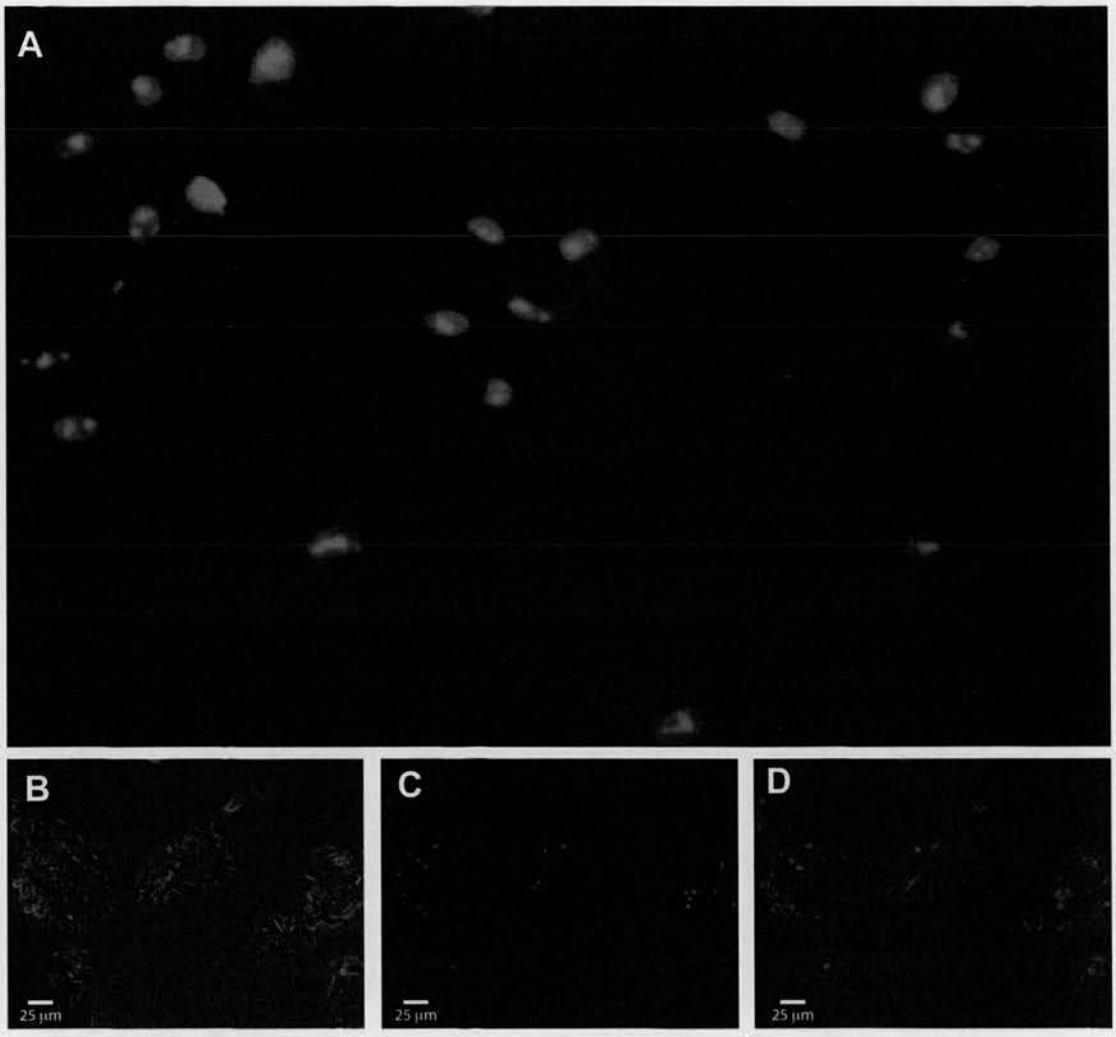

Figure 4.3.2.1. Mitochondrial superoxide fluoresces red with MitoSOX™ staining.

Naïve C3A cells grown in two-chamber slides were incubated with MitoSOX™ for 60 minutes at 37°C. The slides were viewed under fluorescent microscopy. A, Representative image of naïve cells incubated with MitoSOX™ emitting bright red fluorescence indicating the presence of superoxide; B, Phase contrast image; C, Fluorescent image; D, Phase contrast and fluorescent images merged (magnification x40).

4.3.2.2. Enhanced mitochondrial superoxide formation with LPON

To determine the effect of LPON on ROS formation, naïve C3A cells grown in two-chamber slides were incubated with MitoSOX™ for either 45 or 60 minutes at 37°C. The supernatant was then removed and cells were rinsed, before the addition of 500µl of HBSS with or without LPON into each chamber. Additionally, HBSS with DNP (250µM) (negative control) or HBSS with oligomycin (5 µg/ml) (positive control) were added to separate group of cells.

Oligomycin is an ATP synthase inhibitor and acts by blocking the passage of protons through the mitochondrial ATP synthase. This results in an increase in mitochondrial membrane potential ($\Delta\Psi_m$). As discussed in section 1.4.3, proton extrusion and forward electron transfer are inhibited with a significant rise in $\Delta\Psi_m$. Under these circumstances, NADH oxidation is impaired leading to a rise in NADH concentration thus promoting electron leaks and superoxide formation (122). Furthermore, reverse electron transport (RET) can occur, which can potentially enhance superoxide formation.

Conversely, a reduction in $\Delta\Psi_m$ decreases superoxide production (123). Uncoupler such as 2,4-dinitrophenol (DNP) can render the inner membrane permeable to protons, thereby lowering the $\Delta\Psi_m$. Even at low concentrations, these uncouplers have been shown to considerably reduce the rate of mitochondrial superoxide production (123).

Figure 4.3.2.2 and 4.3.2.3 are representative images of mitochondrial superoxide formation after a 45- and 60-minute labeling with MitoSOX™ respectively. The addition of LPON (Panel B) to the naïve C3A cells visibly resulted in higher mitochondrial superoxide formation than the untreated cells (Panel A). The quantification of the

fluorescent area using ImageJ confirmed these findings (Panel E). The rise in mitochondrial superoxide formation with LPON was comparable to that seen with oligomycin. Indeed, LPON resulted in a higher superoxide formation than oligomycin when labeled with MitoSOX™ for 60 minutes. In contrast, mitochondrial superoxide formation with DNP was similar to the untreated cells and was considerably lower than that seen with LPON or oligomycin.

4.3.3. Cell viability is unaltered with LPON

We determined cell viability by measuring the LDH retention in cells that have been treated with LPON for 72 hours as described in section 2.1.6. LPON did not alter cell viability (LPON 97.9 ± 0.33, oleate 98.2 ± 0.32, untreated 98.3 ± 0.39 % LDH activity retained; P=0.63).

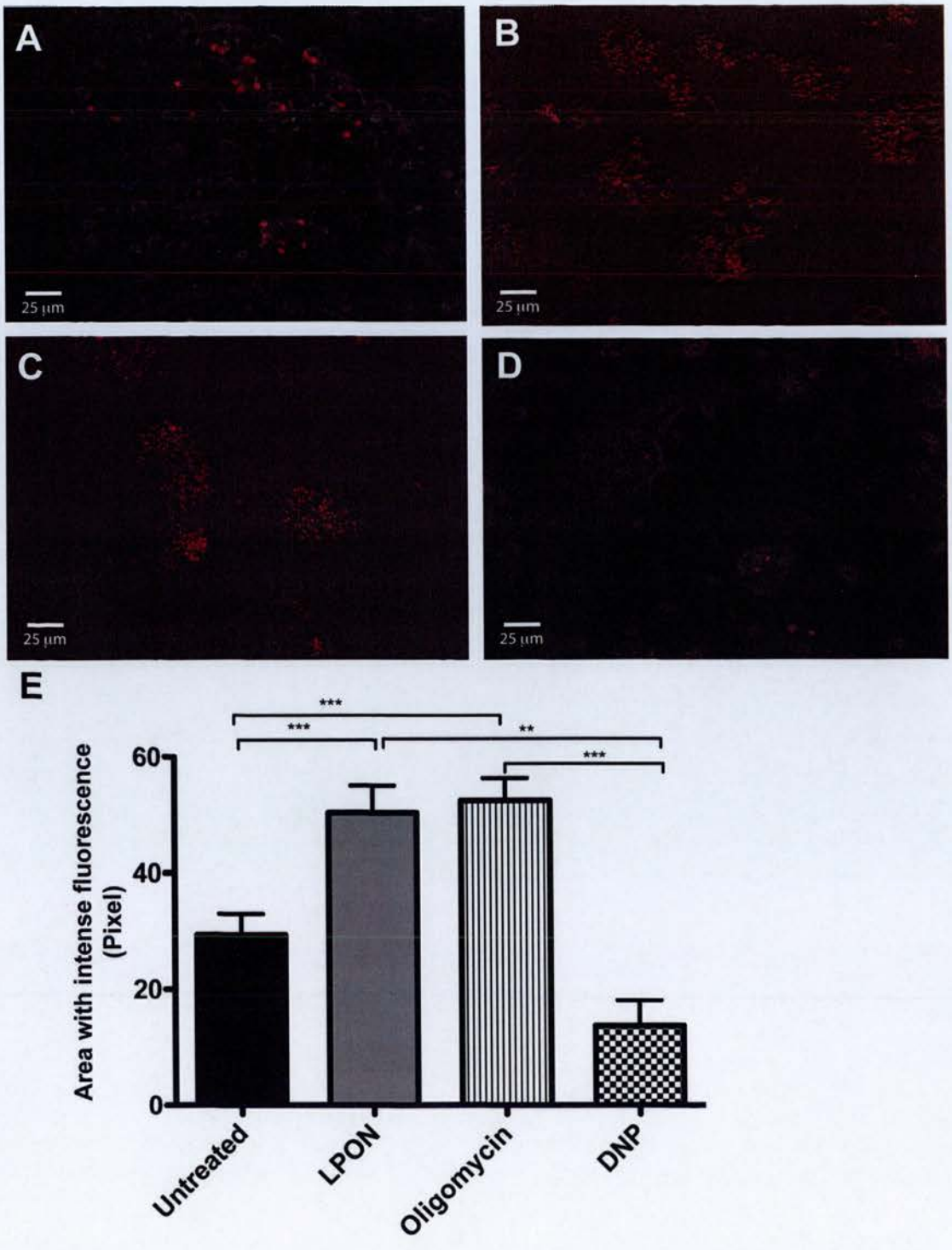

Figure 4.3.2.2. Mitochondrial superoxide formation after a 45-minute labeling with MitoSOX™.

A, Untreated; B, LPON; C, Oligomycin; D, DNP; E, Area with intense fluorescence quantified using ImageJ. Naïve C3A cells grown in two-chamber slides. Confluent cells were then incubated with MitoSOX™ for 45 minutes at 37°C. Cells were rinsed before being treated with 500µl of HBSS with or without LPON into each chamber. Additionally, HBSS with DNP (250µM) or HBSS with oligomycin (5µg/ml) were added to separate group of cells. Oligomycin hyperpolarizes mitochondria thus increasing the leakage of electrons enhancing superoxide formation. In contrast, 2,4-dinitrophenol (DNP) lowers the $\Delta\Psi_m$, hence diminishing the rate of superoxide production by mitochondria. Panel A-D are fluorescent images viewed under fluorescent microscopy and E, fluorescent area quantified using ImageJ. Data are presented as mean ± SEM; $P<0.0001$; $^{***}P<0.001$, $^{**}P<0.01$.

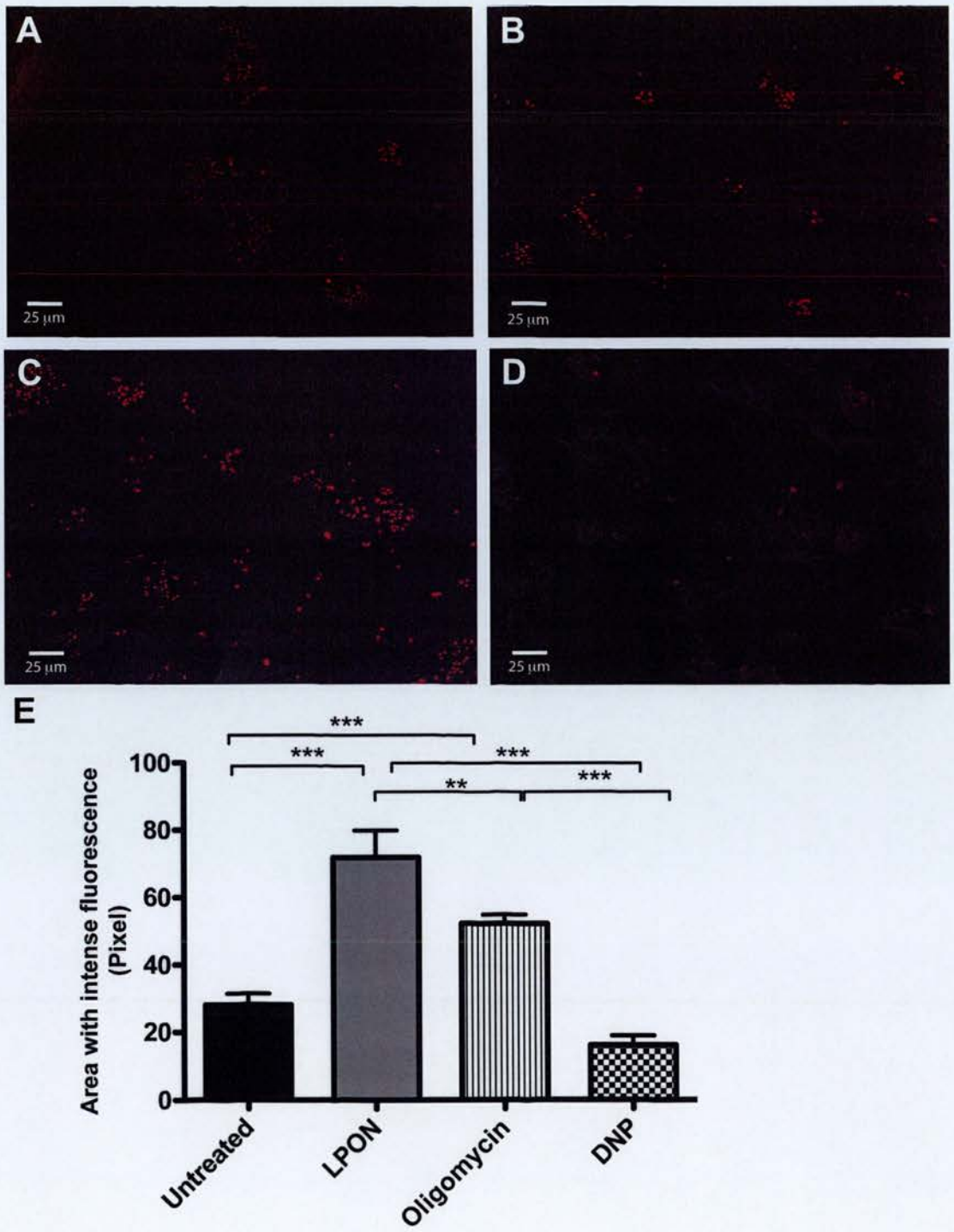

Figure 4.3.2.3. Mitochondrial superoxide formation after a 60-minute labeling with MitoSOX™.

A, Untreated; B, LPON; C, Oligomycin; D, DNP; E, Area with intense fluorescence quantified using ImageJ. Naïve C3A cells grown in two-chamber slides. Confluent cells were then incubated with MitoSOX™ for 60 minutes at 37°C as described previously. Cells were rinsed before being treated with 500µl of HBSS with or without LPON into each chamber. Additionally, HBSS with DNP (250µM) or HBSS with oligomycin (5µg/ml) were added to separate group of cells. Panel A-D are fluorescent images viewed under fluorescent microscopy and E, Fluorescent area quantified using ImageJ. Data are presented as mean ± SEM; $P<0.0001$; $^{***}P<0.001$, $^{**}P<0.01$.

4.4. Discussion and conclusion

Our aim was to design an *in vitro* model of cellular steatosis that would recapitulate the sequence of events proposed to occur in dietary-induced NAFLD. We postulated that the combination of energy substrates, LPON, would fulfill the three prerequisites for such an *in vitro* model; adequate cellular steatosis, exaggerated cell respiration and enhanced superoxide formation. We have confirmed previously that LPON induces significant cellular steatosis. This chapter is focused on whether LPON would augment respiration and increase superoxide formation.

The main findings in this chapter are:

1. LPON acutely increased cell respiration in naïve C3A cells.
2. The rise in acute respiration with LPON was paralleled by an increase in superoxide formation.
3. Despite enhanced superoxide formation, prolonged treatment with LPON did not affect cell viability.

These findings highlight two important points. First, LPON fulfills the three prerequisites of an *in vitro* cellular steatosis model aiming to recapitulate the proposed sequence of events in dietary-induced NAFLD. The sequence is instigated by increased energy substrates, which promotes an extensive triglyceride accumulation in tandem with enhanced acute respiration with a resultant rise in superoxide formation. The focus is then to examine the long-term impact of this chain of events on mitochondrial respiration, superoxide formation and metabolic alterations.

It is salient to note that the effect of LPON on acute respiration reflects the synergistic effect of all its components. Interestingly, despite their differences in β-oxidation, the acute treatment with either oleate or octanoate alone resulted in a similar rise in respiration.

Second, the cellular viability after a 72-hour treatment with LPON remains unaltered. Thus, we propose that LPON is a viable *in vitro* cellular steatosis model to dissect the relationship between cellular steatosis, ROS and mitochondrial function.

5. CHAPTER FIVE

THE CHRONIC EFFECT OF ENERGY SUBSTRATE EXPOSURE ON MITOCHONDRIAL RESPIRATION

5.1. Introduction

There is robust evidence to support mitochondrial impairment and abnormal energy homeostasis in NAFLD (32, 40, 62-64, 124). This evidence has been predominantly inferred from steatohepatitis, thus leaving an uncertainty as to whether similar events can also occur with simple steatosis. Furthermore, it is unclear whether increased hepatic fat content can contribute to the mitochondrial dysfunction. Yet, reduction in hepatic triglyceride accumulation is often construed as a marker of improvement in NAFLD.

Oxidative stress is thought to be the crux of molecular events leading to mitochondrial dysfunction (32, 40, 46, 92). In support of this, intracellular antioxidant, N-acetylcysteine (NAC) has been shown to enhance mitochondrial function in adipocytes, cardiac and skeletal muscle (98-100). Similarly, NAC prevents the development of cirrhosis, ameliorates steatohepatitis and improves insulin resistance in hepatocytes (85, 125, 126). However, the effects of NAC on hepatic mitochondrial respiration particularly in the presence of triglyceride accumulation remain unclear.

We have previously shown that the combination of energy substrates, lactate, pyruvate, octanoate and ammonia (LPON) acutely increased respiration leading to enhanced mitochondrial superoxide formation; a sequence of events akin to that proposed to occur in dietary-induced NAFLD. In this chapter, we examine the effect of chronic LPON exposure on mitochondrial respiration. More important, we address a fundamental question: does steatosis *per se* exert deleterious effects on mitochondrial function?

The aims of this chapter are:

1. To examine the effect of prolonged LPON treatment on mitochondrial respiration
2. To determine the impact of triglyceride *per se* in modulating respiration.
3. To investigate whether a reduction in steatosis would improve mitochondrial function.
4. To examine whether energy substrates would alter mitochondrial structure.

5.2. Methods

5.2.1. Cell respiration in treated cells

Confluent C3A cells grown in 25cm^2 flasks were treated with the specified combination of energy substrates for 72 hours. Cells were rinsed with HBSS, trypsinized and centrifuged for 2 minutes. Cells were resuspended in MEME with FBS (2ml) and counted to obtain 0.5x10^6 cells in single suspension. Cells were added to each well of the BD™ Oxygen Biosensor 96-well plate containing HBSS, HBSS+LPON and HBSS+LPON+DNP (250μM). The fluorescent plate was read using CytoFluor Reader Series 4000 for 40 cycles, for 40 minutes (excitation at 485nm and emission at 590nm). The respiration rates were measured from the linear portion of the slope of fluorescence rise. Data are presented as fold of change from the untreated cells or as arbitrary fluorescent unit (AFU).

5.2.2. The effect of N-acetylcysteine (NAC) on respiration

We examined the effect of NAC (10mM) on triglyceride accumulation and cell respiration in LPON treated cells. C3A cells grown in six-well plates were simultaneously treated with LPON and NAC for 72 hours. Intracellular triglyceride was quantified as described in section 3.2.2 and normalised to the total protein content. Cell respiration was determined as described in section 5.2.1.

5.2.3. The effect of metformin on respiration and triglyceride accumulation

Although metformin has been widely used in the treatment of Type 2 diabetes, its

mechanism of action remains unclear. Recent evidence has suggested that some of its effect may have been mediated by adenosine monophosphate activated protein kinase (AMPK) (127). This mechanism has also been proposed to underlie its lowering of triglyceride in HepG2 cells (128). In this study, we used metformin (50nM-2mM) to induce triglyceride reduction in LPON treated cells. Cells grown in six-well plates were simultaneously treated with LPON and metformin at specified concentrations for 72 hours. Intracellular triglyceride was determined as described in section 3.2.2 and normalised to the total protein content. Cell respiration was determined as described in section 5.2.1. The effect of metformin on cell viability was determined as described in section 2.1.6.

5.2.4. Cytosolic and mitochondrial NADH/NAD^+ ratio

Decreased mitochondrial respiration impairs NADH oxidation to NAD^+. Thus, NADH/NAD^+ ratio is influenced by mitochondrial respiration as well as by the rate of NADH formation. Mitochondrial and cytosolic NADH/NAD^+ ratios were determined from the ratio of β-hydroxybutyrate to acetoacetate and the ratio of lactate to pyruvate respectively. Lactate, pyruvate, β-hydroxybutyrate, and acetoacetate in the culture medium were measured using Bergmeyer's enzymatic methods (129). This method allows immediate measurements at the end of the treatment, as β-hydroxybutyrate, in particular, is an unstable compound. Briefly, acetoacetate concentration is determined from the NADH consumed by β-hydroxybutyrate dehydrogenase in the reaction:

Acetoacetate + NADH → β-hydroxybutyrate +NAD^+

Conversely, β-hydroxybutyrate concentration corresponds to NADH produced. The assays for acetoacetate (1 ml of 0.12mg of NADH for 1ml of PBS (with calcium and

magnesium)) and β-hydroxybutyrate (NAD^+ (50mg), glycine (3g), water (100ml), hydrate hydrazine (2ml) and LDH (100µl)) were added to aliquoted sample (200µl) and homogenized. The baseline NADH was determined using spectrophotometer set at 340nm (the λ_{max} for NADH). β-Hydroxybutyrate dehydrogenase (10µl) was then added to each sample and the second spectrophotometer analysis was performed after 60 minutes.

Similarly, based on the reaction catalyzed by lactate dehydrogenase (LDH):

Lactate + NAD^+ → Pyruvate + NADH + H^+

lactate concentration corresponds to NADH produced whereas pyruvate concentration is proportional to NADH consumed. For lactate measurements, the assay (NAD^+ (50mg), glycine (3g), water (100ml), hydrate hydrazine (2ml) and LDH (100µl)) was added to the sample (10µl). The samples were homogenised and left for 90 minutes at room temperature before spectrophotometer analysis. For pyruvate, the assay ($NADH^+$ 0.12mg for 1ml of PBS) was added to the sample (50µl) and homogenised before the first spectrophotometer analysis. LDH (10µl) was then added to each sample and the second analysis was performed after 15 minutes.

5.2.5. Electron microscopy

To examine whether treatment with energy substrates altered mitochondrial structure, treated cells were prepared for electron microscopy as described in section 3.2.4. Mitochondria from four separate images from different sections were analyzed. The outline of the mitochondria was traced individually to determine the cross-sectional area using ImageJ. The scale was set to µm using the scale bar on the images as reference.

5.3. Results

5.3.1. Basal mitochondrial respiration diminishes with LPON

We have shown that LPON resulted in acute rise in respiration. Here, the chronic impact of LPON on basal respiration was determined. Because LPON resulted in similar triglyceride accumulation but contrasting acute respiration to that seen with oleate, we next focused on the following groups; oleate, LPON and untreated (control). Additionally, lipid accumulation with oleate has been shown previously to have a relatively low ROS formation (85, 107). To examine the effect of ROS on mitochondrial function, cell respiration was also measured in additional cells that were concomitantly treated with LPON and NAC (10mM) for 72 hours. To further confirm the role of ROS, we have included LPON cells treated simultaneously with another antioxidant, α-tocopherol (0.4mM) for the entire treatment period.

Figure 5.3.1 shows that the acute rise in cell respiration observed with LPON was not sustained; respiration with LPON at 72 hours was significantly lower than the untreated cells. Despite the contrasting triglyceride accumulation, basal respiration was similar in the oleate and untreated cells. Furthermore, as demonstrated in Figure 5.3.1, both antioxidants preserved basal respiration in LPON treated cells. Respiration was 62% and 53% higher in LPON cells that were treated simultaneously with NAC and α-tocopherol respectively, when compared to cells treated with LPON alone (Figure 5.3.1).

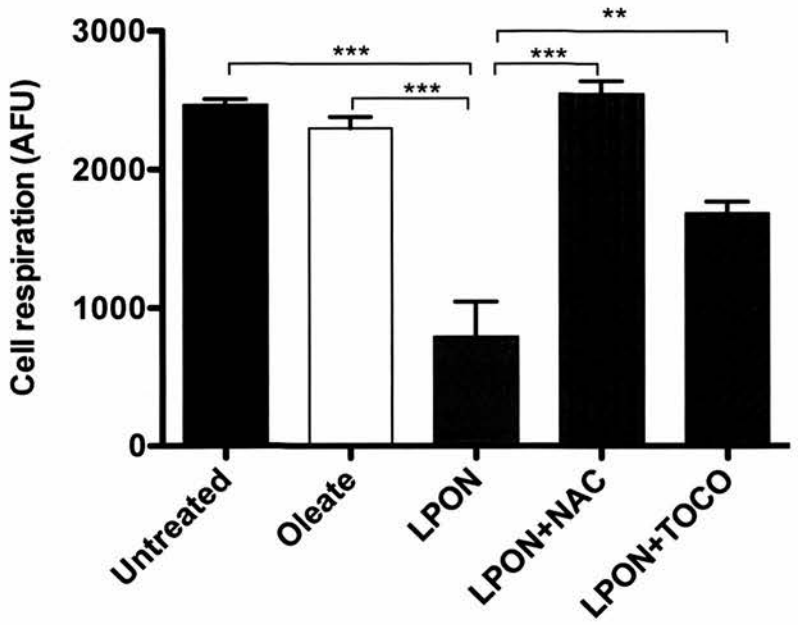

Figure 5.3.1. Basal respiration in cells concomitantly treated with LPON and NAC or α-tocopherol.

BD™ Oxygen Biosensor System was used to determine basal cell respiration as described in section 5.2.1. Additional cells were simultaneously treated with LPON and NAC or α-tocopherol for 72 hours. The fluorescent plates were read in CytoFluor Reader Series 4000 for 40 cycles, for 40 minutes. Cell respiration was measured from the linear portion of the slope of fluorescence rise. Data are presented as mean ± SEM; $P<0.0001$; $^{***}P<0.001$, $^{**}P<0.01$; NAC, N-acetylcysteine; TOCO, α-tocopherol.

5.3.2. NAC restores substrate-induced respiration

In human NAFLD, oxidative stress is often compounded by an ongoing surge of energy substrates. Thus, to examine the impact of further energy substrate exposure on LPON treated cells; HBSS containing LPON was added to all groups immediately before measurement of cell respiration. Further LPON would also confirm that the reduction in basal respiration observed with LPON is neither attributable to decreased substrate availability nor it is related to a suboptimal intermediary metabolism.

All groups demonstrated increased respiration with further LPON (Figure 5.3.2). However, respiration for the LPON-pretreated cells remained lower than the untreated cells. The combination of LPON with NAC or α-tocopherol restored cell respiration by 25% and 20% respectively, when compared with LPON treatment alone (Figure 5.3.2). Interestingly, oleate treated cells also had lower substrate-induced respiration than the untreated cells, but was still significantly higher when compared with LPON.

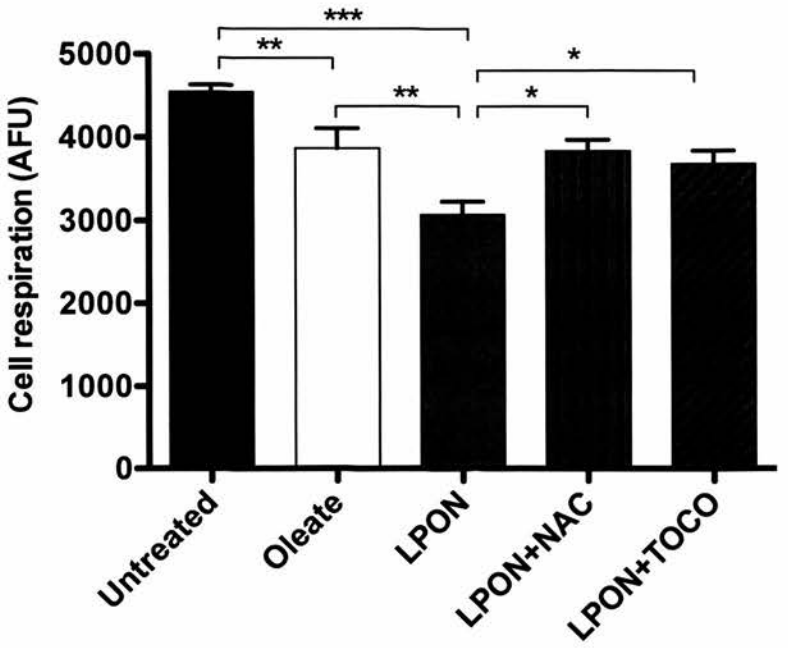

Figure 5.3.2. Substrate-induced respiration in treated cells.

Further LPON was added to all groups prior to the measurement of respiration using BD™ Oxygen Biosensor System as described in section 5.2.1. The fluorescent plates were read in CytoFluor Reader Series 4000 for 40 cycles, for 40 minutes. Cell respiration was measured from the linear portion of the slope of fluorescence rise. Data are presented as mean ± SEM; $P<0.0001$; $^{***}P<0.001$, $^{**}P<0.01$, $^{*}P<0.05$; NAC, N-acetylcysteine; TOCO, α-tocopherol.

5.3.3. NAC does not ameliorate mitochondrial chain impairment

To examine the maximal capacity of mitochondrial respiratory chain, DNP was added to all treated groups. DNP-induced uncoupling dissipates mitochondrial proton gradient. This forces a maximal rise in respiration to preserve the gradient, essential to maintain ATP formation. In the presence of DNP, the rise in cell respiration was significantly lower with the LPON-treated cells when compared with the untreated cells, suggesting decreased mitochondrial respiratory chain capacity. In contrast, the rise in respiration induced by DNP with oleate, LP, LPO and octanoate were comparable to that seen with the control cells (Figure 5.3.3 Panel A), showing an overall lack of impact on the respiratory chain under these conditions. Interestingly, neither NAC nor α-tocopherol significantly improved the respiration in LPON treated cells (Figure 5.3.3 Panel B).

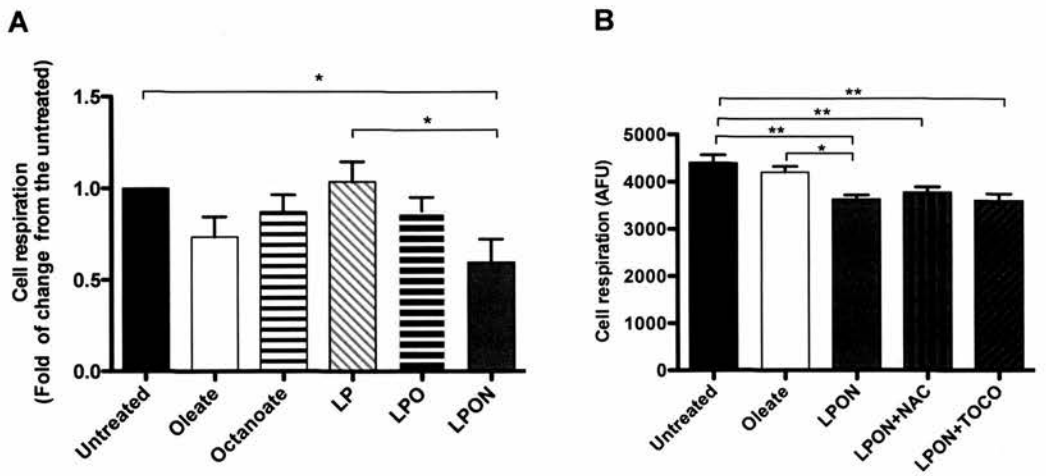

Figure 5.3.3. Impaired maximal mitochondrial chain capacity with LPON.

A, Respiration in treated cells suspended in HBSS+LPON+2,4 dinitrophenol (DNP); B, Respiration in cells treated simultaneously with NAC and α-tocopherol in the presence of LPON+DNP. Separate groups of LPON cells were simultaneously treated with NAC (10mM) or of α-tocopherol (0.4mM) for 72 hours. Cells in single suspension were added to BD™ Oxygen Biosensor 96-well plate containing LPON+DNP (250μM). The fluorescent plates were then read in CytoFluor Reader Series 4000 for 40 cycles, for 40 minutes. Cell respiration was measured from the linear portion of the slope of fluorescence rise. Data are presented as mean ± SEM; A, P=0.0003; B, P=0.0009; $^{**}P<0.01$, $^{*}P<0.05$; NAC, N-acetylcysteine; TOCO, α-tocopherol.

5.3.4. NAC does not reduce triglyceride accumulation

Next, to examine whether the recovery in cell respiration with NAC was associated with a reduction in triglyceride accumulation, triglyceride concentrations in cells co-treated with LPON and NAC were measured after a 72-hour treatment. The addition of NAC to LPON did not alter triglyceride concentration (LPON 235.3 ± 12.2 vs LPON+NAC 237.3 ± 7.2 μg/g of total protein, P=0.9).

5.3.5. The effect of triglyceride reduction induced by metformin on respiration

The reduction in triglyceride is often construed as a marker of improvement in NAFLD. However, it is still unclear whether a reduction in triglyceride *per se* has beneficial impact on mitochondrial function. Metformin has been shown to decrease triglyceride accumulation in HepG2 cells (128). Using metformin concentrations previously shown to decrease triglyceride accumulation, we examined whether the triglyceride reduction would improve mitochondrial function in LPON treated cells (128).

5.3.5.1. Metformin does not affect cell viability in LPON treated cells

Cell viability was not compromised by metformin (50nM-2mM) as evidenced by the percentage of intracellular LDH retention (Figure 5.3.5.1).

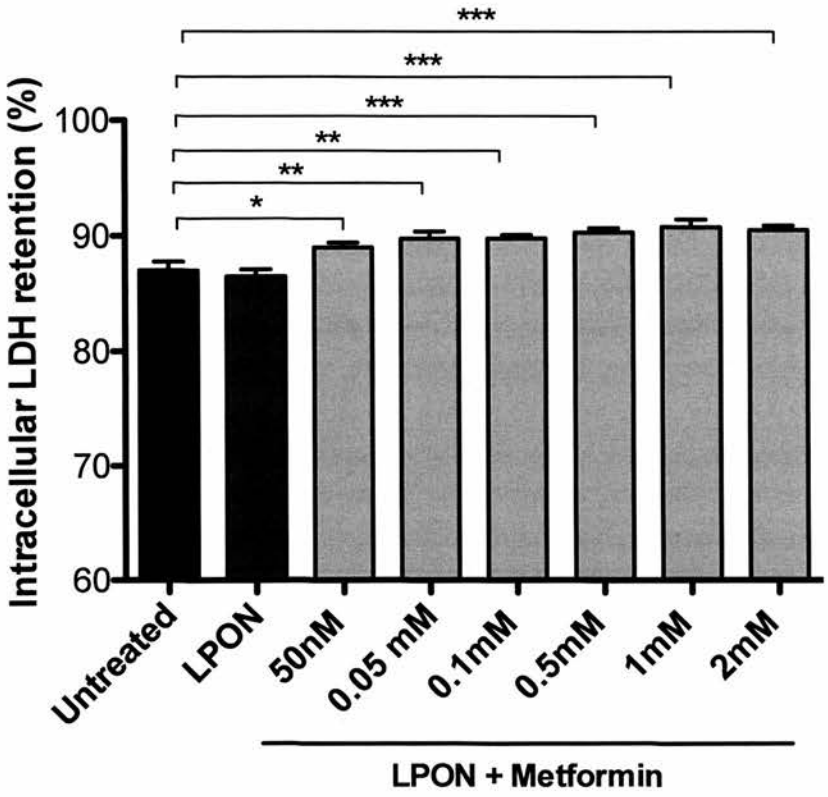

Figure 5.3.5.1. Cell viability in cells treated with metformin and LPON.

Percentage of intracellular LDH retention was determined in cells that have been simultaneously treated with LPON+metformin (50nM-2mM) after 72 hour using the method described in section 2.1.6. Data are presented as mean ± SEM; $P<0.0001$; $^{***}P<0.001$, $^{**}P<0.01$, $^{*}P<0.05$.

5.3.5.2. Triglyceride reduction with metformin does not improved respiration

To induce triglyceride reduction, cells were treated with LPON+metformin (50nM-2mM) for the treatment duration. Figure 5.3.5.2 Panel A shows that the concomitant treatment with metformin at the concentration of 0.5, 1 and 2mM resulted in lower triglyceride concentration in LPON cells when compared with LPON treatment alone. However, the significant reduction in triglyceride with metformin (2mM) did not improve respiration in LPON cells. As shown in Figure 5.3.5.2 Panel B, basal respiration with LPON+metformin was lower than seen in the untreated or LPON treatment alone.

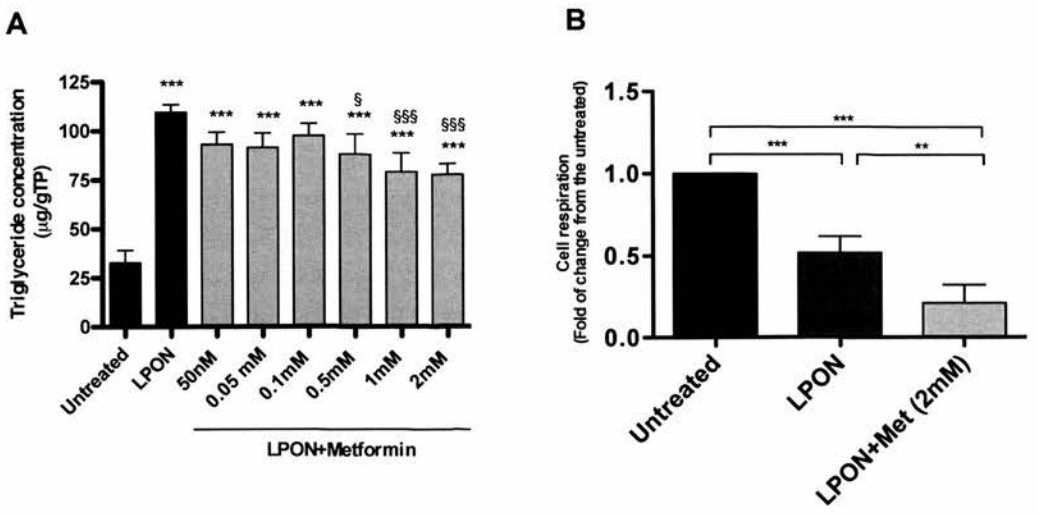

Figure 5.3.5.2. The effect of metformin on triglyceride and basal respiration in LPON treated cells.

A, Triglyceride concentrations in cells treated with LPON+metformin; B, Basal respiration in cells simultaneously treated with LPON+metformin (2mM). A, Cells were treated with LPON+metformin at specified concentrations for 72 hours. Intracellular triglyceride accumulation was determined as described in section 3.2.2 and normalized to total protein content as outlined in section 2.2.5. Data are presented as mean ± SEM; $P<0.0001$; $^{***}P<0.001$ vs untreated; $^{§§§}P<0.001$, $^{§}P<0.05$ vs LPON. B, To investigate whether the reduction in triglyceride accumulation would improve mitochondrial function, basal respiration (described in section 5.2.1) was measured in cells treated with LPON and metformin (2mM) for 72 hours. Data are presented as mean ± SEM; $P=0.008$; $^{***}P<0.001$, $^{**}P<0.01$, $^{*}P<0.05$ vs untreated.

5.3.5.3. Reduced NADH oxidation with metformin

Impaired mitochondrial respiration can reduce NADH oxidation to NAD^+ leading to a rise in mitochondrial NADH/NAD^+ ratio. This reduces the shuttling of NADH from cytosolic into the mitochondria. Thus, the cytosolic NADH/NAD^+ ratio would also rise in parallel to the increase in mitochondrial NADH/NAD^+ ratio. To investigate whether LPON+metformin reduces NADH oxidation, the ratios of β-hydroxybutyrate to acetoacetate (mitochondrial NADH/NAD^+ ratio) and lactate to pyruvate ratio (cytosolic NADH/NAD^+ ratio) were determined. Figure 5.3.5.3 Panel A shows a progressive rise in mitochondrial NADH/NAD^+ ratio mirroring the rising concentrations of metformin suggesting a dose-dependent effect of metformin on mitochondrial respiratory chain. Metformin at 1 and 2mM increased mitochondrial NADH/NAD^+ ratio in LPON treated cells by two- and four-fold respectively. Panel B shows that cytosolic NADH/NAD^+ ratio rose with the increasing concentrations of metformin suggesting a reduction in NADH shuttling from the cytoplasm.

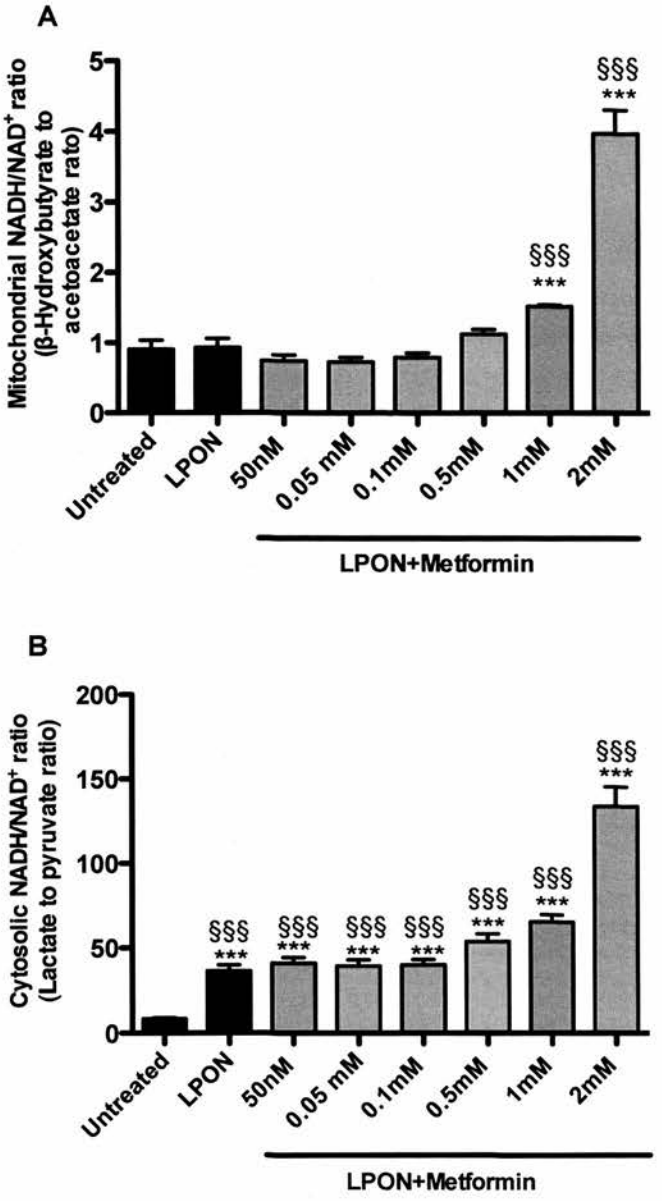

Figure 5.3.5.3. NADH/NAD$^+$ ratio in cells treated LPON and metformin.

A, Mitochondrial NADH/NAD$^+$ ratio; B, Cytosolic NADH/NAD$^+$ ratio. To investigate whether decreased respiration with metformin was paralleled by increased NADH/NAD$^+$ ratio, β-hydroxybutyrate to acetoacetate (mitochondrial NADH/NAD$^+$) and lactate to pyruvate ratio (cytosolic NADH/NAD$^+$) were determined. Data are presented as mean ± SEM; A, $P<0.0001$; $^{***}P<0.001$ vs untreated; $^{§§§}P<0.001$ vs LPON; B, $P<0.0001$; $^{***}P<0.001$ vs untreated, $^{§§§}P<0.001$ vs LPON+metformin (2mM).

5.3.6. Altered mitochondrial structure is most pronounced with LPON

Impaired mitochondrial function in NAFLD is often paralleled by alterations in mitochondrial structure, the most striking of which, is the development of enlarged mitochondria (32, 77, 78). Transmission electron microscopy revealed that mitochondrial cross-sectional area was lower in LPON when compared to oleate or the untreated group (Figure 5.3.6.1). Figure 5.3.6.2 demonstrates representative electron microscopy images of treated cells viewed at the magnification x8400. The cristae in octanoate, oleate and treated cells, but not LPON, were distinct. Figure 5.3.6.3 represents electron microscopy images of mitochondria from cells treated with LPON and octanoate. Despite the similarities in the cross-sectional area, mitochondrial morphology was different. In LPON treated cells, the mitochondria were elongated and the cristae were indistinct.

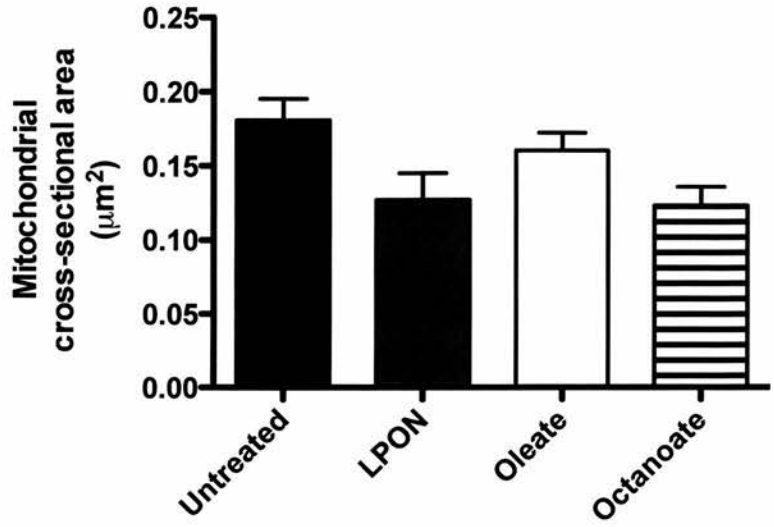

Figure 5.3.6.1. Cross-sectional area of the mitochondria in treated cells.

C3A cells treated for 72 hours were prepared for electron microscopy as described in section 3.2.4. Cross-sectional area of the mitochondria from four different random sections of each group was measured using ImageJ. Data are presented as mean ± SEM; P=0.04.

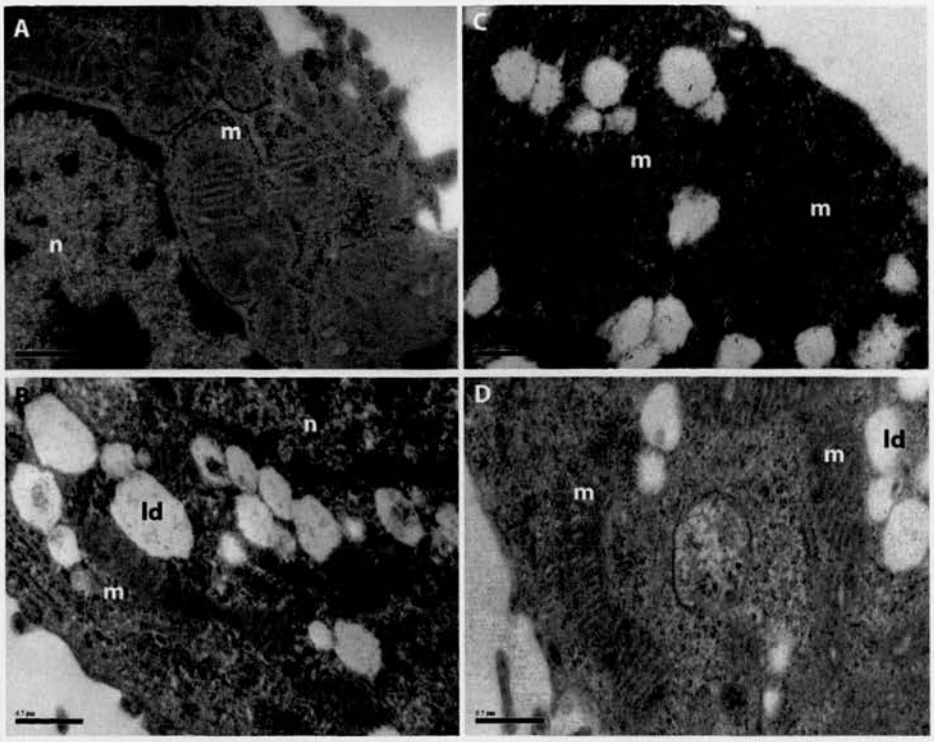

Figure 5.3.6.2. Electron microscopy images of mitochondria in treated cells.

A, Untreated; B, LPON; C, Octanoate; D, Oleate. C3A cells were treated for 72 hours and prepared for electron microscopy as previously described in section 3.2.4; (m, mitochondria; ld, lipid droplets and n, nucleus; magnification x8400).

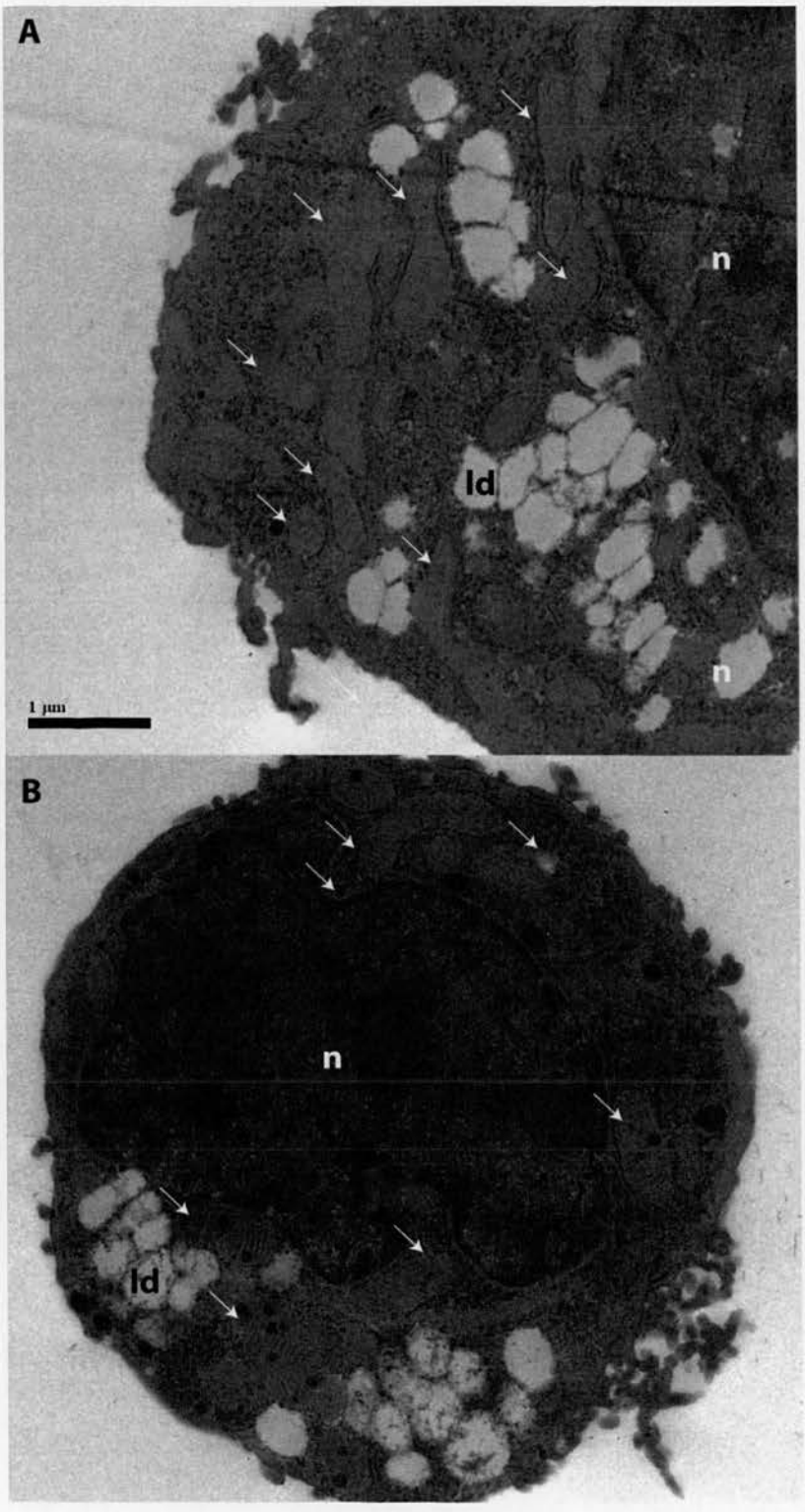

Figure 5.3.6.3. Electron microscopy images of mitochondria in treated cells. A, LPON; B, Octanoate; (white arrows, mitochondria; n, nucleus; lipid droplets; magnification x2100).

5.4. Discussion and conclusion

This chapter is focused on the effect of enhanced mitochondrial respiration and increased superoxide formation on mitochondrial respiration. More important, we address a fundamental question: does steatosis in the absence of ROS exert a deleterious effect on mitochondrial function?

The main findings of this chapter are:

1. Prolonged LPON treatment led to a significant reduction in basal and substrate-induced respiration, as well as diminished mitochondrial chain capacity.
2. Cell respiration was improved in cells treated simultaneously with LPON and NAC or α-tocopherol.
3. Reduction in triglyceride accumulation with metformin did not improve mitochondrial function.
4. Impaired mitochondrial respiration with LPON was associated with altered mitochondrial structure.

These data highlight two important points. First, the capacity of an energy substrate to generate ROS rather than its ability to induce cellular steatosis is the determinant to the subsequent mitochondrial function. In support of this, respiration was preserved with oleate treated cells despite similar triglyceride concentration to that seen in cells treated with LPON. Sustained basal and substrate-induced respiration in the presence of the antioxidants further suggests ROS involvement in promoting the mitochondrial impairment. Moreover, the mitochondrial morphological changes observed with LPON are similar to the alterations previously described in the presence of oxidative stress (32, 82).

Second, a reduction in intracellular triglyceride does not necessarily lead to an improvement in mitochondrial function. We have shown that metformin did not restore mitochondrial function despite the reduction in triglyceride accumulation. Indeed, the dose-dependent rise in mitochondrial and cytosolic NADH/NAD^+ ratio with metformin are consistent with a progressive decline in NADH oxidation, which can occur with impaired mitochondrial respiration. It is worth noting that the overall triglyceride concentrations in Figure 5.3.5.2 were lower than previously observed (Figure 3.3.3). These variations might have been attributable to the differences in cell passage; a reduction in *de novo* lipogenesis in later passage has been previously shown in human fibroblasts (130).

Taken together, our data suggest that the enhanced ROS formation with LPON leads to a significant mitochondrial impairment. This is in accord with several previous studies (32, 59). Thus, the sequence of events instigated by increased energy substrates with LPON is similar to that observed in human and animal model with NAFLD; increased respiration with concomitant rise in ROS formation culminates in altered mitochondrial function. More important, our data address a fundamental point; in the absence of ROS, triglyceride accumulation does not impair mitochondrial respiration.

6. CHAPTER SIX

LPON CELLULAR STEATOSIS IS CHARACTERIZED BY CHRONIC OXIDATIVE STRESS

6.1. Introduction

The association between mitochondrial impairment with enhanced ROS formation is well established (75). The accepted hypothesis is that ROS promote mitochondrial dysfunction, which in turn, perpetuates ROS formation, creating a vicious cycle thus promoting chronic oxidative stress, the hallmark of dietary-induced steatohepatitis.

Thus far, we have shown *in vitro* that enhanced ROS formation, rather than intracellular triglyceride accumulation *per se*, leads to impaired mitochondrial respiration. In this chapter, we examine whether altered mitochondrial respiration in the LPON cellular steatosis model would lead to further ROS formation and oxidative stress. We have postulated that decreased mitochondrial respiration with LPON would promote further ROS release driven by the presumed decline in NADH oxidation. It is anticipated that the heightened ROS formation would result in oxidative stress mirrored by enhanced lipid peroxidation.

The extent of lipid peroxidation is a particularly reliable marker of oxidative stress in NAFLD (46). Lipid is abundant in NAFLD. Thus, the potential for lipid peroxidation can be substantial. The resultant reactive aldehydes can instigate the release of pro-inflammatory cytokines. Furthermore, the peroxidation byproducts can undergo further

oxidative process, which generate additional ROS. Increased polyunsaturated fatty acids (PUFA) peroxidation has also been associated with enhanced formation of dicarboxylic acid from ω-oxidation (131, 132). In turn, dicarboxylic acid enters the peroxisomal β-oxidation pathway (133, 134). Unlike mitochondrial β-oxidation, peroxisomal β-oxidation is not associated with ATP production but instead, each sequence generates a myriad of ROS predominantly H_2O_2.

The aims of this chapter are:

1. To examine whether the reduction in mitochondrial respiration would modulate superoxide formation.
2. To determine whether the acute rise in superoxide formation with LPON would lead to increased oxidative stress.

6.2. Methods

6.2.1. Measurement of superoxide formation

Mitochondrial superoxide production was measured using the live-cell permeable fluorescent probe MitoSOX™ as described in 4.2.2. For fluorescent microscopy, cells were treated with specified energy substrates in two-chamber slides until 70% confluent. Treated C3A cells were then incubated with MitoSOX™ for 45 minutes at 37°C. The supernatant was then removed and cells were rinsed, before the addition of 500µl of HBSS into each chamber. The slides were kept at 37°C and viewed under fluorescent microscopy. Phase contrast and fluorescent field images were obtained and then merged using image editor software, Photoshop CS4, (Adobe Systems Incorporated, San Jose, CA, USA). Fluorescence intensity from each image was analysed using ImageJ. For FACS analysis, treated cells were trypsinized for 5 minutes, rinsed with HBSS and centrifuged. Cells were resuspended in HBSS or LPON to determine the superoxide formation during basal or substrate-induced respiration respectively, before FACS analysis (FACS Calibur™, BD Biosciences, CA, USA).

6.2.2. Metabolomics profiling of oxidative stress markers

Metabolomics is an emerging analytical method to identify and quantify metabolites in a biological system. Oxidative stress markers including the end products of lipid peroxidation can be identified using this method. For metabolomics, treated C3A cells were centrifuged (1000*g*) for 10 minutes at 37°C. The cell pellet was resuspended in 1ml of supernatant, transferred to a 1.5ml tube, and the final pellet was obtained by further centrifugation (3000*g*) for 5 minutes followed by a complete removal of supernatant.

Metabolites were extracted from the cell pellet by the addition of 200µl of chloroform/methanol/water (1:3:1) with vigorous mixing for 1 hour at 4°C. Precipitated proteins and cellular debris were removed by centrifugation (13000*g*) for 5 minutes. Supernatant was kept at –80°C until liquid chromatography (LC)-mass spectrometry (MS) analysis within 2 weeks. Additional control samples included cell-free growth medium and extraction solvent served as blanks.

The LC separation was performed using hydrophilic interaction chromatography with a ZIC–HILIC 150 x 4.6 mm, 5µm column (Merck Sequant, Umeå, Sweden), operated by an UltiMate 3000 RSLC liquid chromatography system (Dionex, Camberley, Surrey, UK). The separation consisted of a linear gradient from 80% B to 20% B over 30 minutes, followed by an 8-minute wash with 5% B, and 8-minute reequilibration with 80% B, where solvent B was 0.08% formic acid in acetonitrile, and solvent A was 0.1% formic acid in water. The flow rate was 300µL/minute, column temperature 20°C, injection volume 10µL, and samples were maintained at 4°C. The mass spectrometry was performed using an Orbitrap Exactive (Thermo Fisher Scientific, Hemel Hempstead, UK) with a HESI 2 probe. The spectrometer was operated in polarity switching mode, with the following settings: resolution 50,000 m/z range 70–1400. Ionisation voltages were +4.5 kV and –3.5 kV in positive and negative modes respectively.

Raw LC-MS data were processed with a combination of XCMS Centwave for peak picking (http://metlin.scripps.edu/xcms/), and mzMatch for alignment and annotation of related peaks (http://mzmatch.sourceforge.net/). Metabolite identification was performed by matching masses and retention times to the database with mass accuracy

window of 3 ppm (if two formulae were within 3ppm the closest match was taken) and RT window of 35% (by in-house VBA scripts). Additional automated noise and MS artifact filtering procedures were applied to remove peak sets that contained: 1) peaks that were present at equal or higher abundance in the blank solvent samples 2) all peaks lower than the intensity threshold (10,000) 3) shoulder or duplicate peaks within the same mass (3 ppm) and retention time (0.2 min) window 4) common MS artifacts 5) irreproducible intensities (relative standard deviation > 0.5) across replicate samples.

6.3. Results

6.3.1. Basal mitochondrial superoxide is diminished with chronic LPON exposure

We have previously shown that basal respiration with LPON was significantly diminished after 72 hours. To examine whether the reduction in basal respiration would affect superoxide formation, cells were labeled with MitoSOX™ for superoxide quantification. Figure 6.3.1 Panel A and B consist of representative fluorescent microscopy images of mitochondrial superoxide formation in the untreated and LPON treated cells respectively. Panel C shows the quantification of fluorescent area using ImageJ. Basal mitochondrial superoxide formation after a 72-hour treatment was similar between LPON and the untreated cells. This finding was further confirmed by FACS analysis (Panel D). Despite the contrasting basal respiration, mitochondrial superoxide formation was similar in LPON and the untreated cells.

6.3.2. Increased mitochondrial superoxide with further LPON exposure

Substrate-driven respiration was also diminished in LPON treated cells. Therefore, we examined the magnitude of superoxide formation during substrate-driven respiration. Treated cells labeled with MitoSOX™ were resuspended in further LPON prior to FACS analysis. As demonstrated in Figure 6.3.2, there was a dramatic rise in the peak fluorescence intensity with LPON suggesting that superoxide formation were significantly upregulated in these cells in the presence of further energy substrates despite the reduction in respiration. In contrast, superoxide formation with oleate treated cells remained similar to that seen with the untreated cells.

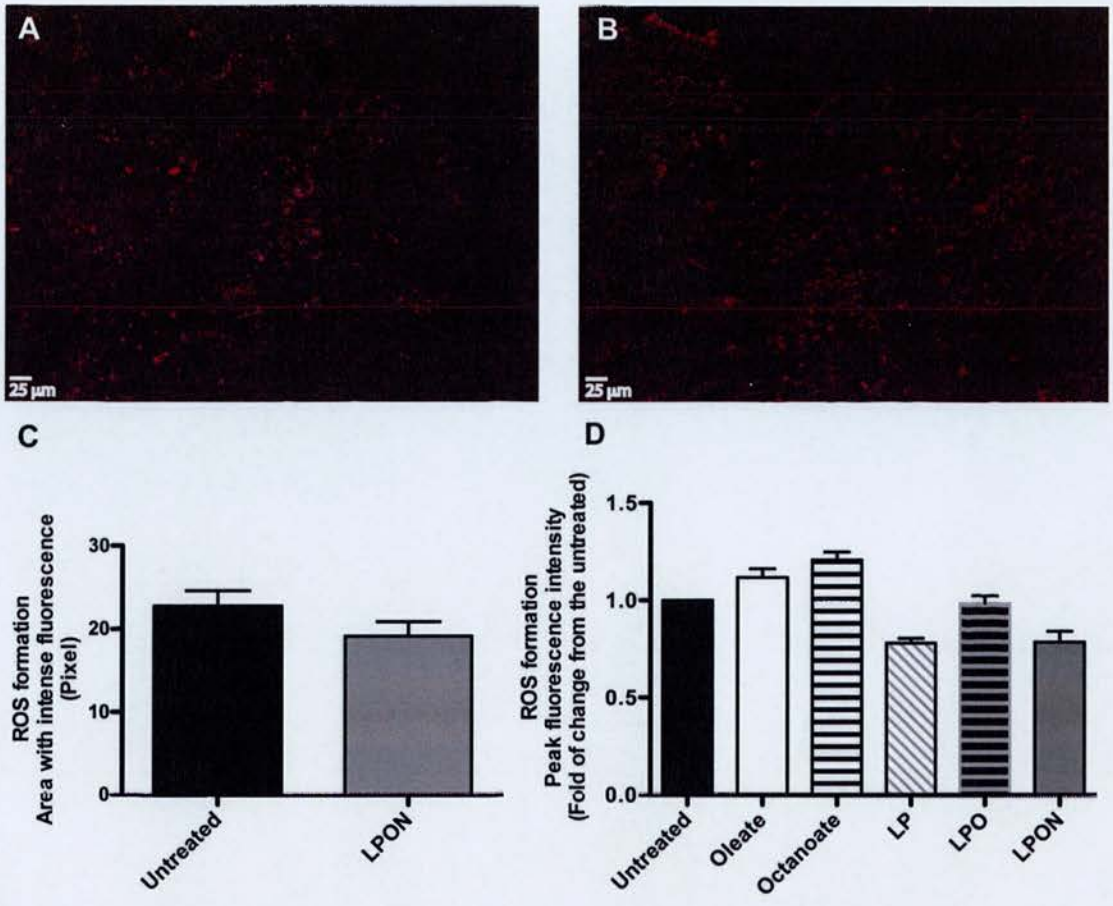

Figure 6.3.1. Basal mitochondrial superoxide formation in treated cells.

A, Untreated cells; B, LPON treated cells, labeled with MitoSOX™ viewed under fluorescent microscopy; C, ImageJ analysis of fluorescent area in cells labeled with MitoSOX™; D, Peak fluorescence in treated groups quantified by FACS. A-C, Cells treated in two-chamber slides for 72 hours were incubated in MitoSOX™ for 45 minutes before fluorescent microscopy (magnification x10). Fluorescent area was analysed using ImageJ. Data are presented as mean ± SEM; P=0.15 (unpaired t-test). D, Cells treated in 25cm^2 flasks were trypsinized and incubated with MitoSOX™ for 45 minutes. Cells were then rinsed, centrifuged and resuspended in HBSS. Data are presented as mean ± SEM; P=0.14 (one-way ANOVA with Newman-Keuls post-hoc tests).

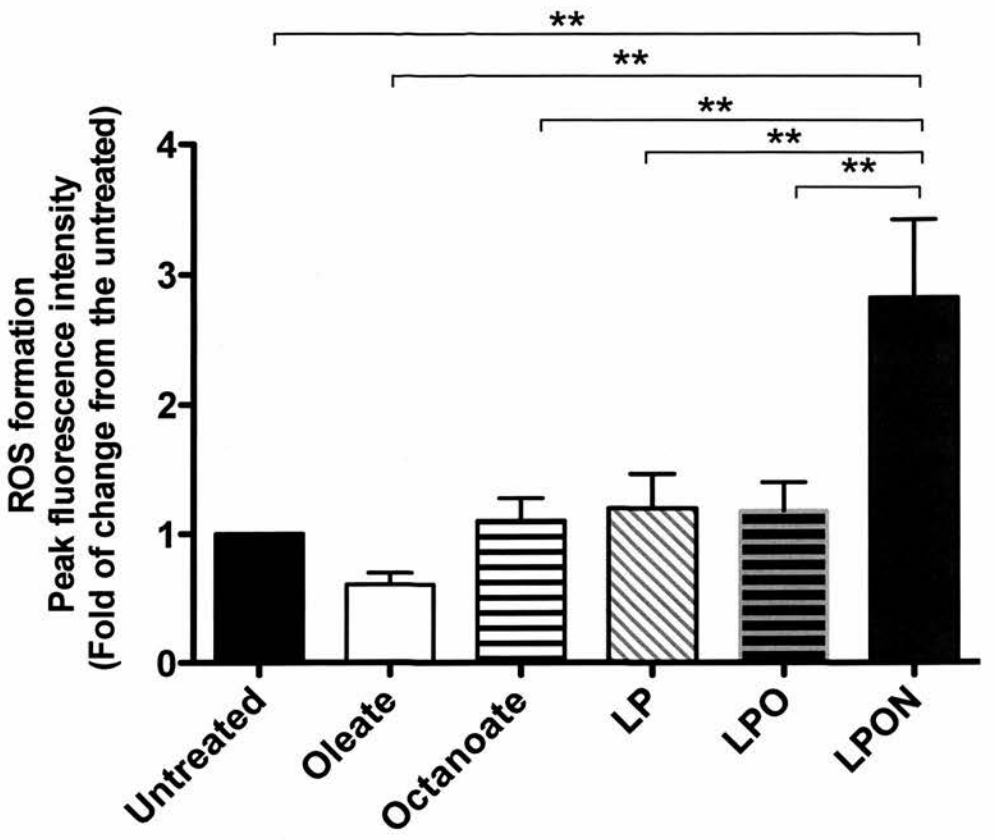

Figure 6.3.2. Mitochondrial superoxide formation during substrate driven respiration.

Cells treated in 25cm^2 flasks were trypsinized and incubated with MitoSOX^{TM} for 45 minutes at 37°C. Cells were then rinsed, centrifuged and resuspended in further LPON before FACS analysis. Data are presented as mean ± SEM; P=0.005, $^{**}P$<0.01.

6.3.3. LPON is associated with oxidative stress

Next, we determined whether LPON was associated with increased oxidative stress. The byproduct of lipid peroxidation has been proposed to be a reliable marker of oxidative stress *in vivo* and *in vitro*. In oxidative stress, the formation of lipid hydroperoxides is enhanced and their enzymatic or non-enzymatic alterations would produce intermediates such as reactive aldehydes (46). Using metabolomics profiling, lipid peroxidation intermediates were identified and quantified. Given the contrasting respiration between LPON and oleate (despite similar triglyceride accumulation), we focused on the following groups; untreated (control), LPON and oleate.

6.3.3.1. Enhanced lipid peroxidation with LPON

A total of six metabolites of fatty acid-derived aldehydes were identified (Figure 6.3.3.1). As shown in Figure 6.3.3.1, LPON treated cells had a non-statistically significant rise in 4-HNE and its precursor, 3-nonenal, when compared with oleate. In contrast, the levels of pentadecanal, 2-hexenal and 2,4-octadienal are significantly higher with LPON than seen with either oleate or the untreated cells.

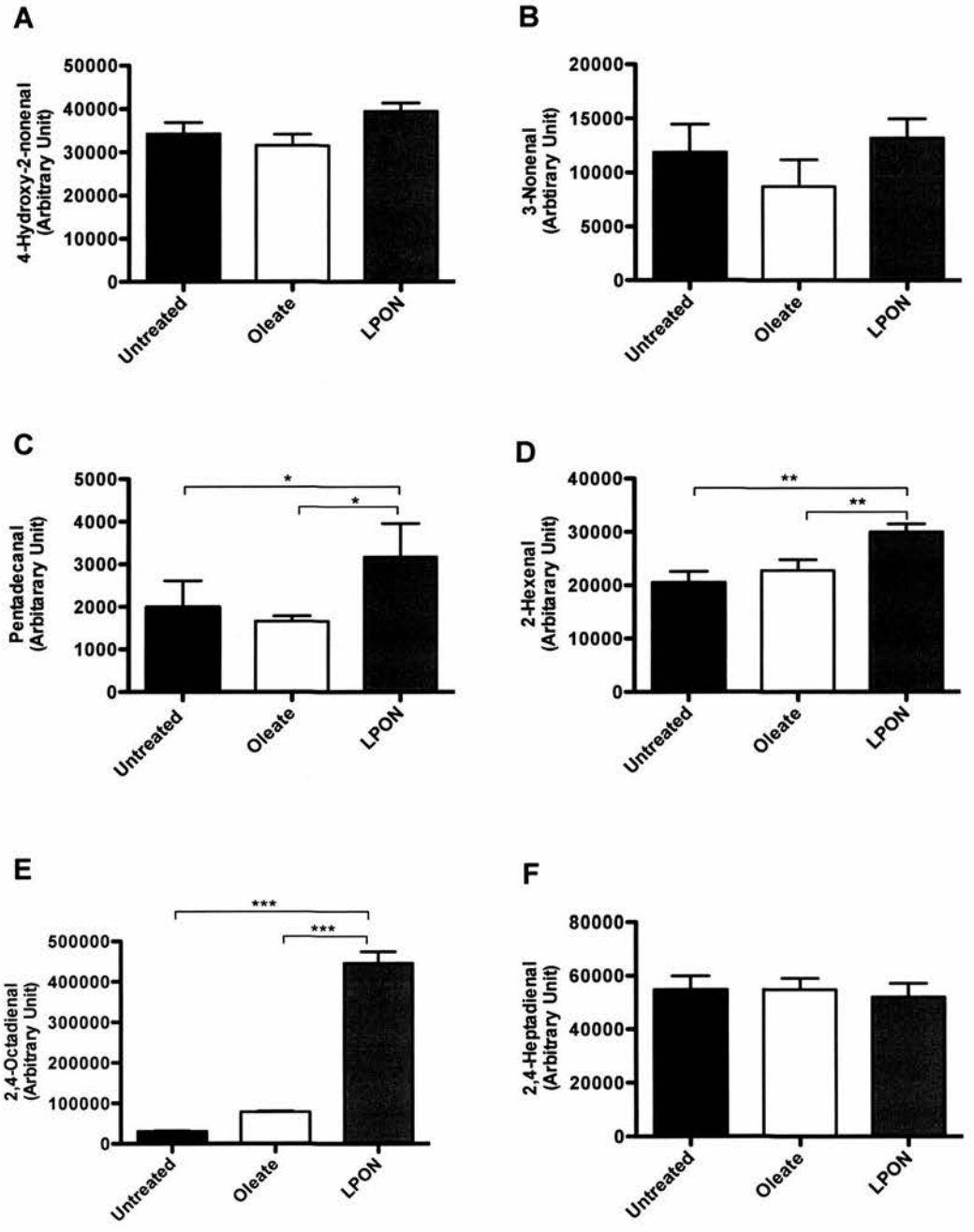

Figure 6.3.3.1. Lipid peroxidation intermediates in treated cells.

A, 4-HNE; B, 3-Nonenal; C, Pentadecanal; D, 2-Hexenal; E, 2,4-Octadienal; F, 2,4-Heptadienal. Metabolites were identified using metabolomics in cells treated with specified substrates for 72 hours. Data are presented as mean ± SD; *P* values: A, 0.13; B, 0.12; C, 0.04; D, 0.001; E, <0.0001; F, 0.72; $^{***}P<0.001$, $^{**}P<0.01$, $^{*}P<0.05$.

6.3.3.2. Isoprostane is increased with LPON

Isoprostanes are prostaglandin-like substances produced primarily by non-enzymatic peroxidation of arachidonic acid. Among the isoprostanes discovered to date, F2-isoprostanes, the isomeric compounds of cyclooxygenase-derived $PGF_{2\alpha}$, have been regarded as the most reliable marker of oxidative stress/lipid peroxidation status *in vivo* (135, 136). Furthermore, F2-isoprostanes have been implicated in the pathogenesis of hepatic fibrosis (137). Using the metabolomics approach, we identified a metabolite that corresponded to F2-isoprostane. Figure 6.3.3.2 represents the concentration of 9S,11R,15S-trihydroxy-2,3-dinor-5Z,13E-prostadienoic acid-cyclo (8S,12R) (2,3-dinor-8-iso-$PGF_{2\alpha}$), an F2-isoprostane, in treated cells. The concentration of 2,3-dinor-8-iso-$PGF_{2\alpha}$ was significantly higher with LPON when compared with oleate and the untreated cells.

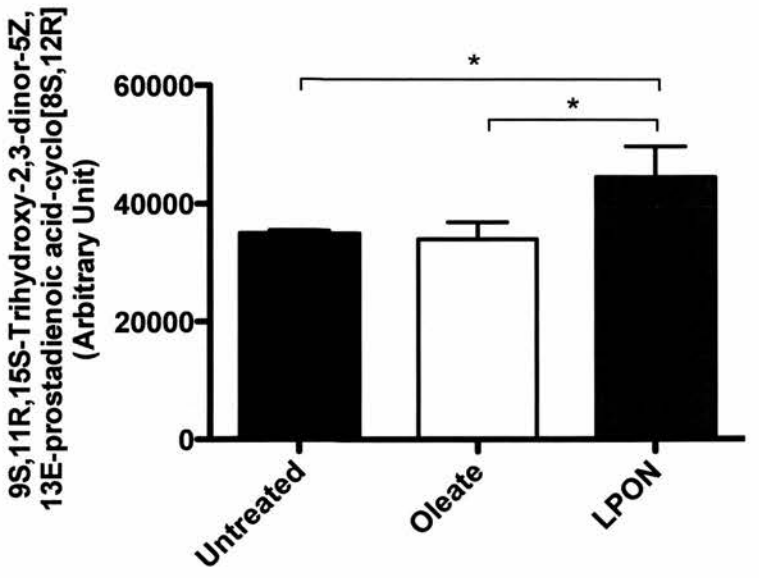

Figure 6.3.3.2. The concentration of F2-isoprostane in treated cells.

F2-isoprostane is regarded as a reliable marker of oxidative stress *in vivo*. 9S,11R,15S-Trihydroxy-2,3-dinor-5Z,13E-prostadienoic acid-cyclo (8S,12R) (2,3-dinor-8-iso-$PGF_{2\alpha}$), a metabolite of F2-isoprostane, was identified using metabolomics in treated cells. Data are presented as mean ± SD; $P=0.01$, $^{*}P<0.01$.

6.3.3.3. Increased dicarboxylic acid concentrations with LPON

Medium and short chain dicarboxylic acids have also been proposed to be a marker of oxidative stress (132). In NAFLD, measuring dicarboxylic acids as a marker of oxidative stress can potentially provide an insight into β-oxidative capacity; the presence of dicarboxylic acid suggests mitochondrial β-oxidation overload. Their presence also heralds an ongoing ROS formation. The oxidation of dicarboxylic acids by peroxisomal β-oxidation generates a considerable amount of ROS. Additionally, dicarboxylic acids have also been shown to diminish respiration (133). Using metabolomics analysis, a total of 19 metabolites that corresponded to dicarboxylic acid were identified (Table 1). The concentration of all nine medium chain (C8-C12)) dicarboxylic acids were significantly higher with LPON when compared with the untreated or oleate (Table 6.3.3.3 and Figure 6.3.3.3.1). Similarly, the levels of C13 and C14 dicarboxylic acid were higher with LPON. Taken together, these findings are consistent with increased oxidative stress as well as overwhelmed mitochondrial β-oxidation. Interestingly, the concentrations of very long chain dicarboxylic acids (>C16) were similar between LPON and the untreated cells (Table 6.3.3.3).

Chemical Structure	Dicarboxylic acid	LPON (Fold of change from untreated)	Oleate (Fold of change from untreated)
Short chain (<C8)			
$C_6H_{10}O_4$	Adipate	0.31	0.46
$C_7H_{12}O_4$	Heptanedioic acid	1.12	0.90
Medium chain (C8-C12)			
$C_8H_{14}O_4$	Suberic acid	1.29*	1.02
$C_{10}H_{18}O_4$	Decanedioic acid	1.53*	0.99
$C_{10}H_{18}O_5$	3-hydroxysebacic acid	1.51*	0.86
$C_{11}H_{20}O_4$	Undecanedioic acid	1.41*	1.01
$C_{12}H_{20}O_4$	Traumatic acid	2.43*	0.90
$C_{12}H_{22}O_4$	Dodecanedioic acid	2.68*	0.97
$C_{12}H_{22}O_5$	3-hydroxydodecanedioic acid	1.77*	1.00
$C_{12}H_{14}O_4$	2E,4E,8E,10E-Dodecatetraenedioic acid	1.60*	1.05
Long chain (>C13)			
$C_{13}H_{24}O_4$	Brassilic acid	1.41*	1.01
$C_{14}H_{26}O_4$	Tetradecanedioic acid	1.50*	0.86
$C_{14}H_{26}O_5$	3-hydroxy-tetradecanedioic acid	1.56*	1.00
$C_{16}H_{30}O_4$	Hexadecanedioic acid	1.10	0.92
$C_{17}H_{32}O_4$	2-methyl-hexadecanedioic acid	1.26*	0.92
$C_{20}H_{38}O_4$	Eicosanedioic acid	1.02	0.95
$C_{21}H_{40}O_4$	Heneicosanedioic acid	0.90	1.14
$C_{23}H_{44}O_4$	Tricosanedioic acid	0.98	0.97
$C_{26}H_{50}O_4$	Hexacosanedioic acid	0.90	1.14

Table 6.3.3.3. Dicarboxylic acids concentrations in treated cells.

The concentration of dicarboxylic acid determined using metabolomics in treated cells. <C8, short chain; C8-C12, medium chain; >C13, long chain dicarboxylic acids. Data presented as fold of change from the untreated; $^{*}P<0.05$.

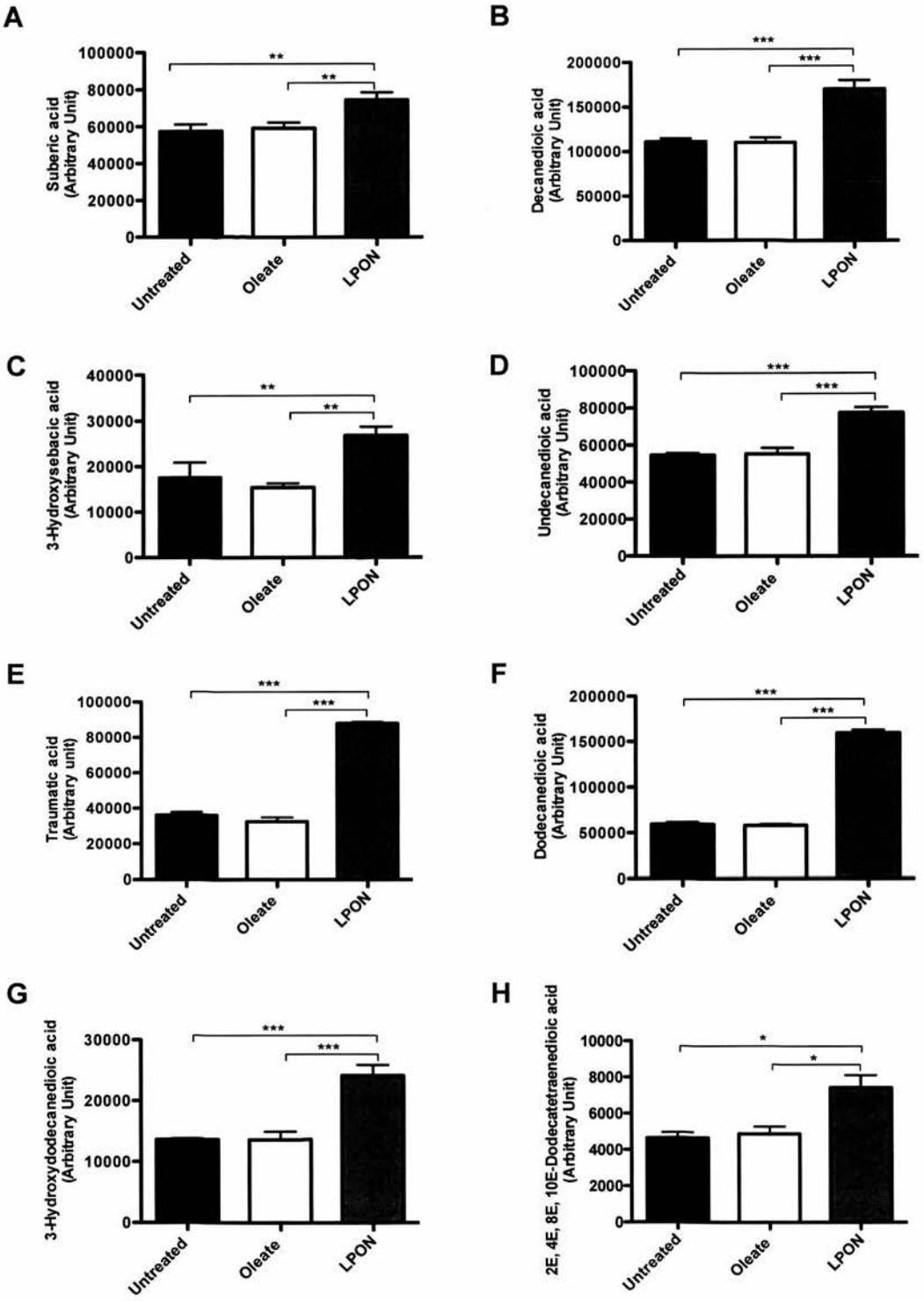
A
Suberic acid (Arbitrary Unit)
100000
80000
60000
40000
20000
0
**
**
Untreated
Oleate
LPON
B
Decanedioic acid (Arbitrary Unit)
200000
150000
100000
50000
0
***
***
Untreated
Oleate
LPON
C
3-Hydroxysebacic acid (Arbitrary Unit)
40000
30000
20000
10000
0
**
**
Untreated
Oleate
LPON
D
Undecanedioic acid (Arbitrary Unit)
100000
80000
60000
40000
20000
0
***
***
Untreated
Oleate
LPON
E
Traumatic acid (Arbitrary unit)
100000
80000
60000
40000
20000
0
***
***
Untreated
Oleate
LPON
F
Dodecanedioic acid (Arbitrary Unit)
200000
150000
100000
50000
0
***
***
Untreated
Oleate
LPON
G
3-Hydroxydodecanedioic acid (Arbitrary Unit)
30000
20000
10000
0
***
***
Untreated
Oleate
LPON
H
2E, 4E, 8E, 10E-Dodecatetraenedioic acid (Arbitrary Unit)
10000
8000
6000
4000
2000
0
*
*
Untreated
Oleate
LPON

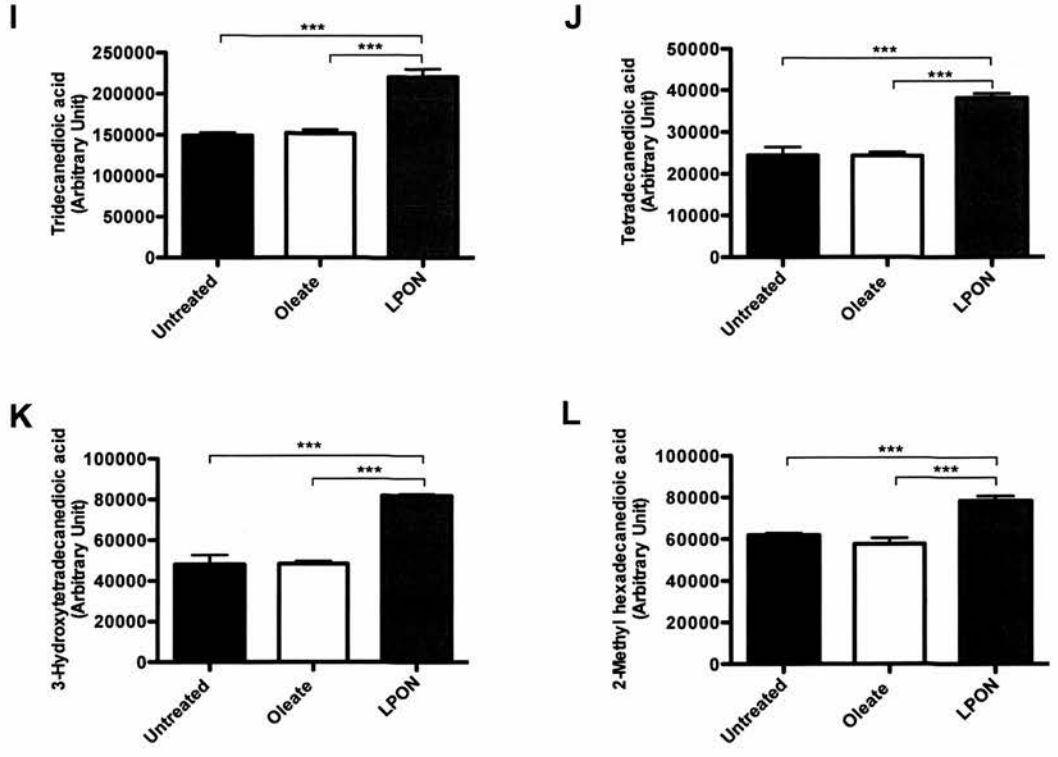

Figure 6.3.3.3.1. Increased dicarboxylic acids concentration in LPON cells.

Metabolites that corresponded to dicarboxylic acids were identified using metabolomics. A, Suberic acid (P=0.002); B, Decanedioic acid (P<0.0001); C, 3-Hydroxysebacic acid (P=0.001); D, Undecanedioic acid (P<0.0001); E, Traumatic acid (P<0.0001); F, Dodecanedioic acid (P<0.0001); G, 3-Hydroxydodecanedioic acid (P<0.0001); H, 2E,4E,8E,10E-Dodecatetraenedioic acid (P=0.01); I, Brassilic acid (P<0.0001); J, Tetradecanedioic acid (P<0.0001); K, 3-Hydroxytetradecanedioic acid (P<0.0001); L, 2-Methylhexadecanedioic acid (P<0.0001). With the exception of 2-methylhexadecanedioic acid, all were <C14. Data are presented as mean ± SD; $^{***}P$<0.001, $^{**}P$<0.01, $^{*}P$<0.05.

6.4. Discussion and conclusion

This chapter examines whether the reduction in mitochondrial respiration observed in the LPON *in vitro* model of cellular steatosis is associated further superoxide formation and oxidative stress.

The main findings of this chapter are:

1. Basal mitochondrial superoxide formation was downregulated in parallel with the diminished basal respiration with LPON.
2. Exposure to further energy substrates dramatically increased the superoxide production in LPON treated cells.
3. Despite the downregulation of basal superoxide formation, LPON was associated with increased lipid peroxidation and dicarboxylic acid formation indicative of oxidative stress.

These data highlight four important points. First, the reduction in basal ROS after a 72-hour treatment with LPON was unexpected. It was anticipated that diminished basal respiration would have led to an increase in superoxide formation driven by the potential reduction in NADH oxidation. It is possible that the initial surge of ROS may have instigated metabolic adaptations to curb further ROS formation. Thus, determining the modulators of mitochondrial ROS formation notably mitochondrial membrane potential and $NADH/NAD^+$ ratio would be instrumental in dissecting the underlying mechanism.

Second, the capacity for ROS formation is actually enhanced in LPON treated cells. This is evidenced by a significant rise in the substrate-induced ROS. It is likely that

diminished mitochondrial respiration hinders the oxidation of NADH generated from further energy substrates leading to a significant increase in NADH/NAD^+ ratio. More important, this indicates that further exposure to energy substrates can overcome any potential mechanism responsible for minimizing ROS formation. This is particularly relevant to human steatohepatitis where ongoing surge of energy substrates is likely to occur.

The differences in the superoxide formation between cells treated with LPO and LPON further emphasized that mitochondrial impairment, not triglyceride accumulation, is responsible for sustaining oxidative stress. Treatment with LPO led to an extensive triglyceride accumulation but with preserved mitochondrial respiration. This maintains efficient NADH oxidation even in the presence of further energy substrates. Whether these differences can be attributable to the presence of ammonia in LPON remains unclear. However, mitochondrial respiration in cells that have been treated with the combination of lactate, pyruvate, oleate and ammonia for 72 hours remains unaltered (unpublished data from our group; data not shown). Further, metabolomic profiling on these cells or cells treated with ammonia alone does not support the presence of oxidative stress (unpublished data from our group; data not shown). Taken together, these data suggest that the rise in ROS incurred by LPON represents a synergistic effect of all its components rather than that of ammonia alone.

Third, despite the relatively low basal ROS formation, the evidence of oxidative stress is already apparent in LPON cells as evidenced by the increased formation of fatty aldehydes, dicarboxylic acids and isoprostane. This is likely to be attributable to the acute rise in superoxide formation coupled with the abundance of substrates susceptible

to peroxidation from the enhanced *de novo* lipogenesis.

Finally, increased dicarboxylic acid concentration with LPON highlight the presence of fatty acid dysregulation that can occur with substrate overload. Enhanced dicarboxylic acid formation suggests increased ω-oxidation, a minor fatty acid oxidative pathway inducible in the presence free fatty acid overload or in conditions that overwhelm mitochondrial β-oxidation. Additionally, dicarboxylic acids can act as a ligand of the hepatic lipid sensor, PPAR-α, to induce all three fatty acid oxidative pathways; ω-oxidation, peroxisomal β-oxidation and the already strained mitochondrial β-oxidation with a resultant rise in ROS burden.

In conclusion, ROS beget more ROS. Although we have not demonstrated a sustain rise in superoxide, the presence of excessive H_2O_2 (and potentially other ROS) from the ω- and peroxisomal β-oxidation cannot be excluded. Mitochondrial impairment only serves to enhance the inherent capacity to form further ROS. This is likely to sustain oxidative stress in steatohepatitis particularly in the presence of incessant supply of energy substrates.

7. CHAPTER SEVEN

THE REGULATION OF MITOCHONDRIAL ROS FORMATION

7.1. Introduction

In the previous chapter, we have demonstrated an unanticipated downregulation of basal ROS with LPON despite evidence to suggest mitochondrial impairment. This raises the question whether adaptations to minimize ROS formation have already occurred. In this chapter, we focus on factors that may have modulated the superoxide formation in LPON treated cells.

As previously discussed, there are two main factors that regulate mitochondrial ROS formation. First, ROS can be modulated by mitochondrial $NADH/NAD^+$ ratio. Increased concentration of the electron carrier, NADH, accelerates the formation of superoxide. In normal mitochondria, such rise in NADH is swiftly met by an active respiration, thus maintaining efficient NADH oxidation to lower the $NADH/NAD^+$ ratio. Second, superoxide production is highly sensitive to the changes in mitochondrial membrane potential ($\Delta\Psi_m$). Increased $\Delta\Psi_m$ inhibits respiration; hence NADH concentration rises, bolstering the superoxide formation. Conversely, a reduction in mitochondrial $\Delta\Psi_m$ either by an efficient ATP formation or through uncoupled respiration mitigates superoxide formation.

The aim of this chapter is to identify potential factors that may have modulated ROS in treated cells, specifically:

1. Mitochondrial membrane potential ($\Delta\Psi_m$)
2. Mitochondrial (and cytosolic) NADH/NAD^+ ratio
3. Uncoupled respiration.

7.2. Methods

7.2.1. Determining mitochondrial membrane potential using JC-1

The lipophilic cationic probe, JC-1 (Invitrogen, NY, USA) can detect $\Delta\Psi_m$ in intact cells. JC-1 forms multimers (J-aggregates) and monomers in the presence of high and low $\Delta\Psi_m$ respectively. The difference in the emission spectra between the monomer form (green range (530nm)) and J aggregates (red-orange range (590nm)) allows the assessment of $\Delta\Psi_m$ using FACS and fluorescent microscopy. The level of $\Delta\Psi_m$ can be calculated from the ratio of median fluorescence intensity of red (detected in FL2 channel) to green (detected in FL1 channel). Thus, mitochondrial hyperpolarization is indicated by an increase in the red to green fluorescence intensity ratio and vice versa. For fluorescent microscopy, cells were grown and treated in two-chamber slides for 72 hours. Cells were labeled with 5μM of JC-1 for 20 minutes at 37°C as adherent cells and viewed under LSM510 fluorescent microscope. Fluorescent images were merged using image editor software, Photoshop CS4, and the intensity was analysed using ImageJ. Briefly, each image was set to a threshold, and the intensity was determined using 'analyze particle'. For FACS, C3A cells were grown and treated in 25cm^2 flask. Stock solution for JC-1 was prepared by adding 500μl of HBSS. Treated cells were rinsed and incubated with 2ml of JC-1 for 20 minutes in 37°C. Cells were then trypsinized, centrifuged and the supernatants were discarded. Cells were resuspended in 5ml of HBSS and FACS analysis was performed.

7.2.2. Cell respiration in the presence of oligomycin

Confluent cells treated with the specified combination of energy substrates for 72 hours were rinsed, trypsinised and centrifuged as described in section 5.2.3. Cells were

resuspended in 2ml of MEME (with FBS) and were added to the BD™ Oxygen Biosensor 96-well plate containing LPON+Oligomycin (5 μg/ml). The fluorescent plate was then read in CytoFluor Reader Series 4000 for 40 cycles, for 40 minutes. Respiration was measured from the linear portion of the slope of fluorescence rise. Data are presented as arbitrary fluorescent unit (AFU).

7.2.3. Mitochondrial and cytosolic NADH to NAD^+ ratio

Mitochondrial and cytosolic $NADH/NAD^+$ ratio were determined from the ratio of β-hydroxybutyrate to acetoacetate and lactate to pyruvate respectively, as described in section 5.2.4. The presence of lactate and pyruvate in the LPON culture supernatant would preclude any conclusive determination of cytosolic $NADH/NAD^+$ ratio. For this reason, treated cells were rinsed and allowed to reach a steady state for 24 hours in MEME without additional FCS or energy substrates. Cells from all groups were then incubated for 4 hours in PBS and octanoate (2mM) prior to the measurement of mitochondrial and cytosolic NADH to NAD^+ ratio.

7.3. Results

7.3.1. Increased mitochondrial membrane potential with LPON

Using the probe JC-1, we determined the $\Delta\Psi_m$ by calculating the ratio of median intensity of red to green fluorescence. Figure 7.3.1.1 demonstrates representative fluorescent image of red (Panel A) and green (Panel B) from LPON treated cells labeled with JC-1. These images were merged to highlight the red to green fluorescent intensity ratio (Panel C). Figure 7.3.1.2 (Panel A to E) are merged images of treated cells. Panel F shows that ImageJ analysis of the fluorescence intensity suggests higher $\Delta\Psi_m$ with LPON than the untreated cells. Indeed, FACS analysis confirms this finding. As demonstrated in Figure 7.3.1.3, LPON treatment led to increased $\Delta\Psi_m$ when compared with the untreated cells. In contrast, $\Delta\Psi_m$ in oleate treated cells was unaltered. We have also included separate groups of LPON cells that have been concomitantly treated with NAC for the entire treatment. As shown in Figure 7.3.1.3, cells that have been treated with LPON+NAC had lower $\Delta\Psi_m$ than cells treated with LPON alone.

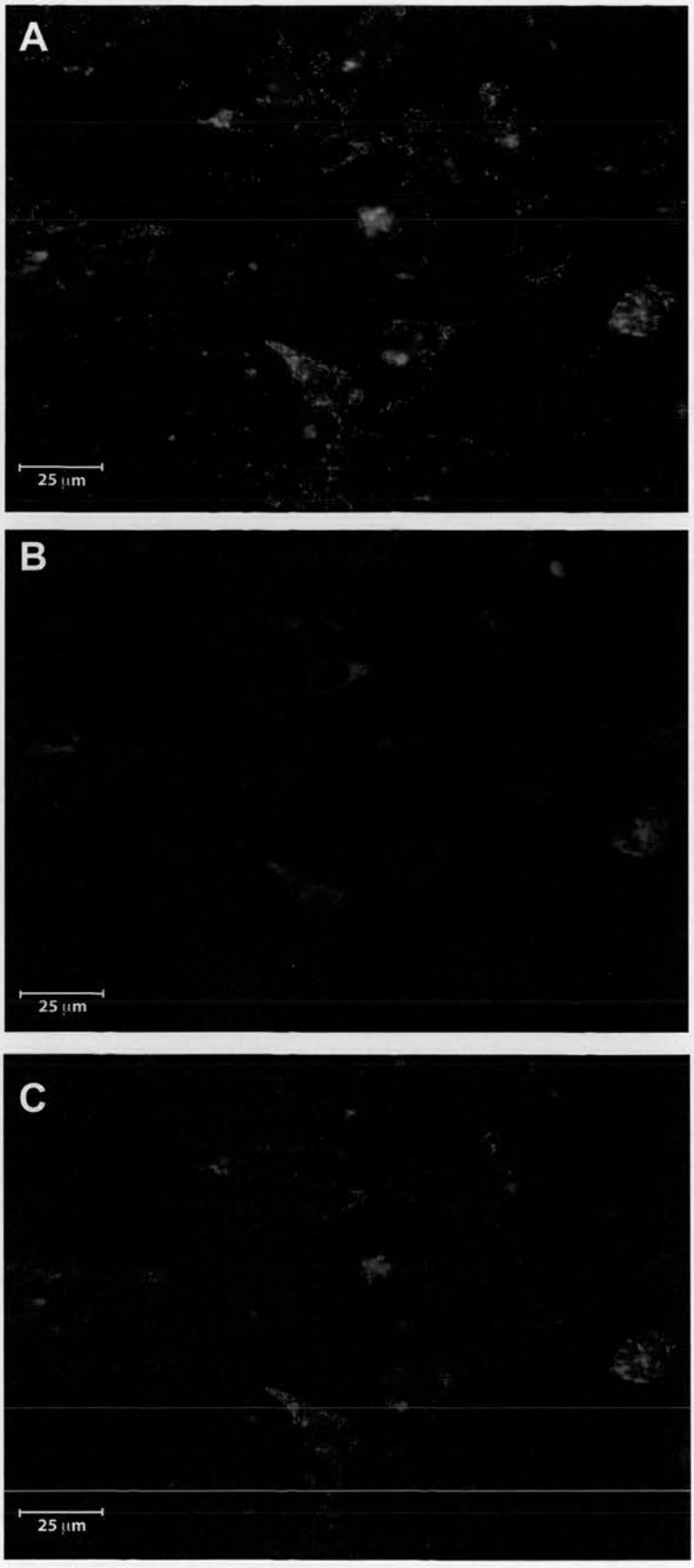

Figure 7.3.1.1

Figure 7.3.1.1. Mitochondrial membrane potential ($\Delta\Psi_m$) in LPON treated cells.

A, Red fluorescent and B, Green fluorescent image viewed under fluorescent microscopy; C, The fluorescent images merged to determine red to green fluorescent ratio. The lipophilic cationic fluorescent probe, JC-1, was used to detect $\Delta\Psi_m$. Treated cells in two-chamber slides were labeled with 5μM of JC-1 for 20 minutes at 37°C as adherent cells. Labeled cells were then viewed under fluorescent microscopy. The ratio of red-orange range (590nm) to green range (530nm) represents $\Delta\Psi_m$. To this end, red and green fluorescent images were merged using Adobe Photoshop software with threshold set at 50%.

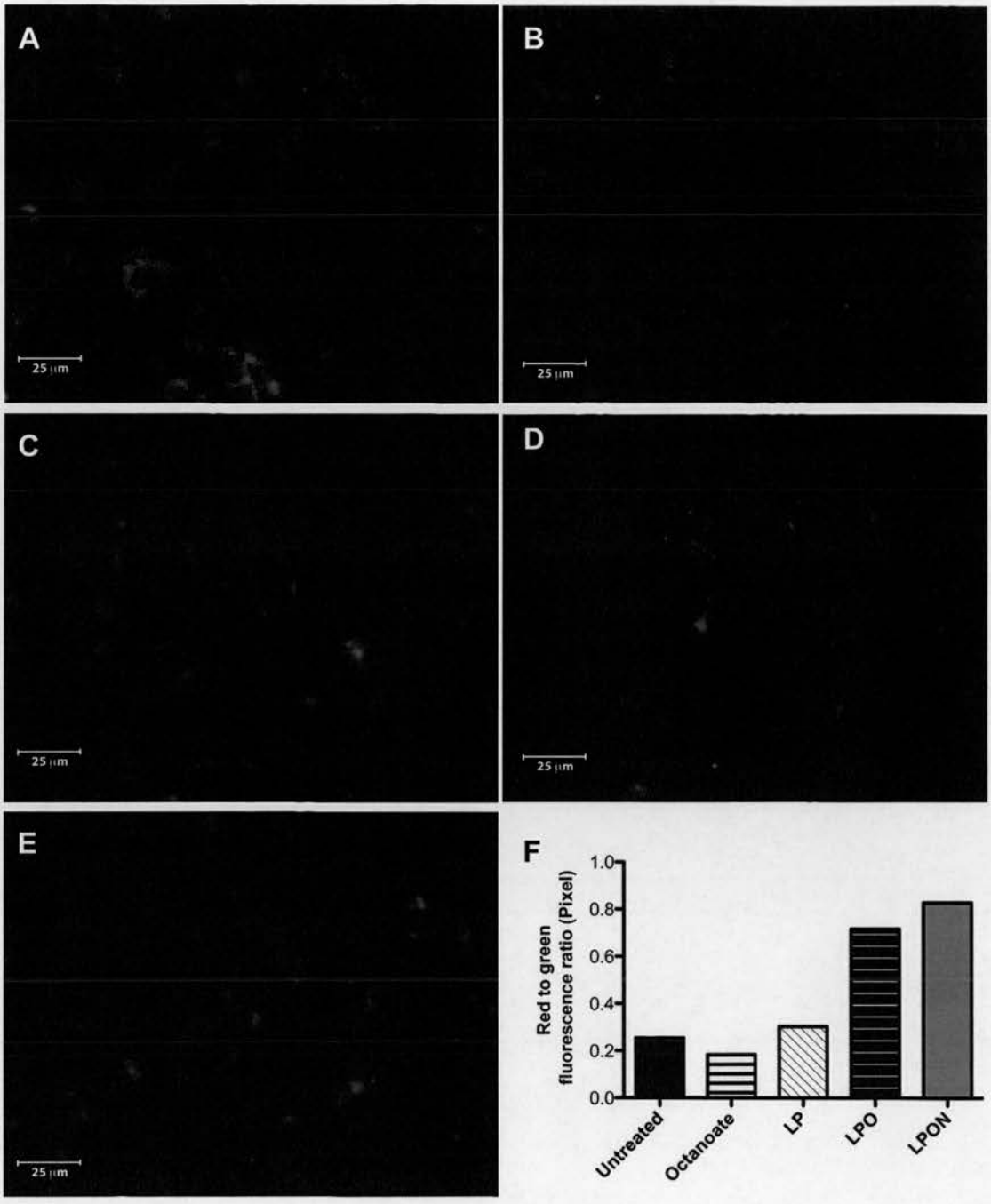

Figure 7.3.1.2. Mitochondrial membrane potential ($\Delta\Psi_m$) in treated cells.

Merged fluorescent images of A, Untreated; B, Octanoate; C, LP; D, LPO; E, LPON labeled with JC-1; F, Mean of red to green fluorescent intensity ratio obtained from the images (Panel A-E) quantified using ImageJ as described in section 7.2.1. Cells were grown and treated for 72 hours in two-chamber slides. Cells were then labeled with 5µM of JC-1 for 20 minutes at 37°C as adherent cells as described in section 7.2.1.

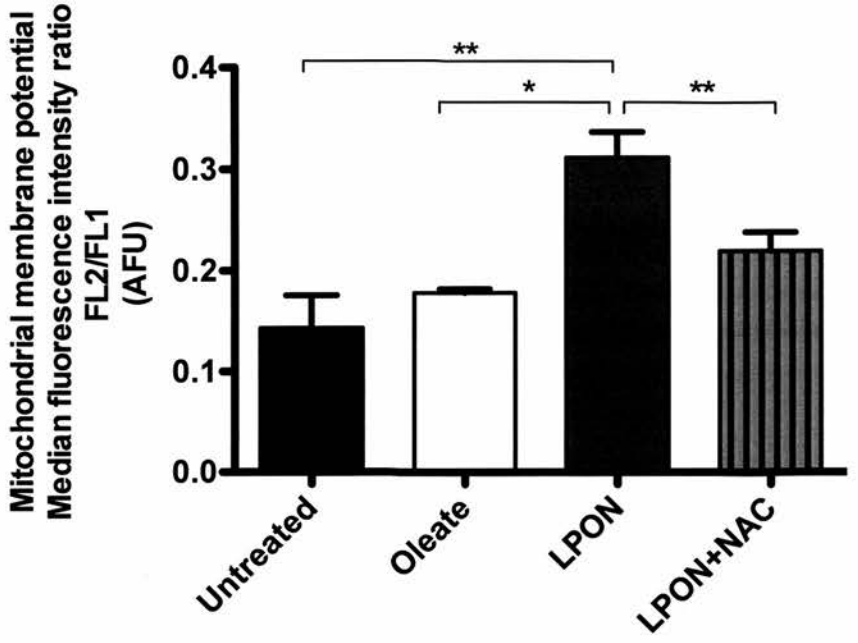

Figure 7.3.1.3. Fluorescent intensity from JC-1 labeled cells quantified by FACS. Treated cells were trypsinized and labeled with JC-1. Cells were rinsed, centrifuged and resuspended in HBSS immediately before FACS analysis. $\Delta\Psi_m$ is determined by calculating the ratio of median intensity of red to green fluorescence (FL2/FL1). Data are presented as mean ± SEM; P=0.003; $^{**}P<0.01$, $^{*}P<0.05$.

7.3.2. LPON increases cytosolic but not mitochondrial NADH/NAD$^+$ ratio

Next, we examined the impact of LPON on NADH/NAD$^+$ ratio. We anticipated that mitochondrial impairment with LPON would promote an increase in NADH/NAD$^+$ ratio. However, the previously demonstrated low basal superoxide formation with LPON is not consistent with increased NADH concentration. Indeed, as demonstrated in Figure 7.3.2. Panel A, mitochondrial NADH/NAD$^+$ ratio with LPON was similar to that seen in the untreated cells. This may explain decreased basal ROS formation but is not expected in the presence of diminished respiration. Figure 7.3.2. Panel B demonstrates a more reduced cytosolic compartment with LPON when compared with the untreated cells suggesting decreased NADH shuttling into the mitochondria, which is expected to occur in mitochondrial impairment.

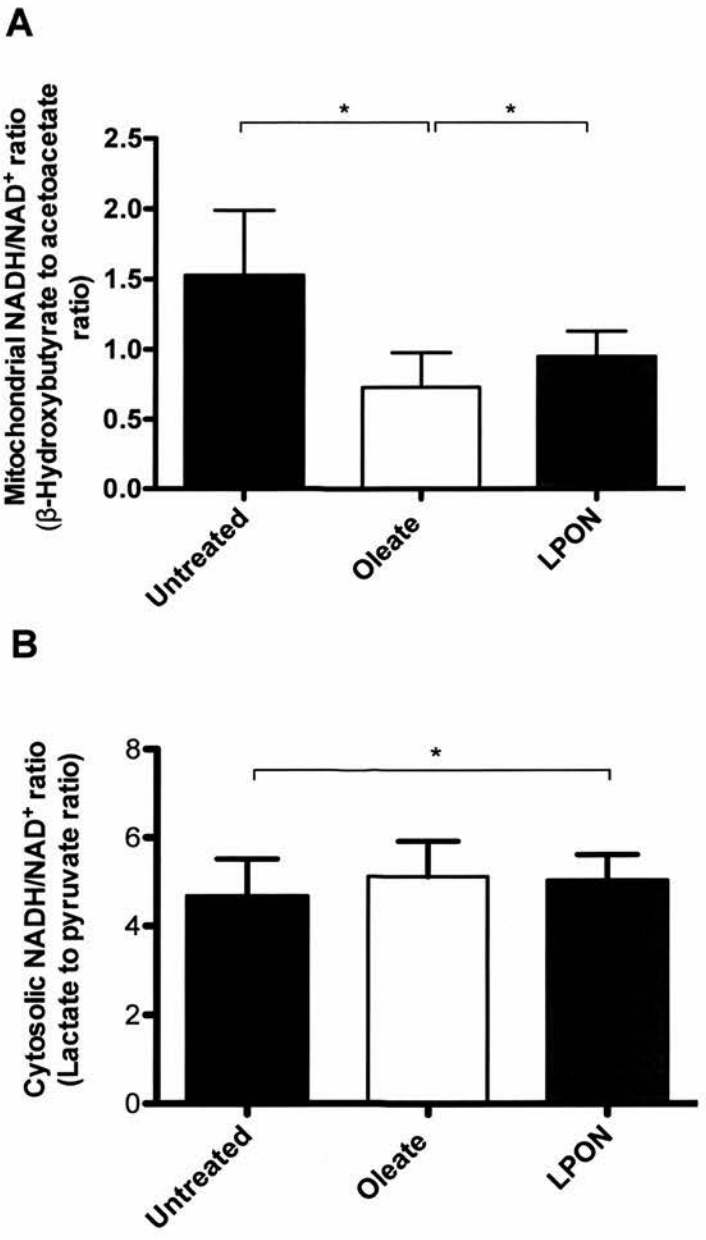

Figure 7.3.2. Mitochondrial and cytosolic NADH/NAD$^+$ ratio in treated cells.

A, Mitochondrial NADH/NAD$^+$ ratio; B, Cytosolic NADH/NAD$^+$ ratio. To determine the mitochondrial and cytosolic NADH/NAD$^+$ ratios, β-hydroxybutyrate to acetoacetate and lactate to pyruvate ratios were measured after a 72-hour treatment as described in section 7.2.3. Data are presented as mean ± SEM; A, P=0.03; $^*P$<0.05; B, P=0.04; $^*P$<0.05.

7.3.3. Further exposure to energy substrates enhances NADH/NAD$^+$ ratio

We have previously shown that the addition of further energy substrates resulted in a significant rise in superoxide formation in LPON treated cells (Figure 6.3.2). Because steatohepatitis is characterized by chronic oxidative stress, which in part, is sustained by the recurrent surge of energy substrates, we examined the impact of further LPON on mitochondrial NADH/NAD$^+$ ratio. Additionally, to dissect the individual contribution from each component of LPON, we focused on the following groups: LPON, LP, octanoate and untreated cells (control). Treated cells were rinsed and fresh culture media as specified for each group were added. Cells were treated for another 72 hours. β-Hydroxybutyrate to acetoacetate and lactate to pyruvate ratios were determined as described in section 6.2.5. Figure 7.3.3 demonstrates higher mitochondrial NADH/NAD$^+$ ratio with LPON when compared with the untreated cells indicating decreased NADH oxidation at the level of respiratory chain. The finding of higher mitochondrial NADH/NAD$^+$ ratio with LPON than either LP or octanoate suggests the synergistic effect of the energy substrates in sustaining the reduction in NADH oxidation. In contrast, cytosolic NADH/NAD$^+$ ratio was unexpectedly similar in all groups. It is possible that the similarity reflects the eventual decline in cytosolic NADH formation with metabolic changes such as gluconeogenesis, known to occur in association with mitochondrial impairment (98).

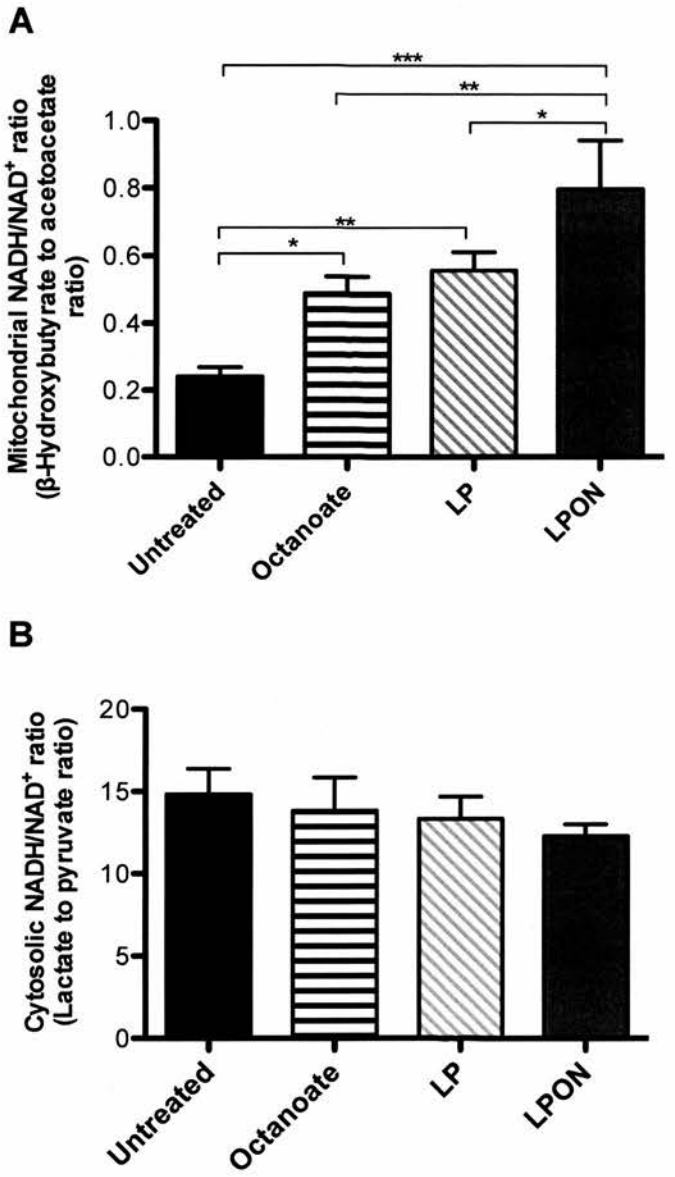

Figure 7.3.3. NADH/NAD$^+$ ratio in treated cells with further energy substrate.

A, Mitochondrial; B, Cytosolic NADH/NAD$^+$ ratio in treated cells exposed to further energy substrates. Fresh media were added to the treated cells and left for another 72 hours. Cells were then rinsed and incubated in fresh MEME (without energy substrates or FCS) for 24 hours, before a 4-hour incubation with octanoate (4mM) in PBS. β-Hydroxybutyrate to acetoacetate and lactate to pyruvate ratio were determined as described in section 6.2.5. Data are presented as mean ± SEM; A, $P<0.0001$; B, $P=0.52$; $^{***}P<0.001$, $^{**}P<0.01$, $^{*}P<0.05$.

7.3.4. NAC and α-tocopherol enhances uncoupled respiration

Another factor that can influence the level of superoxide formation is the modulation of $\Delta\Psi_m$ by proton leak. Superoxide, free fatty acids and lipid peroxidation intermediates such as HNE, have all been shown to induce proton leak by activating uncoupling proteins (UCP) (70-73). UCP allows proton slipping into the matrix independent of ATP synthase thus lowering the $\Delta\Psi_m$, diminishing superoxide formation and inducing the compensatory uncoupled respiration in the process. To examine whether proton leak influenced superoxide formation in the treated cells, respiration were measured in the presence of oligomycin. Oligomycin blocks the passage of protons through the ATP synthase leading to mitochondrial hyperpolarization thus abolishing respiration. Therefore, the respiratory activity is directly proportional to the proton leak.

In the presence of oligomycin, cell respiration was significantly diminished (Figure 7.3.4 Panel A). However, the degree of uncoupled respiration differed among the groups (Figure 7.3.4 Panel B). LPON showed a non-statistically significant trend of higher uncoupled respiration than oleate or untreated cells. Intriguingly, simultaneous treatment with LPON and either NAC or α-tocopherol had resulted in a significantly higher uncoupled respiration than the untreated cells.

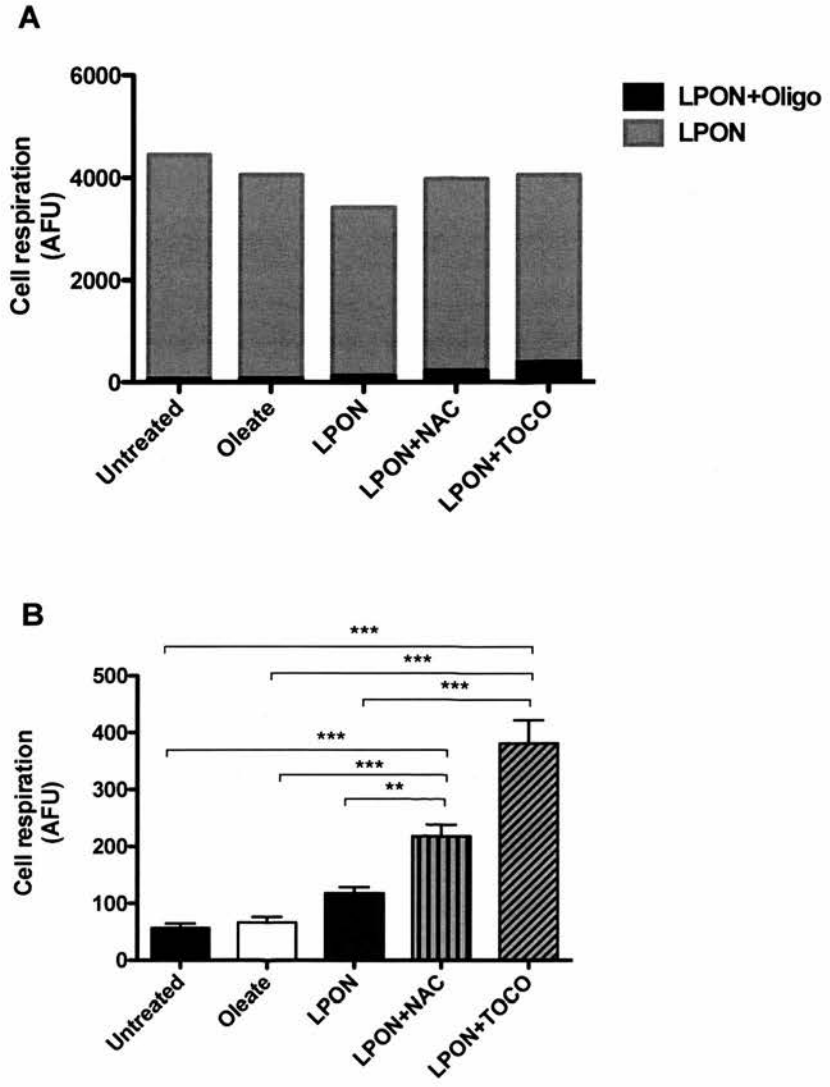

Figure 7.3.4. Cell respiration in the presence of oligomycin.

A, The effect of oligomycin on respiration; grey bar, cell respiring on LPON alone; black bar, cell respiring on LPON+oligomycin (5mg/ml); B, The varying degrees of uncoupled respiration in treated cells respiring on LPON+oligomycin (represented by black bars in A). Cells in single suspension were added to BD™ Oxygen Biosensor 96-well containing LPON+oligomycin. The fluorescent plates were read in CytoFluor Reader Series 4000 for 40 cycles, for 40 minutes. Cell respiration was determined from the linear portion of the slope of fluorescence rise. Data are presented as mean ± SEM; A, $P<0.0001$ for the variation attributable to oligomycin (two-way ANOVA); B, $P<0.0001$; $^{***}P<0.001$, $^{**}P<0.01$.

7.4. Discussion and conclusion

This chapter is focused on the modulators of superoxide formation in the treated cells. In particular, we examine the potential mechanisms that lead to the downregulation of basal ROS in LPON treated cells.

The main findings of this chapter are:

1. LPON was associated with increased $\Delta\Psi_m$.
2. Decreased basal ROS observed with LPON was mirrored by a relatively low mitochondrial NADH/NAD^+ ratio. Similarly, enhanced ROS formation following a further exposure to the energy substrates was paralleled by sustained rise in mitochondrial NADH/NAD^+ ratio.
3. The antioxidant, NAC, lowered the $\Delta\Psi_m$ and induced uncoupled respiration in LPON treated cells.

These findings highlight four important points. First, the relatively low mitochondrial NADH/NAD^+ in LPON treated cells may have been the mechanism underpinning the unexpected downregulation of basal ROS with LPON. Such a reduction in mitochondrial NADH/NAD^+ ratio can represent either enhanced NADH oxidation or decreased NADH delivery to the respiratory chain. A prerequisite for enhanced NADH oxidation is efficient mitochondrial respiration. This is exemplified by the association between preserved mitochondrial respiration and a relatively low NADH/NAD^+ ratio in oleate treated cells. In effect, active respiration with oleate maintains NADH oxidation and thereby lowering the NADH/NAD^+ ratio. Accordingly, diminished mitochondrial respiration with LPON is expected to hamper NADH oxidation, thus,

increasing the NADH/NAD$^+$ ratio. Indeed, mitochondrial NADH/NAD$^+$ ratio with LPON was higher than that seen in oleate treated cells. However, it was lower than anticipated; there was no significant difference between LPON and the untreated cells despite contrasting respiration. This raises the question whether NADH delivery to the respiratory chain may have been diminished with LPON and whether such reduction represents a metabolic adaptation gearing to minimize ROS formation.

Second, further exposures to energy substrates can potentially sustain oxidative stress. In support of this, mitochondrial NADH/NAD$^+$ (and potentially ROS formation) was increased in LPON pretreated cells after a further 72 hours of treatment. Importantly, this suggests that a continual substrates exposure can overwhelm any potential metabolic adaptations that serve to mitigate oxidative stress. This is likely to be an important mechanism of chronic oxidative stress in dietary-induced steatohepatitis.

Third, the increase in $\Delta\Psi_m$ with LPON may have reflected a relative or an absolute decline in ATP formation. The acute rise in respiration, hence active proton extrusion, may have initially bolstered ATP formation in LPON treated cells. However, the concomitant oxidative stress can affect the terminal complexes of the respiratory chain including ATP synthase, thus diminishing ATP formation. Consequently, the proton reentry into the matrix declines with the resultant rise in $\Delta\Psi_m$. In turn, increased $\Delta\Psi_m$ can diminish mitochondrial respiration further. The reduction of $\Delta\Psi_m$ by NAC supports the role of oxidative stress in modulating $\Delta\Psi_m$, the subsequent ROS formation and mitochondrial respiration.

Finally, another mechanism that may have contributed to lower $\Delta\Psi_m$ with NAC is

enhanced uncoupled respiration. This is a novel finding of this study. It is unknown whether NAC induces uncoupling proteins that might have led to the rise in uncoupled respiration. This effect may underlie the lack of improvement in respiration with NAC in the presence of the uncoupling agent, DNP. Although the uncoupled respiration may have also played a role in preserving basal and substrate-induced respiration seen with NAC, the actual contribution would have been modest. It accounted for a mere 5.6% of the 26% rise in the substrate-induced respiration observed with NAC.

In conclusion, increased energy substrates and the ensuing oxidative stress lead to an increase in $\Delta\Psi_m$, which in turn, diminishes respiration and promotes ROS formation. Excessive oxidative stress may have led to adaptations including a reduction in the mitochondrial $NADH/NAD^+$ ratio to deter a further increase in ROS formation. However, an ongoing exposure to energy substrate can overcome such adaptations resulting in chronic oxidative stress.

8. CHAPTER EIGHT

METABOLIC ADAPTATIONS ASSOCIATED WITH IMPAIRED MITOCHONDRIAL RESPIRATION

8.1. Introduction

The unanticipated findings of a relatively low mitochondrial NADH/NAD^+ with a concomitant reduction in basal ROS with LPON highlight the importance of NADH/NAD^+ ratio as one of the principal energy sensors. The three main sensors, NADH/NAD^+, ATP/AMP and acetyl-coA, are pivotal for maintaining the intricate balance between substrate oxidation and ATP formation. Should the substrate availability exceed the energy demand, these sensors can instigate a cascade of metabolic adaptations crucial to preserve ATP homeostasis. In this respect, the initial surge of ROS from substrate oxidation acts as crucial signaling molecules to fine-tune the subsequent metabolic pathways (43).

Such metabolic adaptation would include modulation of the TCA cycle activity, hence the NADH delivery to the respiratory chain. Increased energy substrates in hepatic steatosis is associated with the upregulation of TCA cycle turnover (138). In turn, high NADH concentration leads to decreased activity of pyruvate dehydrogenase, citrate synthase, isocitrate dehydrogenase, and α-ketoglutarate dehydrogenase. Decreased

TCA turnover would divert the superfluous acetyl-coA to non-oxidative pathways (Figure 8.1).

The impact of impaired mitochondrial function on the TCA cycle in steatohepatitis is yet to be delineated. It is likely that the concomitant oxidative stress exerts a considerable influence on the TCA cycle turnover; activities of α-ketoglutarate dehydrogenase, isocitrate dehydrogenase and succinate dehydrogenase have been shown to diminish with oxidative stress (139, 140).

In this study, we hypothesized that the observed reduction in mitochondrial NADH/NAD^+ ratio represents an adaptation to the diminishing mitochondrial capacity, as well as to the concurrent rise in ROS formation. In a milieu that favours NADH accumulation such as diminished respiration, such an adaptation would involve a reduction in the TCA cycle turnover, hence decreasing NADH delivery to the mitochondrial respiratory chain. Consequently, acetyl-coA is diverted towards the non-oxidative pathways.

The aims of this chapter are:

1. To determine the association between mitochondrial impairment and TCA cycle activity in LPON treated cells.
2. To examine the pattern of acetyl-coA partitioning in LPON treated cells.

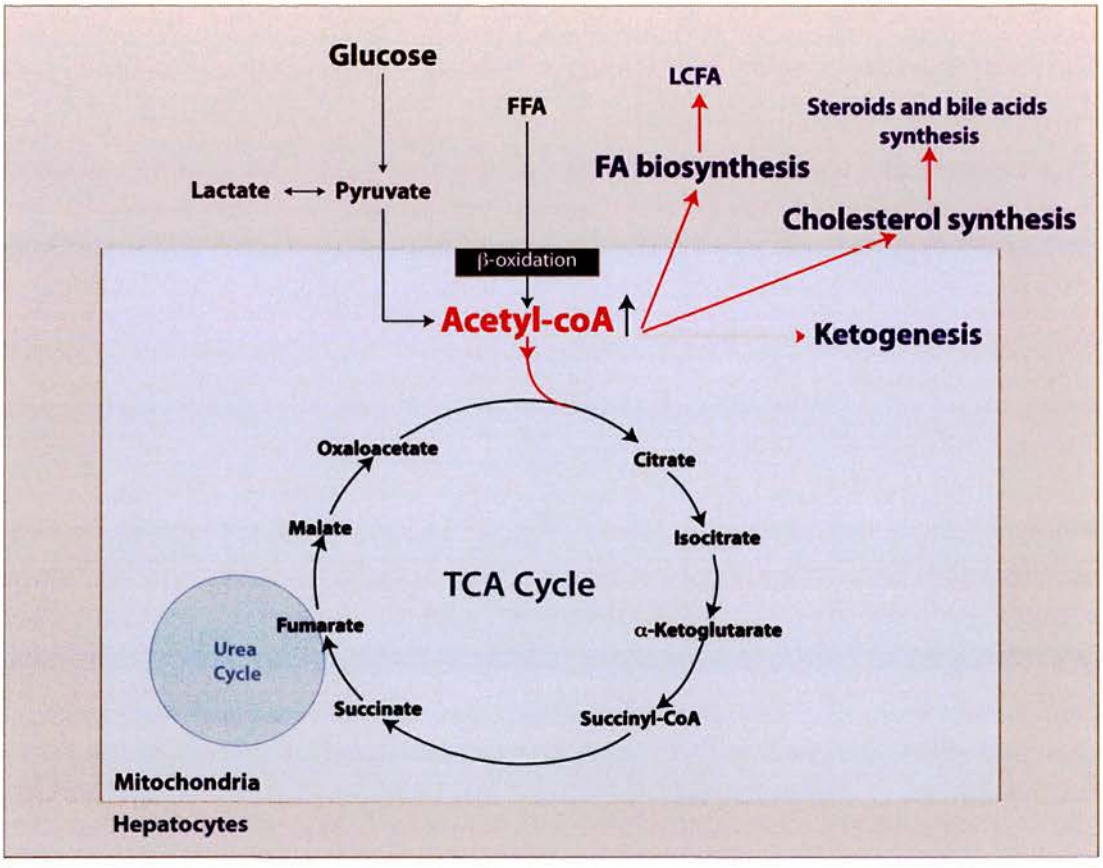

Figure 8.1. Acetyl-coA metabolism.

Acetyl-coA is the crossroad of lipid and glucose metabolism. It enters TCA cycle to generate NADH/$FADH_2$ for ATP formation. It can also be diverted towards ketogenesis, fatty acid biosynthesis or towards mevalonate pathway culminating in the formation of cholesterol. In turn, cholesterol is an important substrate for steroid and bile acid biosynthesis.

8.2. Methods

8.2.1. Metabolomics profiling

The intermediates of the TCA cycle, fatty acid biosynthesis, and mevalonate pathways were identified using metabolomics profiling as previously described in section 6.2.2.

8.2.2. Ketogenesis

The rate of ketogenesis was determined by measuring the concentrations of β-hydroxybutyrate and acetoacetate in cell culture medium immediately after the 72-hour as described in section 5.2.4. Cellular protein was quantified as described in section 2.2.5. The rate of ketogenesis was expressed as μmol/gram of total protein/hour.

8.3. Results

8.3.1. The level of TCA cycle intermediates in treated cells

To investigate whether impaired mitochondrial respiration altered TCA cycle, we conducted metabolomics profiling of TCA cycle metabolites. Using this approach, four TCA cycle intermediates were identified (Figure 8.3.1).

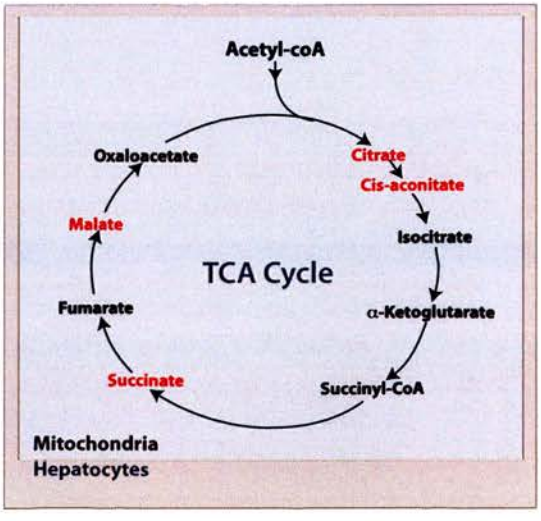

Figure 8.3.1. Schematic diagram of the TCA cycle.
TCA cycle intermediates identified in the metabolomics profiling are highlighted in red.

Figure 8.3.1.1 Panel A, shows that citrate level was lower in LPON than that seen with oleate treated cells consistent with a possible reduction in its formation from acetyl-coA and oxaloacetate. This also suggests decreased acetyl-coA flux into the TCA cycle with LPON. Moreover, the level of malate (Panel D) was significantly higher in LPON than the untreated cells. The conversion of oxaloacetate to malate occurs with increased substrates, hence reducing the availability of oxaloacetate to condense with acetyl-coA. All groups had similar levels of cis-aconitate and succinate (Panel B and C).

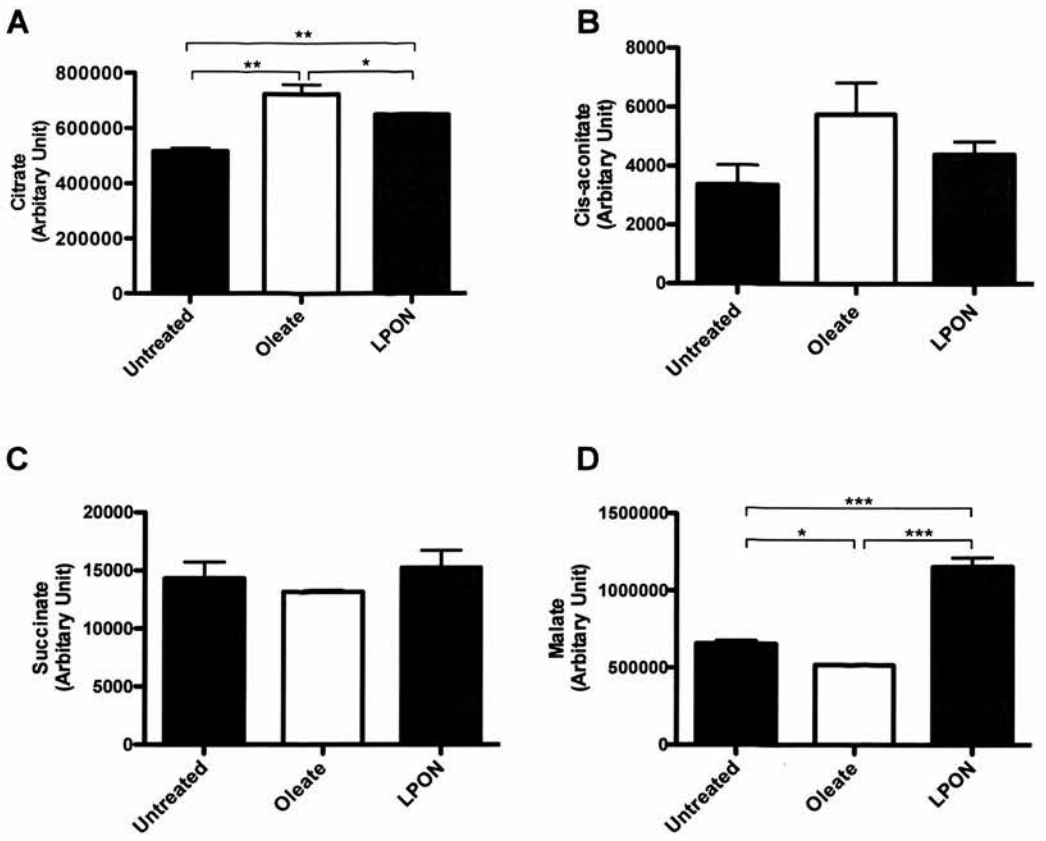

Figure 8.3.1.1. The level of TCA cycle intermediates in treated cells.

A, Citrate; B, Cis-aconitate; C, Succinate and D, Malate. Metabolites corresponded to TCA cycle intermediates were identified using metabolomics analysis in cells treated with the specified substrates. Data are presented as mean ± SD; A, Citrate, P=0.001; B, Cis-aconitate, P=0.16; C, Succinate, P=0.5; D, Malate, P<0.0001; $^{***}P$<0.001, $^{**}P$<0.01, $^{*}P$<0.05.

8.3.2. The diversion of acetyl-coA to non-oxidative pathways

Next, we examined whether altered TCA cycle observed was associated with the diversion of acetyl-coA towards non-oxidative metabolic pathways, specifically, ketogenesis, fatty acid biosynthesis, and the mevalonate pathways (Figure 8.1).

8.3.2.1. Ketogenesis is enhanced with LPON

Figure 8.3.2.1 shows higher ketogenesis with LPON than the untreated cells. Co-treatment of LPON+NAC led to a considerable reduction in ketogenesis by 41% when compared with LPON alone. It is likely that the preserved respiration and the potential reduction in ROS with NAC improved the acetyl-coA flux into the oxidative pathway.

8.3.2.2. Increased fatty acid biosynthesis intermediates with LPON

In the presence of energy substrates excess, citrate is shuttled into the cytoplasm to be reconverted to acetyl-coA, which is subsequently incorporated in fatty acid biosynthesis. We identified three intermediates for fatty acids biosynthesis using metabolomics study. Figure 8.3.2.2 shows that the quantity of fatty acid biosynthesis intermediates identified was higher in LPON compared with untreated cells suggesting increased acetyl-coA diversion towards fatty acid biosynthesis.

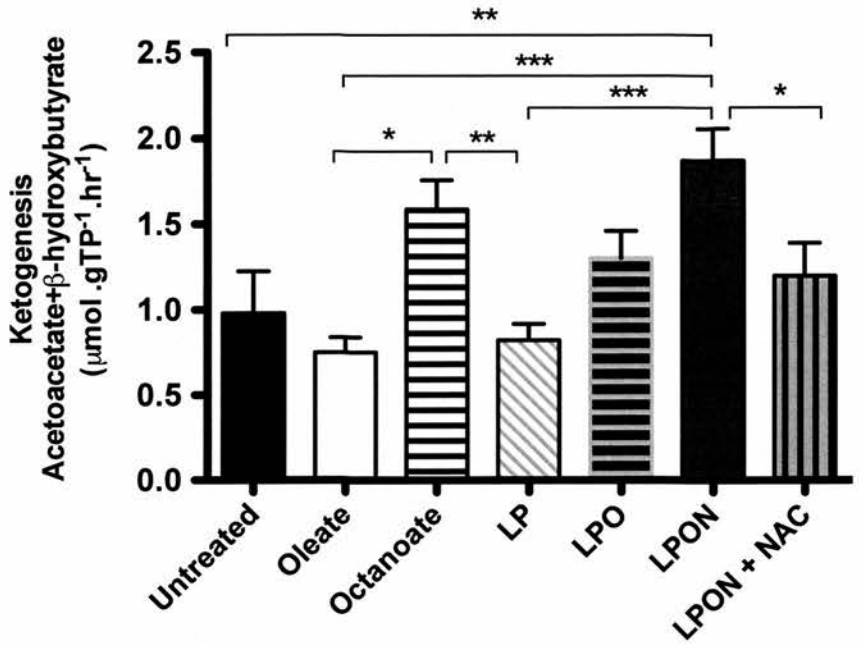

Figure 8.3.2.1. Ketogenesis in treated cells.

C3A cells were treated for 72 hours. A separate group of cells were simultaneously treated with LPON and NAC (10mM). Acetoacetate and β-hydroxybutyrate concentrations were measured in the supernatant after 72 hours as detailed in 5.2.4. Data are presented as mean ± SEM; P=0.0001; $^{***}P<0.001$, $^{**}P<0.01$, $^{*}P<0.05$.

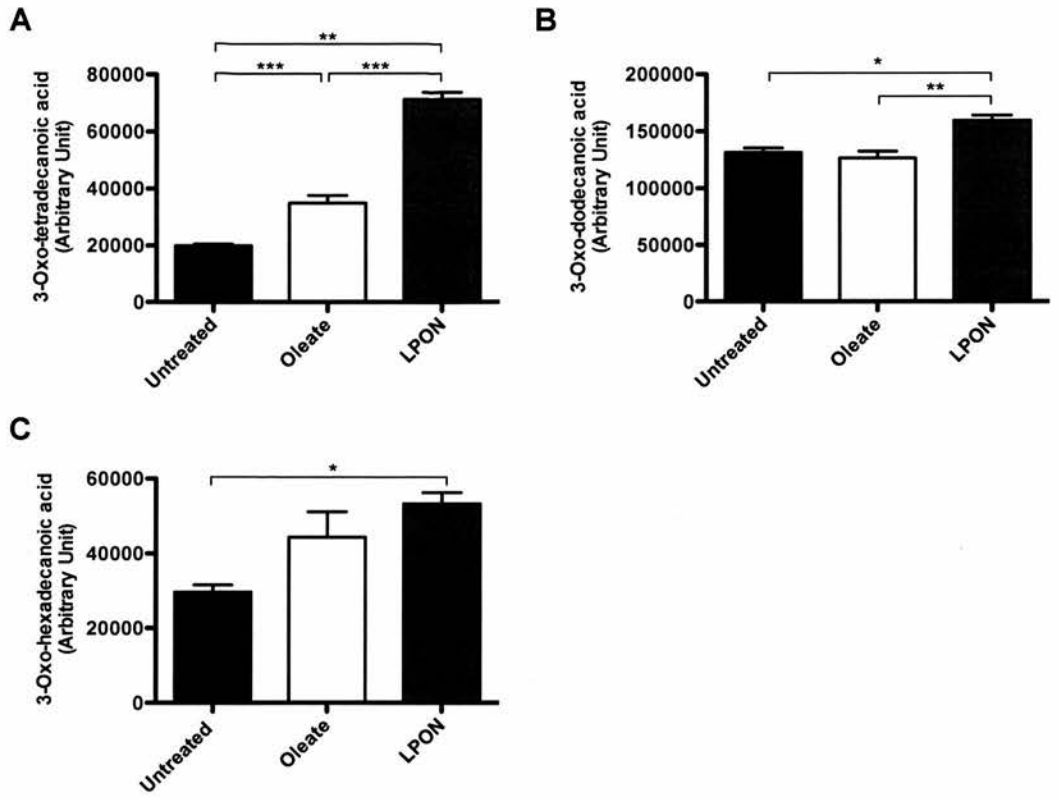

Figure 8.3.2.2. Fatty acid biosynthesis intermediates in treated cells.

A, 3-Oxo-tetradecanoic acid; B, 3-Oxo-decanoic acid; C, 3-Oxo-hexadecanoic acid. Using the metabolomics study, three metabolites corresponded to the fatty acid biosynthesis intermediates were identified in cells treated with the specified combination of energy substrates for 72 hours. Data are presented as mean ± SD; A, $P<0.0001$; B, $P=0.005$; C, $P=0.02$; $^{***}P<0.001$, $^{**}P<0.01$, $^{*}P<0.05$.

8.3.2.3. Mevalonate pathways is not increased with LPON

Acetyl-coA can also be channeled towards mevalonate pathways for the synthesis of cholesterol, steroid hormones and bile acids (Figure 8.3.2.3).

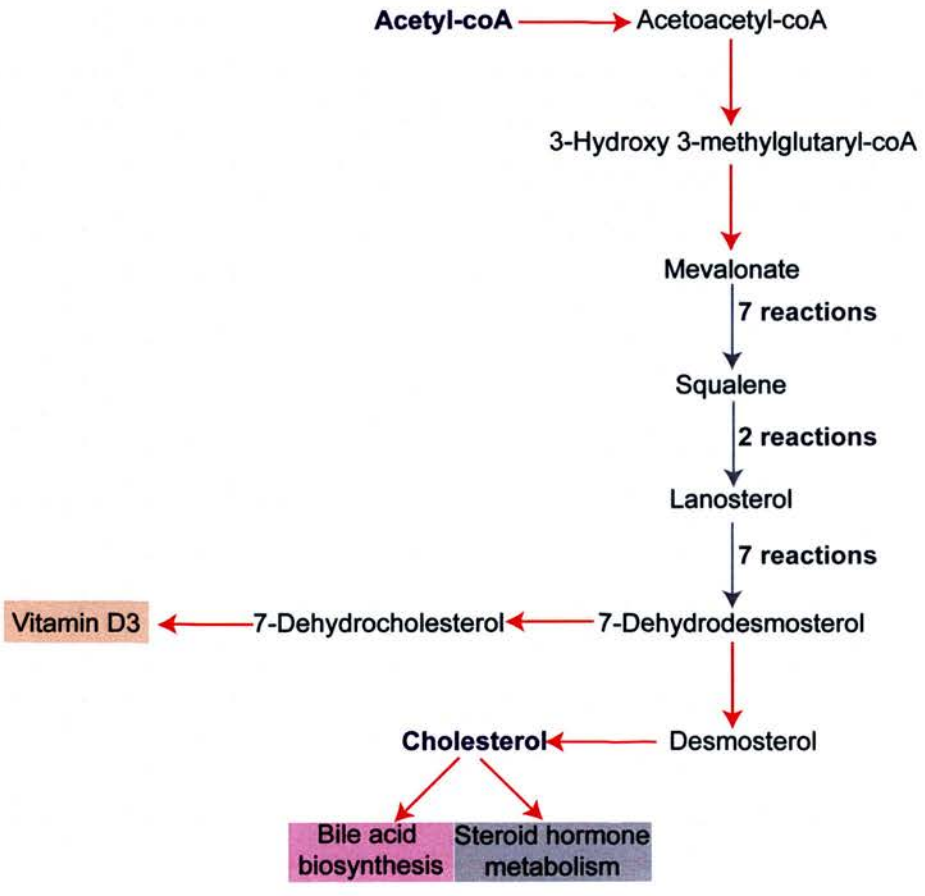

Figure 8.3.2.3. Mevalonate pathways.

Schematic diagram illustrating mevalonate pathway for the synthesis of cholesterol, steroid hormones, bile acids, and vitamin D3.

Using metabolomics analysis, the intermediates of mevalonate pathway were identified; three were intermediates of bile acid synthesis; three were involved in the steroid hormone synthesis, mevalonic acid (the main precursor for mevalonate pathway) and 7-dehydrodemosterol (an intermediate for cholesterol biosynthesis). Figure 8.3.2.3.1 demonstrates the level of mevalonic acid and 7-dehydrodesmosterol. Although these levels were higher with oleate than that seen with LPON, the differences did not reach statistical significance. In contrast, the level of bile acid intermediates; taurocholate (Figure 8.3.2.3.2 Panel A), glycodeoxycholate (Figure 8.3.2.3.2 Panel B), glycocholate (Figure 8.3.2.3.2 Panel C) were significantly elevated with oleate when compared with LPON or the untreated cells. Similarly, the concentrations of cortol, an intermediate for steroid hormone biosynthesis (Figure 8.3.2.3.3 Panel A) and vitamin D3 metabolites (Figure 8.3.2.3.3 Panel B and C) were higher in oleate treated cells when compared with LPON or the untreated cells.

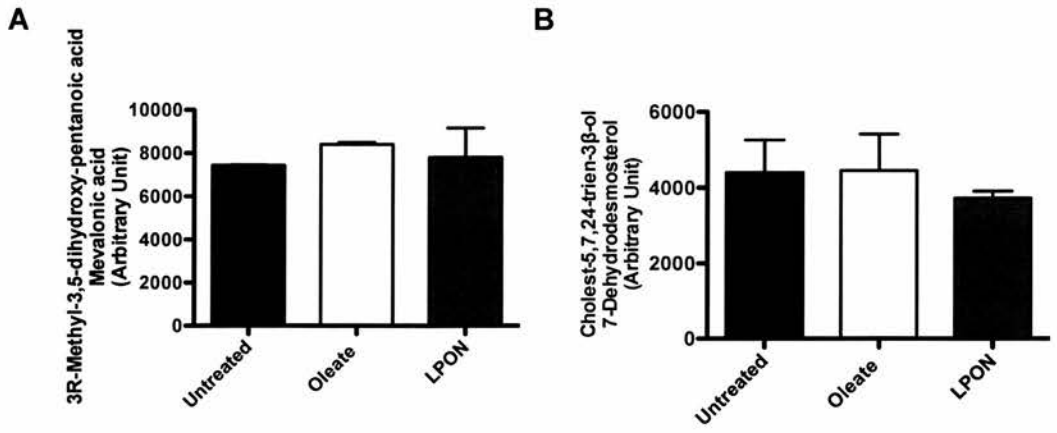

Figure 8.3.2.3.1. The concentration of mevalonate pathway intermediates in treated cells.

A, Mevalonic acid; B, 7-Dehydrodesmosterol. Using metabolomics analysis, metabolites corresponded to the intermediates in cholesterol biosynthesis, mevalonic acid and 7-dehydrodesmosterol, were identified in treated cells. Data are presented as mean ± SD; A, P=0.37; B, P=0.46.

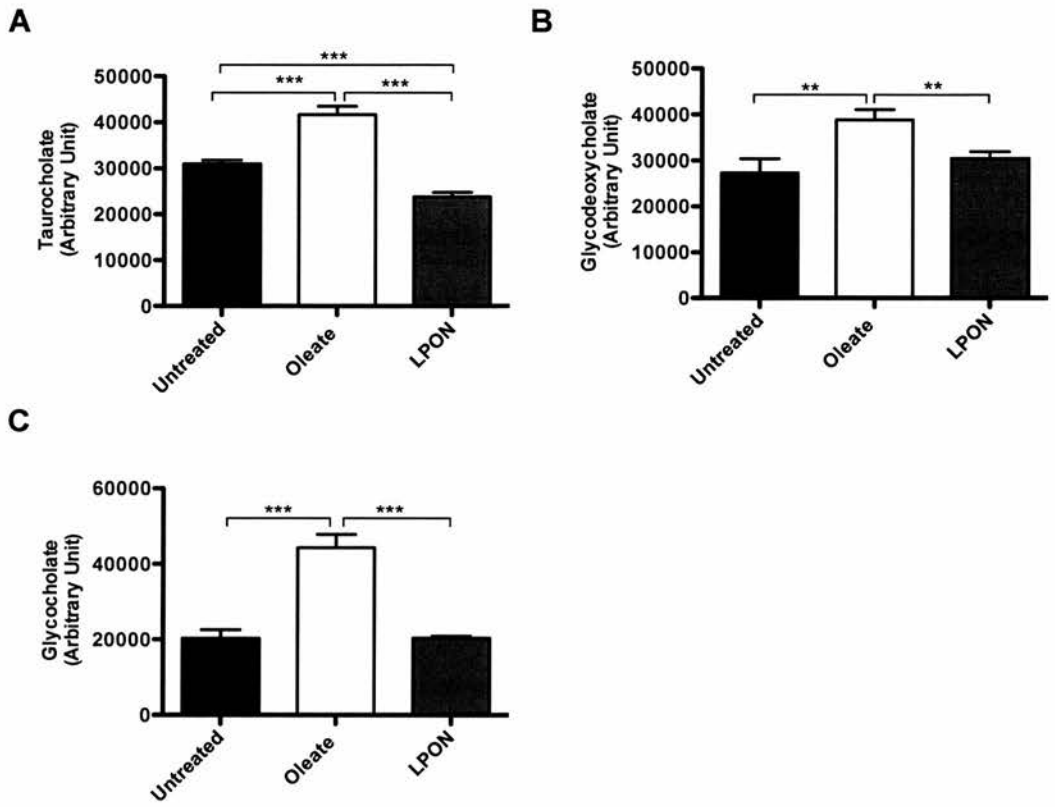

Figure 8.3.2.3.2. The concentration of bile acid intermediates in treated cells.

A, Taurocholate; B, Glycodeoxycholate; C, Glychocolate. Using metabolomics analysis, metabolites corresponded to bile acid intermediates were identified in treated cells. Data are presented as mean ± SD; A, $P<0.0001$; B, $P=0.002$; C, $P<0.0001$; $^{***}P<0.001$, $^{**}P<0.01$.

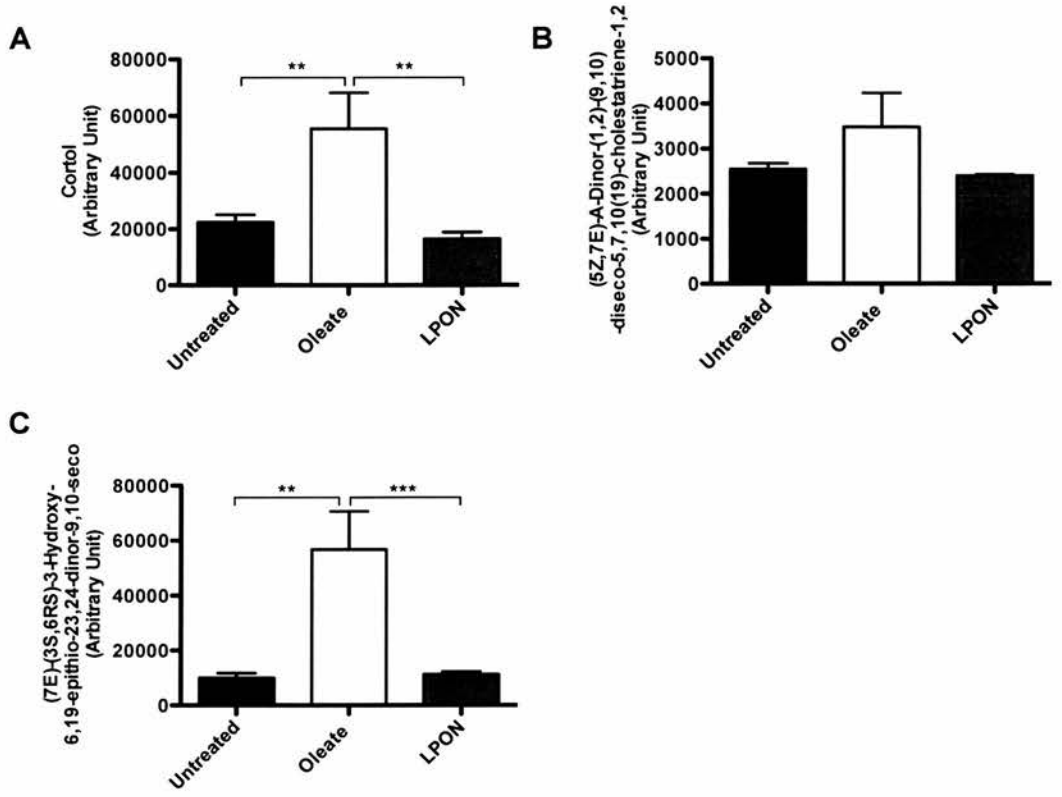

Figure 8.3.2.3.3. The concentration of steroid and vitamin D3 metabolites in treated cells.

A, Cortol; B, (5Z,7E)-A-Dinor-(1,2)-(9,10)-diseco-5,7,10(19)-cholestatriene-1,2,25-triol C, (7E)-(3S,6RS)-3-Hydroxy-6,19-epithio-23,24-dinor-9,10-seco-5(10),7-choladien-22-al S,S-dioxide. Cortol, an intermediate in steroid hormone biosynthesis, and both vitamin D3 metabolites were identified in cells treated with energy substrates for 72 hours. Data are presented as mean ± SD; A, P=0.001; B, P=0.04; C, P=0.0006; $^{***}P<0.001$, $^{**}P<0.01$.

8.4. Discussion and conclusion

In this chapter, we sought to examine whether the observed reduction mitochondrial NADH/NAD^+ ratio represents an adaptation to the diminishing mitochondrial capacity. We postulated that such an adaptation would involve a reduction in the TCA cycle turnover; hence decreasing NADH delivery to the respiratory chain as well as lowering the NADH/NAD^+ ratio.

The main findings of this chapter are:

1. Mitochondrial impairment with LPON was associated with altered TCA cycle.
2. Acetyl-coA in LPON treated cells was diverted towards ketogenesis and fatty acid biosynthesis, but not the mevalonate pathways.

Our data suggest possible decreased TCA cycle turnover in the presence of mitochondrial impairment. In support of this, the concentration of malate was increased with LPON. It is possible that the surge of energy substrates and the subsequent mitochondrial impairment with LPON would initially lead to a rise in NADH/NAD^+ ratio such that it favours the conversion of oxaloacetate to malate (Figure 8.4). The lowering of oxaloacetate can dampen the TCA cycle turnover, thus diminishing the subsequent NADH formation (141). In effect, such reduction in oxaloacetate decreases its availability to condense with acetyl-coA to form citrate. Indeed, citrate levels were lower with LPON compared with oleate. Furthermore, citrate synthase activity is diminished in the presence of oxidative stress as well as in elevated NADH/NAD^+ (98, 142).

The diversion of acetyl-coA towards ketogenesis is yet another classic acute metabolic adaptation to the reduction in TCA cycle activity. Acetyl-coA is also diverted towards free fatty acid synthesis with LPON. However, it is likely that acetyl-coA diversion is influenced by cell demand and ATP availability. For example, acetyl-coA did not appear to be diverted towards the mevalonate pathways with LPON. Indeed, in the absence of ATP formation, for example in mitochondrial dysfunction, mevalonate pathways are down regulated.

These adaptations are necessary in the presence of mitochondrial impairment. Excessive supply of NADH in the presence of electron flow disruption (for example, in ROS-induced mitochondrial injury) can promote further ROS formation. Thus, these adaptations are not only geared to achieve ATP homeostasis but also to minimize ROS formation.

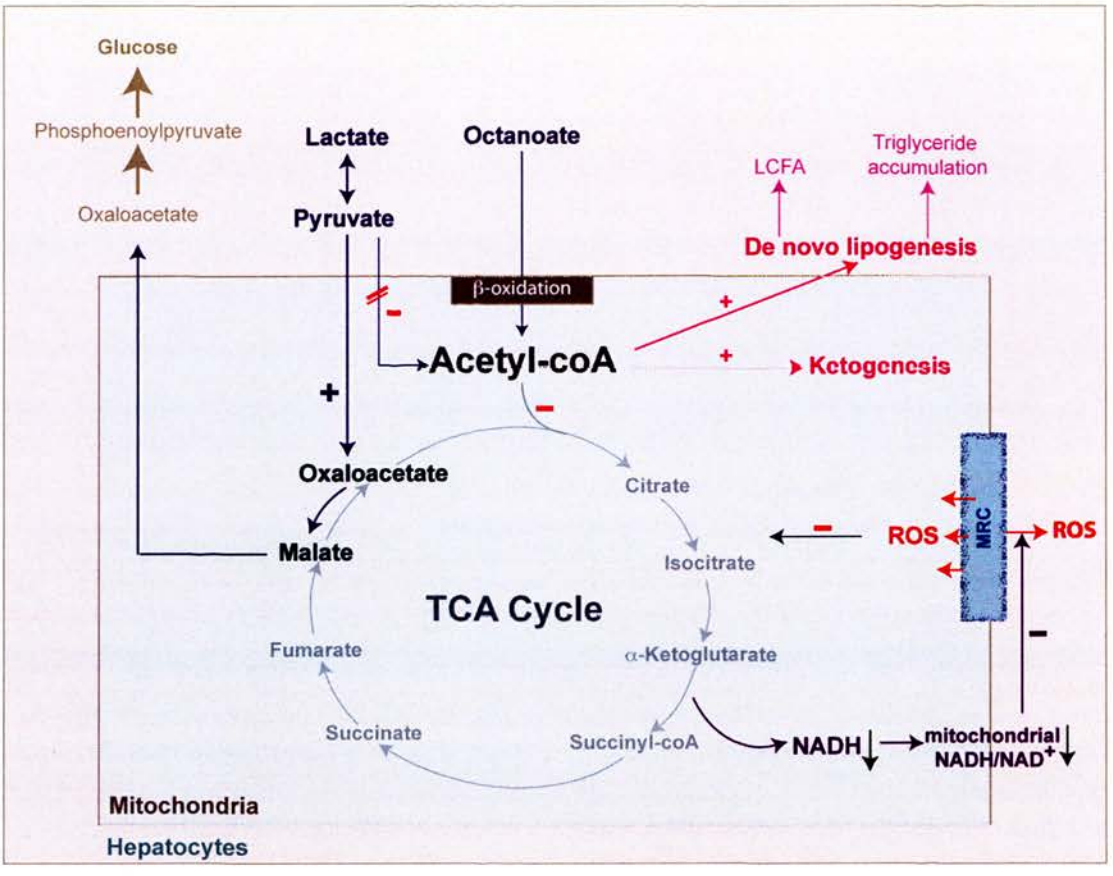

Figure 8.4. Metabolic adaptations instigated by the rise in energy substrates.

Increased energy substrates availability initially enhanced NADH/NAD^+ ratio with resultant rise in mitochondrial ROS formation. This would eventually decrease citrate synthase activity as well as favouring the conversion of oxaloacetate to malate, thus slowing down the TCA cycle turnover. The reduction in the TCA cycle leads to two important consequences. First, NADH formation declines, lowering the NADH/NAD^+ ratio. Second, acetyl-coA accumulates leading to its diversion to non-oxidative pathways.

9. CHAPTER NINE

THE RELATIONSHIP BETWEEN TRIGLYCERIDE ACCUMULATION, REACTIVE OXYGEN SPECIES, MITOCHONDRIAL FUNCTION AND GLUCOSE METABOLISM

9.1. Introduction

The association between insulin resistance and hepatic steatosis is well established. Hepatic triglyceride content has been shown to correlate with hepatic insulin resistance, and reducing hepatic steatosis either pharmacologically or through dietary modification leads to significant improvements in hepatic insulin resistance in humans (89, 90, 143-145). In rodents, manipulation of enzymes involved in triglyceride synthesis to reduce liver fat has been shown to enhance insulin sensitivity.

However, the molecular details that underlie this association remain to be elucidated. Furthermore, there is emerging evidence that supports the dissociation between insulin resistance and hepatic triglyceride accumulation. It is unclear if triglyceride accumulation *per se* mediates insulin resistance or whether it hinges on concurrent factors, notably oxidative stress.

The presence of mitochondrial impairment is adding to the complexity of this relationship. Although mitochondrial function is strongly associated with insulin

resistance, the causal relationship remains unclear; is mitochondrial dysfunction a cause or a consequence, or simply a parallel event to the development of insulin resistance? Importantly, the question remains whether altered glucose metabolism represents a metabolic adaptation to prevent mitochondrial overload in the presence of increased energy substrates and mitochondrial impairment.

The aims of this chapter are:

1. To examine gluconeogenic capacity in the treated cells, and determine the contribution of triglyceride and ROS in gluconeogenesis.
2. To determine the effect of LPON on factors that can modulate endogenous glucose formation specifically glycolysis and glycogen turnover.

9.2. Methods

9.2.1. Glucose and acyl carnitine concentrations

These were identified using the metabolomics approach as described in 6.2.2.

9.2.2. Gluconeogenic capacity

Gluconeogenic capacity was determined by measuring glucose flux following a 4-hour incubation with LPON. Culture supernatant was removed and cells were rinsed with PBS. LPON was then added to all groups. Glucose concentration in the incubation medium was determined at the end of the incubation using Bergmeyer's enzymatic methods (129). Briefly, glucose concentration corresponds to the NADH produced from the following reactions:

$$\text{Glucose} + \text{ATP} \xrightarrow{\text{Hexokinase}} \text{Glucose 6-phosphate}$$

$$\text{Glucose 6-phosphate} + \text{NAD}^+ \xrightarrow[\text{dehydrogenase}]{\text{Glucose 6-phosphate}} \text{Gluconolactone 6-phosphate} + \text{NADH}$$

The assay was prepared using: NAD^+ (0.34mg/ml), ATP (2.5µl/ml), glucose 6-phosphate dehydrogenase (0.25µl/ml), hexokinase (0.5µl/ml) in PBS. The assay (1ml) was added to the supernatant of treated cells (200µl), homogenized and analysed using spectrophotometer (340nm). The concentration was averaged for total protein to obtain µmol. gram of total protein^{-1}.hour^{-1} as described in section 2.1.5.

9.2.3. The effect of insulin on treated cells

Cells were grown and treated with LPON in 6-well plates as previously described. After 72 hours, the supernatant was removed and cells were rinsed. The culture media were

replaced with MEME without FBS for 24 hours. Cells were then rinsed before a 4-hour incubation with insulin at the specified concentrations determined from a dose-response curve (Supplementary Data 2). Glucose flux in the incubation medium was determined as described in section 9.2.2. Lactate and pyruvate concentrations were determined as described in section 6.2.2.

Glycogen is the main source of endogenous glucose formation in the absence of gluconeogenic substrate. Glycogen breakdown results in the formation of glucose 6-phosphate, which can either enter glycolysis or subject to glucose 6-phosphatase to produce glucose (Figure 9.2.3). Thus, the final concentrations of lactate, pyruvate, and glucose (2x(glucose)+lactate+pyruvate) reflect the total flux through glucose 6-phosphate. Similarly, the percentage of glycogen diverted to glucose or glycolysis can be calculated as follows:

Percentage of glycogen diverted to glucose:

$$(2 \times (\text{glucose}) / (2 \times (\text{glucose})) + \text{lactate} + \text{pyruvate}) \times 100$$

Percentage of glycogen diverted to glycolysis:

$$(\text{Lactate} + \text{pyruvate} / (2 \times (\text{glucose})) + \text{lactate} + \text{pyruvate}) \times 100$$

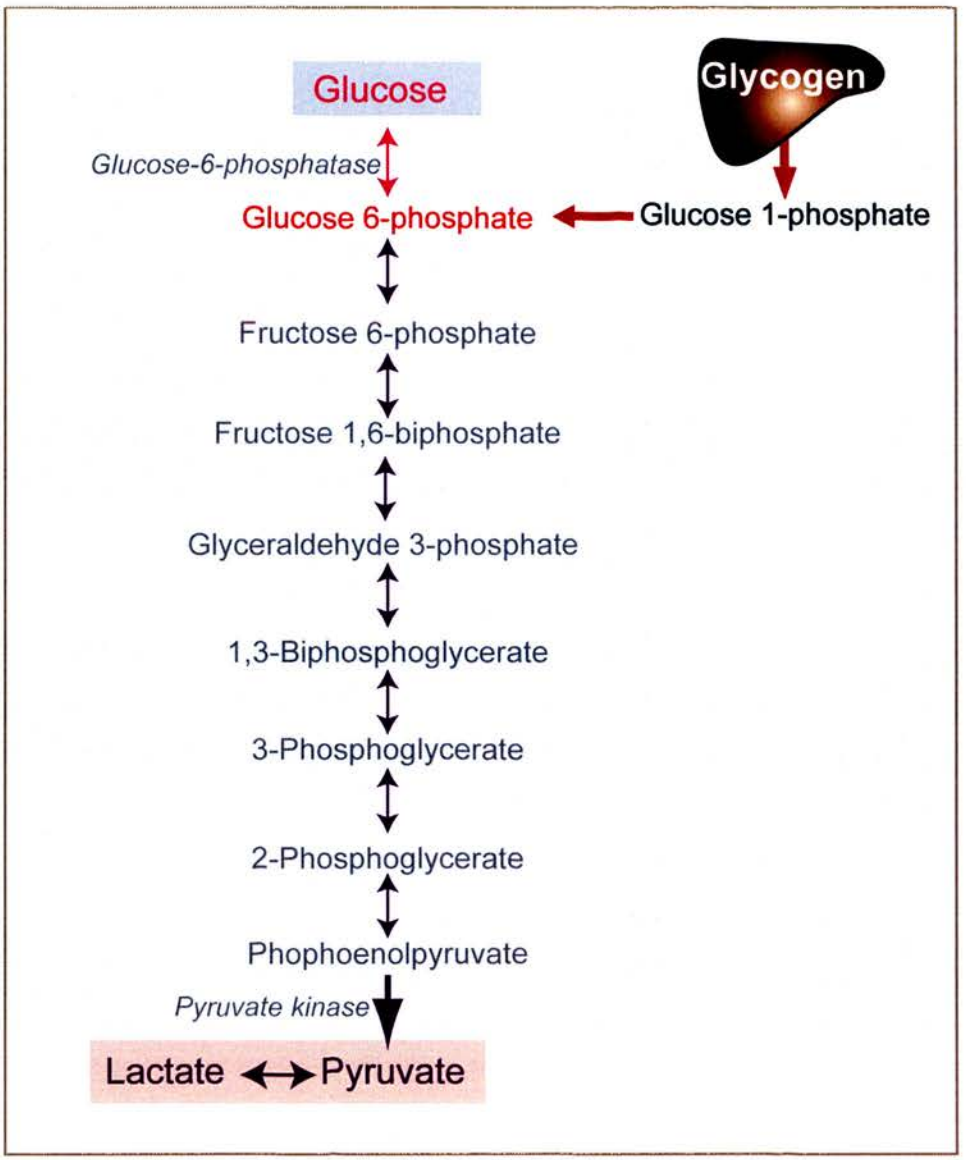

Figure 9.2.3. Flux through glucose 6-phosphate.

Glycogen breakdown results in the formation of glucose 6-phosphate, which can enter the glycolytic pathway (purple arrows) or can be converted to glucose by glucose 6-phosphatase (pink arrow). Thus, the overall flux through glucose 6-phosphate can be determined from the concentrations of glucose, lactate and pyruvate. The percentage of glycogen diverted to glucose and glycolytic pathway can be measured as described above.

9.2.4. Glycogen detection using Periodic Acid Schiff (PAS) Staining

Cells were grown and treated in two-chamber slides until 70% confluent. Cells were fixed in 10% formaldehyde. Mr. Robert Morris from Queen's Medical Research Institute kindly performed the PAS staining. Briefly, slides were rehydrated and oxidized in 0.5% periodic acid solution for 5 minutes. Slides were then rinsed in distilled water, placed in Schiff reagent for 15 minutes, rinsed in warm water for 5 minutes and counterstained in hematoxylin before mounting. Images were viewed under light microscopy. At least three different slides from each group were analysed using ImageJ. A threshold for each image was set to highlight the stained area. Using 'analyze particle' function, the extent of the stained area was quantified and data are expressed in pixel.

9.2.5. Lipid droplets surface area to volume ratio

Cells were cultured on a chamber slide and treated for 72 hours before being stained using BODIPY 493/503 as described in section 3.2.3. To determine the lipid droplets surface area to volume ratio, the stack of 3D BODIPY confocal images were analysed using Volocity 3D image analysis software (Perkin Elmer, Waltham, MA, USA).

9.3. Results

9.3.1. Glucose formation is enhanced in LPON treated cells

Having confirmed the presence of insulin receptors in treated C3A cells (Supplementary data 1.1), we then focused on the impact of LPON on glucose metabolism. In the presence of energy substrate excess, acetyl-coA exerts a negative feedback on pyruvate dehydrogenase (PDH) thus allowing lipid oxidation to take precedence over that of glucose. Using metabolomics, peaks that corresponded to D-glucose were identified at the end of the treatment. As shown in Figure 9.3.1, glucose concentration was higher in LPON than that seen with the untreated cells. In contrast, the concentration of glucose with oleate was similar to the untreated cells.

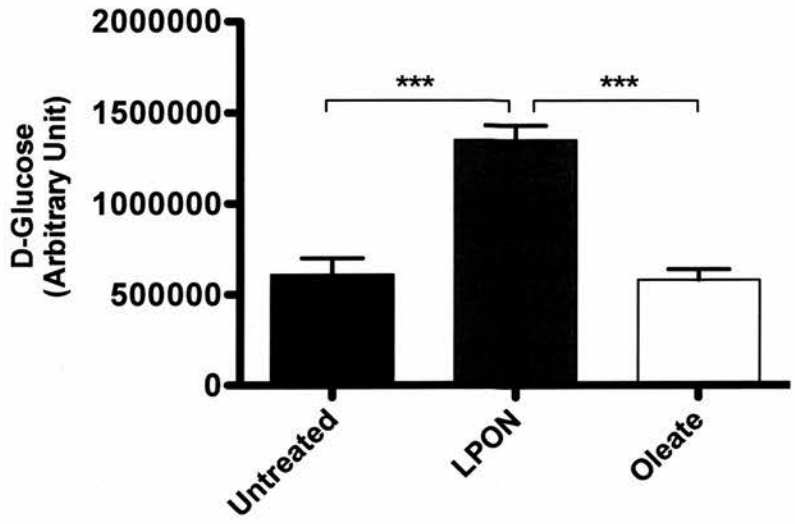

Figure 9.3.1. Glucose concentration in treated cells.

Using the metabolomics technique as described in 9.2.1, peak that corresponded to D-glucose was identified. Cells were treated for 72 hours. Data are presented as mean ± SD; $P<0.0001$; $^{***}P<0.001$.

9.3.2. Gluconeogenic capacity is enhanced in LPON treated cells

To investigate whether increased glucose formation with LPON is attributable to enhanced gluconeogenic capacity, LPON were added to all groups as described in section 9.2.2. Figure 9.3.2 represents glucose concentrations at the end of a 4-hour incubation with LPON. Glucose concentration with LPON was significantly higher than that seen with oleate or the untreated cells consistent with enhanced gluconeogenic capacity in these cells. Importantly, concomitant treatment with NAC resulted in a 43% reduction in glucose formation in the LPON treated cells suggesting the role of ROS in promoting gluconeogenesis. Interestingly, cells treated with octanoate alone had higher gluconeogenic capacity than that seen with oleate treated cells.

9.3.3. Glycolysis is diminished in LPON treated cells

Next, we examined whether enhanced glucose formation with LPON was associated with decreased glycolysis. Glycolysis was determined by measuring lactate and pyruvate concentrations following a 4-hour incubation with glucose (20mM). Figure 9.3.3 demonstrates lower glycolysis with LPON than the untreated cells. Furthermore, despite the similarity in gluconeogenic capacity, glycolysis was lower with LPON compared with LPO.

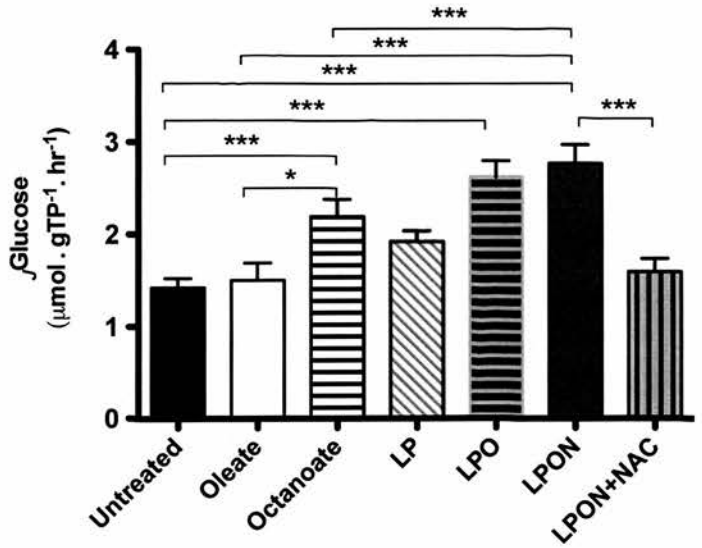

Figure 9.3.2. Gluconeogenic capacity in treated cells.

Glucose flux was determined at the end of a 4-hour incubation period as described in section 9.2.2. Data presented are presented as mean ± SEM; $P<0.0001$; $^{***}P<0.001$, $^{*}P<0.05$. LPON+NAC; LPON+N-acetylcysteine.

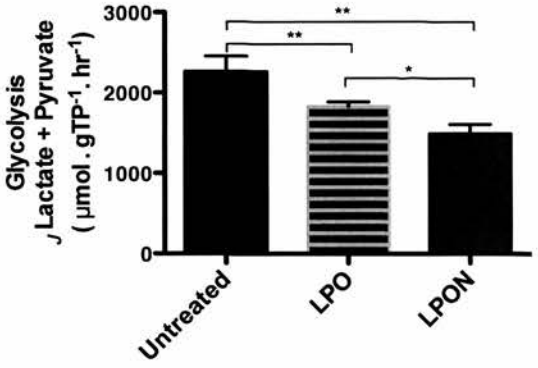

Figure 9.3.3. Glycolysis flux in treated cells.

Culture supernatants from treated cells were replaced with MEME (without FBS) for 24 hours. Cells were then rinsed and incubated in glucose (20mM) in the presence of octanoate (4mM) for 4 hours. Lactate and pyruvate concentrations were measured (section 5.2.4). Data are presented as mean ± SEM; $P<0.0001$; $^{**}P<0.01$, $^{*}P<0.05$.

9.3.4. Glycogen accumulation is reduced with LPON treated cells

We examined the contribution of glycogen turnover towards endogenous glucose formation with LPON. First, we examined whether LPON altered the amount of glycogen accrued in C3A cells. PAS staining was performed and quantified using ImageJ as described in section 9.2.4. Panel A of Figure 9.3.4 shows that glycogen was rendered bright magenta with PAS staining. Panel B and C are representative images of PAS stained untreated and LP cells respectively. Panel D demonstrates a PAS stained image set to a threshold using ImageJ to highlight the magenta area of glycogen accumulation. Panel E and F represent PAS stained images of LPON and octanoate treated cells. LPON and octanoate treated cells have visibly less magenta areas than that seen with LP and untreated cells. Indeed, quantification using ImageJ confirmed that glycogen accumulation in LPON was lower than the untreated cells (Panel G).

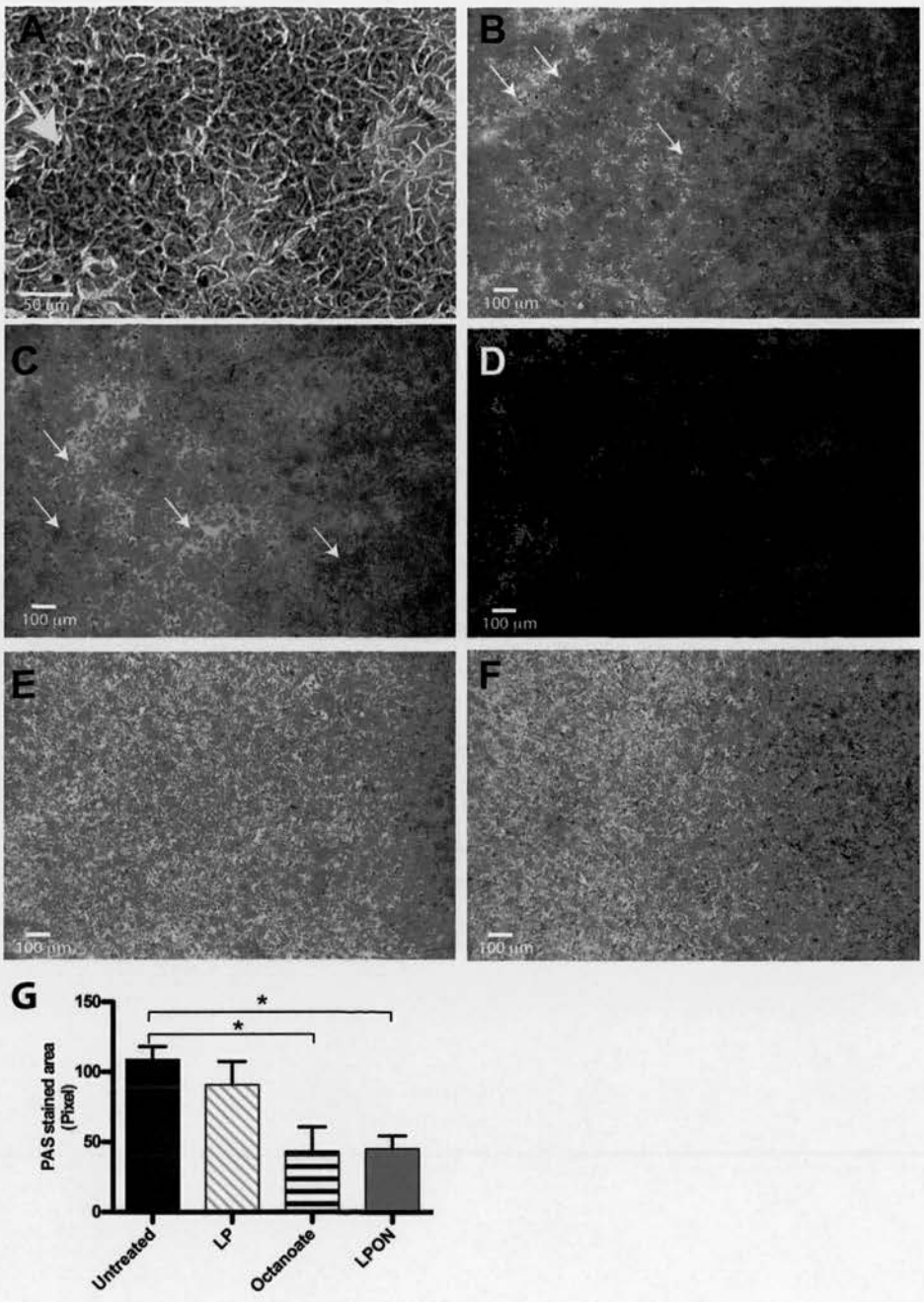

Figure 9.3.4. Glycogen accumulation in treated cells.

A, PAS stained area (indicated by the arrow) in untreated cells viewed under light microscopy (magnification x10); B, PAS stained (white arrow) untreated; C, LP treated cells (magnification x4); D, PAS stained area in LP treated cells highlighted by Image J; E and F, PAS stained LPON and octanoate treated cells respectively; G, Stained area quantified by Image J. PAS staining was performed as described in section 9.2.4. Data are presented as mean ± SEM; $P=0.02$; $^{*}P<0.05$.

9.3.5. Increased glycogen turnover with LPON treated cells

We then determined whether reduced glycogen accumulation with LPON could be attributable to increased glycogen turnover. Additionally, we examined whether the breakdown of glycogen with LPON is partitioned towards glucose formation rather than glycolysis. Glycogen breakdown produces glucose 1-phosphate, which is then converted to glucose 6-phosphate. Glucose 6-phosphate can enter glycolysis producing lactate and pyruvate, or dephosphorylated to form glucose (Figure 9.2.3). Insulin is expected to promote glycolysis and reduce glucose formation. Therefore, we compared the effect of insulin on glucose formation from glycogen in LPON and oleate treated cells. The concentration of insulin used (0-15mM) was determined from a dose response curve (Supplementary data 1.2).

Figure 9.3.5 Panel A shows that the overall flux through glucose 6-phosphatase was significantly higher in LPON than the untreated cells. The presence of insulin (0-15nM) did not alter the overall flux in LPON or the untreated cells. There was a non-statistical significant trend of reduced flux through glucose 6-phosphate with insulin (5nM) in oleate treated cells. In contrast, the percentage of glycogen diverted to glucose was significantly lowered by insulin (5nM) in oleate treated cells. This remained unaltered in LPON and the untreated cells (Panel B). Panel C shows the diversion towards glycolysis. The pattern was diametrical to that seen in glucose formation. There was a non-statistical significant increase in glycolysis with oleate and the untreated cells when compared with LPON.

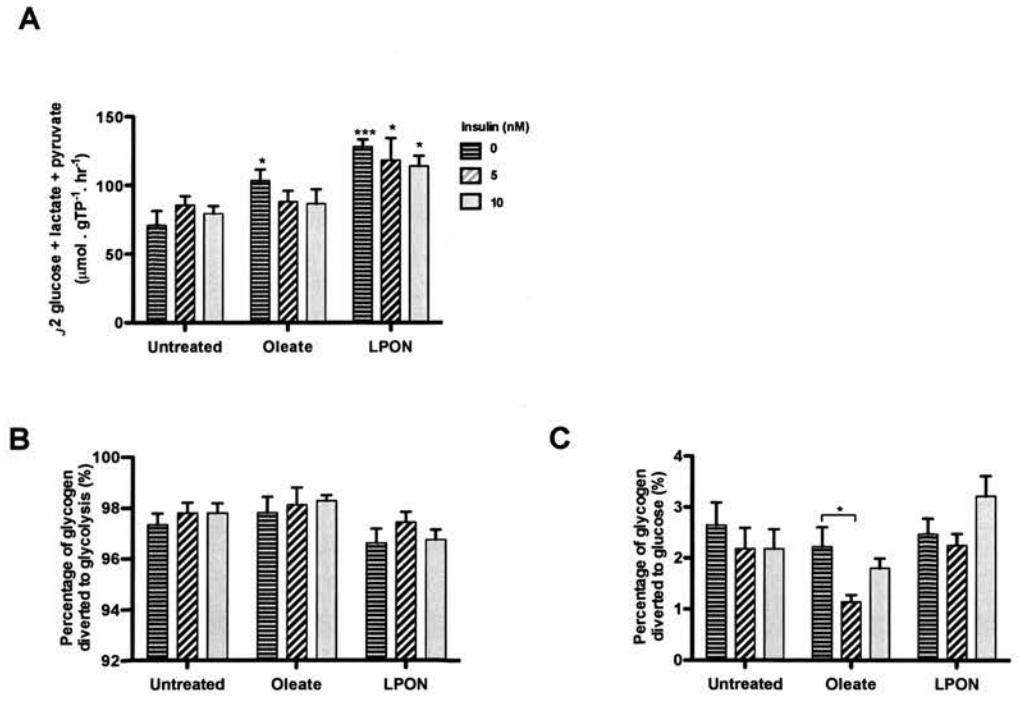

Figure 9.3.5. The effect of insulin on glycogen turnover in treated cells.

A, The overall flux through glucose 6-phosphate; B, The percentage of glycogen diverted towards glucose formation; C, The percentage of glycogen diverted towards glycolysis. Panel A-C, treated cells were incubated with insulin at the specified concentrations. The percentage of glycogen diverted to glucose and glycolysis was calculated as previously described in section 9.2.3. A, $P<0.0001$ for the overall effect of treatment. $^{***}P<0.001$, $^{*}P<0.05$ when compared to the corresponding untreated cells. B, The effect of treatment was significant ($P=0.005$) whilst the effect of insulin on the untreated and LPON cells was not statistically significant ($P=0.07$). $^{*}P<0.05$ between 0 and 5nM of insulin in oleate treated cells. C, The effect of treatment was significant ($P=0.01$) whilst the variation due to insulin did not reach statistical significance ($P=0.3$). Data are presented as mean ± SEM.

9.3.6. Triglyceride reduction with metformin does not lower glucose formation

Next, we examined whether the reduction in triglyceride accumulation induced by metformin would lower glucose concentration in LPON cells. A separate group of cells were treated with LPON and metformin (50nM and 1mM) for 72 hours. We have previously shown that metformin (1mM) reduced triglyceride accumulation in LPON treated cells (Figure 5.3.3.2). The concentration of glucose in the supernatant was measured as described in section 9.2.2. As shown in Figure 9.3.6, metformin did not alter glucose concentration in LPON treated cells.

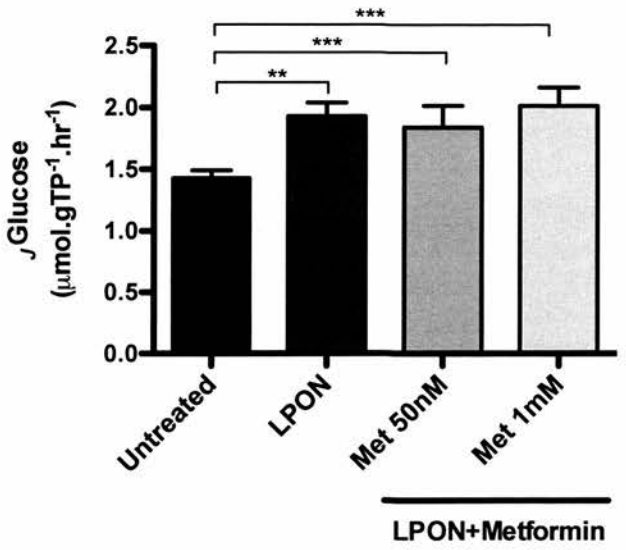

Figure 9.3.6. The effect of metformin on glucose formation in treated cells.

Cells were treated for 72 hours in six-well plates. Separate group of cells were treated with LPON and metformin at the concentration specified. Glucose concentrations in the culture supernatant were measured as described in section 9.2.2. Data are presented as mean ± SD; $P<0.0001$; $^{***}P<0.001$, $^{**}P<0.01$.

9.3.7. Other factors that may have influenced glucose metabolism

The disparity in glucose metabolism between LPON and oleate treated cells suggests that the extent of triglyceride accumulation does not influence glucose metabolism. Furthermore, the reduction in triglyceride accumulation with LPON+metformin did not lower glucose formation. Therefore, we examined two factors that have been proposed to influence insulin sensitivity-the surface area to volume ratio of the lipid droplets and acyl-carnitine concentration.

9.3.7.1. Lipid droplets surface area to volume ratio

Recent evidence suggests that increased surface area to volume ratio enhances insulin sensitivity (146). Conversely, reduced surface ratio to volume as often found with larger droplets is thought to limit the access of lipases leading to incomplete triglyceride hydrolysis. This can result in the formation of DAG, which in turn, can potentially impede insulin signaling through the activation of PKCε. Using 3D image analysis software, we determined the surface area to volume ratio in treated cells. Figure 9.3.7.1 demonstrates that surface area to volume ratio was significantly higher in the untreated and oleate treated cells when compared with LPON cells after 72 hours.

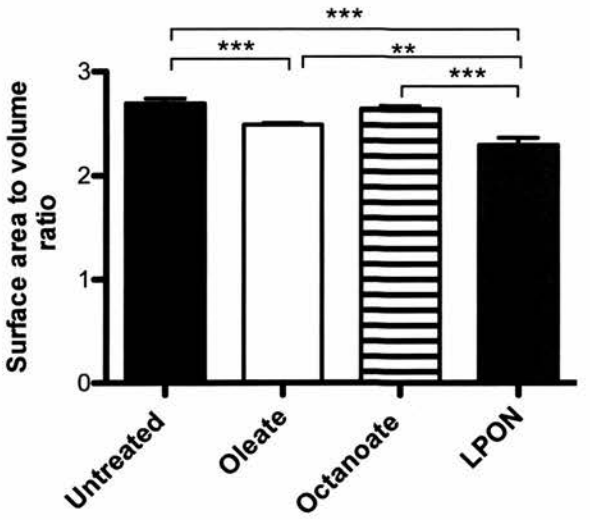

Figure 9.3.7.1. The surface area to volume ratio of lipid droplets accumulated.

Cells were grown in two-chamber slides and treated for 72 hours. The surface area and volume were determined using 3D software, Volocity. Data are presented as mean ± SD; $P<0.0001$; $^{***}P<0.001$, $^{**}P<0.01$.

9.3.7.2. Acyl-carnitine concentrations were higher in LPON treated cells.

Peroxisomal β-oxidation of the long chain fatty acids results in shorter fatty acid chains, which are converted to acyl carnitines. Acyl carnitines, subsequently, enter the mitochondria to undergo complete β-oxidation. Increased concentration of even-chain acyl carnitine (C4-C22) reflects decreased/overwhelmed mitochondrial β-oxidation. Raised even-chain acyl carnitine concentrations have been observed in individuals with Type 2 diabetes and has been associated with impaired fatty acid oxidation in animal models of obesity (147, 148). Increased even-chain species of acyl carnitine concentrations is thought to contribute towards insulin resistance by activating NFκB pathways (149).

Using metabolomics, we identified metabolites that corresponded to acyl carnitines in the treated cells. Figure 9.3.7.2.1 demonstrates increased butanoylcarnitine (C4), hexanoylcarnitine (C6) and octanoylcarnitine (C8) concentrations with LPON when compared with oleate and the untreated cells. In contrast, the odd-chain acyl carnitine; propanoylcarnitine (C3), tiglylcarnitine (C5) and heptanoylcarnitine (C7) concentrations were lower with LPON than oleate or the untreated cells (Figure 9.3.7.2.2). These findings are similar to that observed in individuals with Type 2 diabetes in a previous study (149).

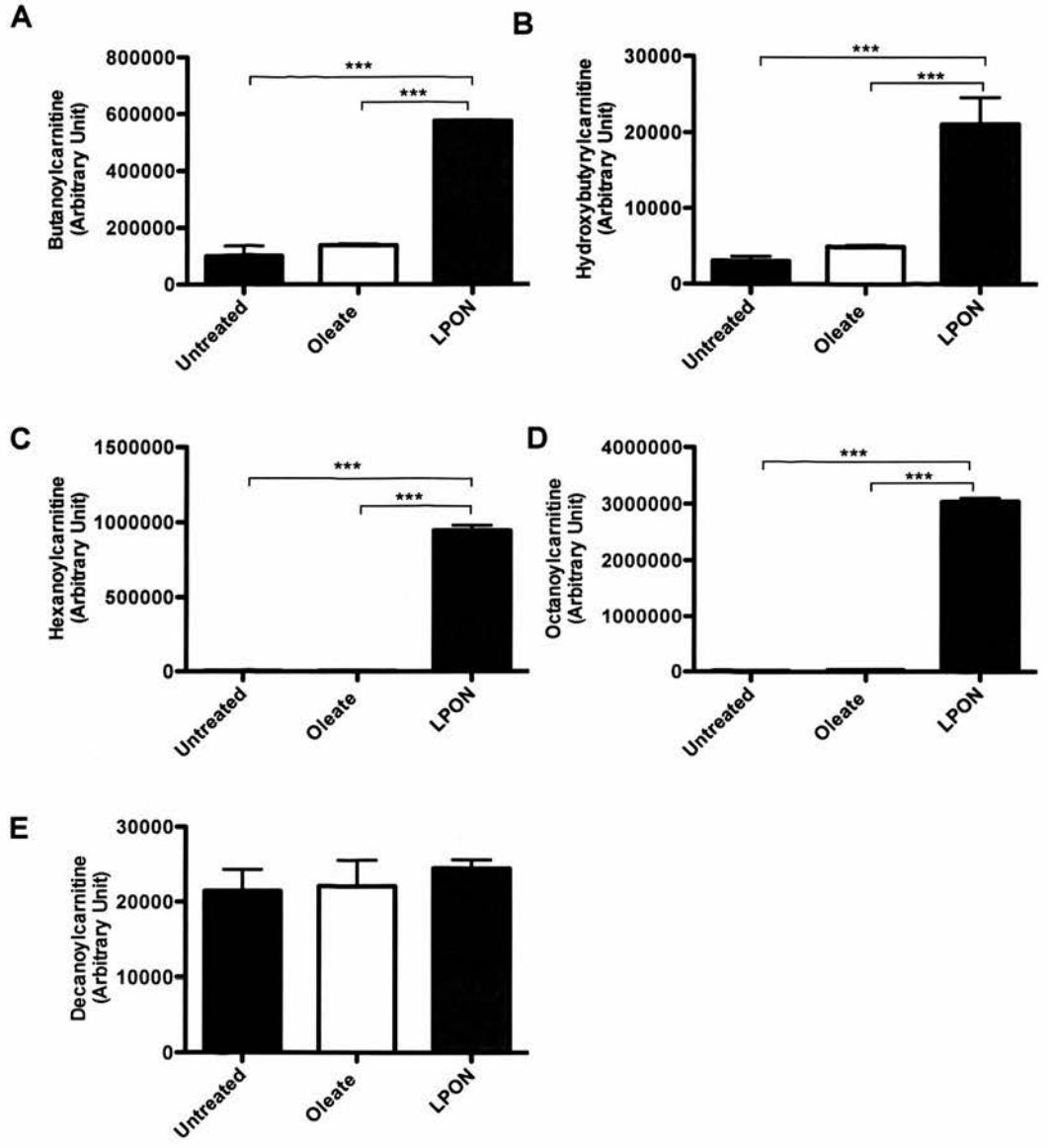

Figure 9.3.7.2.1. Even-chain acyl carnitine concentration in treated cells.

A, Butanoylcarnitine (C4), (P<0.0001); B, Hydroxybutyrylcarnitine (C4), (P<0.0001); C, Hexanoylcarnitine (C6), (P<0.0001); D, Octanoylcarnitine (C8), (P<0.0001); E, Decanoylcarnitine (C10), (P=0.45). The concentrations of acyl carnitine were determined using metabolomics in cells that have been treated for 72 hours. Data are presented as mean ± SD; $^{***}P$<0.001.

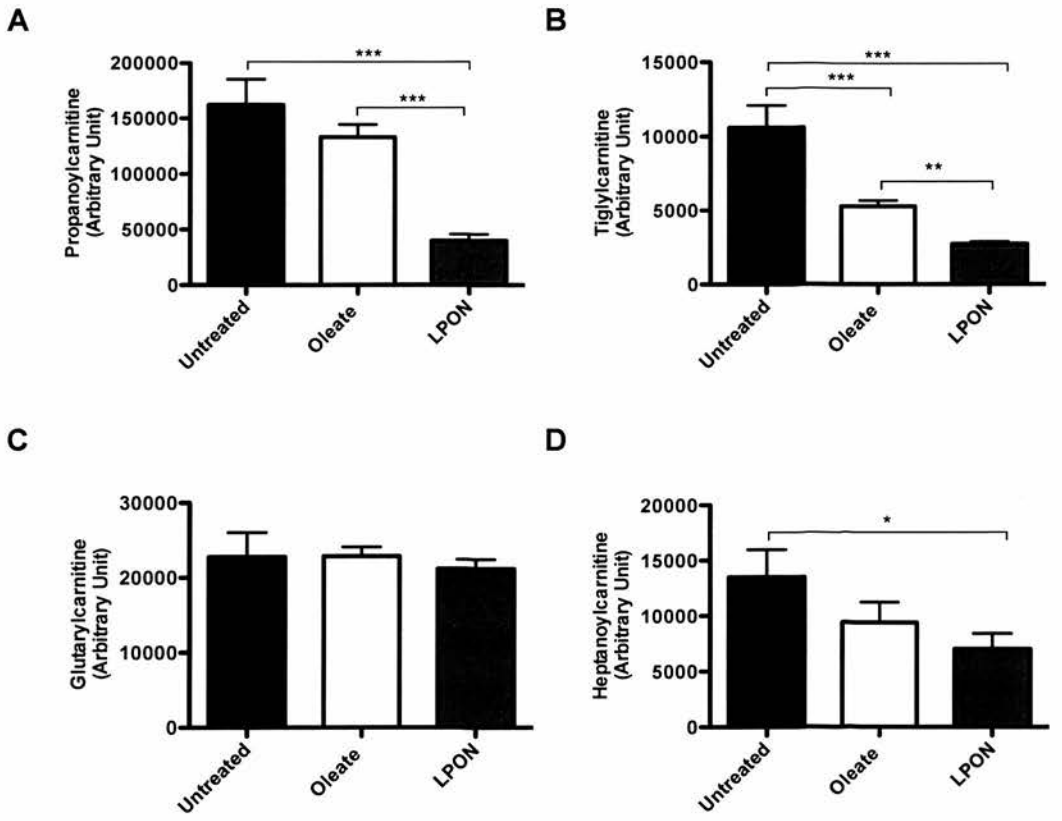

Figure 9.3.7.2.2. Odd-chain acyl carnitine concentration in treated cells.

A, Propanoylcarnitine (C3), (P<0.0001); B, Tiglylcarnitine (C5), (P<0.0001); C, Glutarylcarnitine (C5), (P=0.58); D, Heptanoylcarnitine (C7), (P=0.01). The concentrations of acyl carnitine were determined using metabolomics in cells that have been treated for 72 hours. Data are presented as mean ± SD; $^{***}P$<0.001, $^{**}P$<0.01, $^{*}P$<0.05.

9.4. Discussion and conclusion

In this chapter, we dissect the relationship between glucose metabolism, triglyceride accumulation and mitochondrial function. Our data highlight several important points. First, the extent of triglyceride accumulation does not influence glucose metabolism. Despite the similarity in triglyceride accumulation, LPON, not oleate, had enhanced glucose formation paralleled by increased gluconeogenic capacity, decreased glycolysis, reduced glycogen accumulation and enhanced glycogen turnover. Similarly, triglyceride reduction does not necessarily affect glucose formation. Diminished triglyceride accumulation in cells concomitantly treated with LPON and metformin was not mirrored by a reduction in glucose formation.

The next question is whether altered glucose metabolism observed with LPON is driven by ROS. Indeed, ROS have been proposed to alter insulin signaling (92). The reduction in gluconeogenesis with NAC corroborates the role of ROS in altering glucose metabolism in LPON treated cells. However, increased gluconeogenesis and reduced glycogen accumulation occurred in octanoate treated cells without a discernible rise in ROS formation. In this respect, it is likely that accelerated acetyl-coA formation with octanoate (as evidenced by enhanced ketogenesis) inhibits pyruvate dehydrogenase (PDH), thus diverting pyruvate towards the gluconeogenic pathways. The presence of ROS can augment this further. Decreased TCA cycle activity with concomitant mitochondrial dysfunction in the presence of oxidative stress can augment acetyl-coA accumulation. In contrast, NAC promotes acetyl-coA flux into the TCA cycle, which is likely to underpin its ability to reduced gluconeogenic capacity (150).

Second, the importance of acetyl-coA in glucose metabolism also underlies the observation that impaired glucose tolerance precedes mitochondrial impairment (98). Increased gluconeogenic capacity with octanoate occurs in the presence of preserved mitochondrial function.

Third, abnormal glucose metabolism is associated with the dysregulation of fatty acid metabolism. Enhanced formation of acetyl-coA with LPON promotes *de novo* lipogenesis with resultant long chain fatty acids formation. Enhanced ω- and peroxisomal β-oxidation of long chain fatty acids yields a significant amount of fatty acid intermediates that rely on the mitochondria for complete oxidation. Thus, mitochondrial β-oxidation is overwhelmed as evidenced by higher acyl carnitine concentrations. Similarly, decreased surface area to volume of lipid droplets can result in incomplete triglyceride hydrolysis leading to the formation of DAG in LPON treated cells. Both acyl carnitine and DAG have been implicated in the pathogenesis of insulin resistance (149, 151).

In summary, the formation of acetyl-coA, rather than cellular steatosis *per se*, is an important determinant to glucose dysregulation. Conditions that accelerate acetyl-coA accumulation, for example, an ongoing surge of energy substrate or ROS-induced TCA cycle downregulation is likely to augment this effect further.

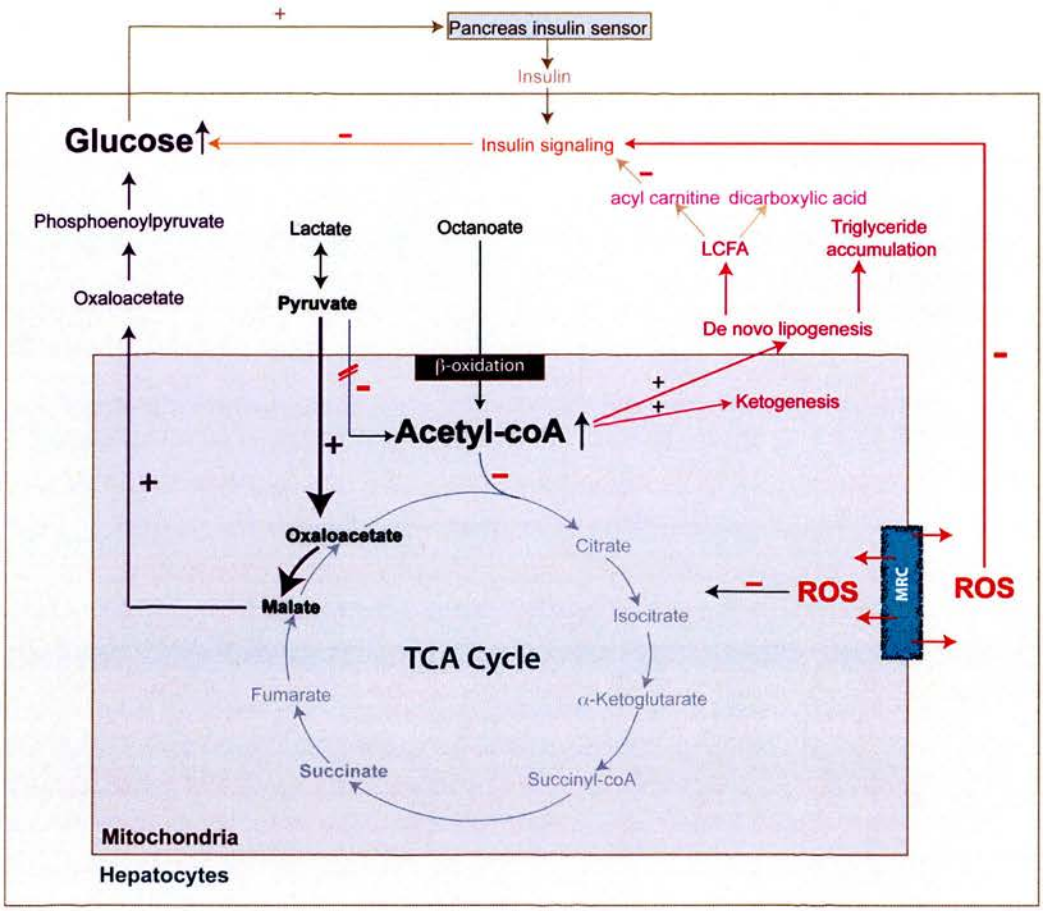

Figure 9.4. The effect of LPON on gluconeogenesis.

The rise in mitochondrial NADH/NAD$^+$ ratio and increased oxidative stress reduce the TCA cycle turnover. Consequently, the acetyl-coA flux into the cycle is decreased. This results in acetyl-coA accumulation, which instigates the pyruvate dehydrogenase to inhibit the conversion of pyruvate to acetyl-coA. As a result, pyruvate is carboxylated to form oxaloacetate. Oxaloactetate is converted to malate and transported out of the mitochondria to form phosphoenoylpyruvate. Phosphoenoylpyruvate enters the gluconeogenic pathway culminating in the production of glucose. The impact of acetyl-coA *per se* occurs even before the onset of mitochondrial dysfunction. However, the onset of mitochondrial dysfunction enhances acetyl-coA accumulation thus amplifying these events. Additionally, increased ROS formation with mitochondrial dysfunction can alter insulin signaling and exacerbate hyperglycaemia.

10. CHAPTER TEN

CONCLUSION

Our study sought to dissect the relationship between fat accumulation, reactive oxygen species and mitochondrial function in NAFLD. Understanding this relationship is a critical question since a considerable proportion of individuals with steatosis progress to steatohepatitis. To address this fundamental question, we have designed *in vitro* models of cellular steatosis using various combinations of physiological energy substrates that are relevant to human dietary nonalcoholic fatty liver disease.

In vitro model of cellular steatosis

The prerequisite of substrate chosen is its ability to induce adequate steatosis in addition to its capacity in promoting tricarboxylic acid cycle (TCA) activity to generate NADH for mitochondrial respiratory chain. We have shown that treatment with oleate or octanoate induced significant triglyceride accumulation in C3A cells. The addition of energy substrates, lactate and pyruvate, to octanoate enhanced the triglyceride accumulation, supporting the hypothesis that these substrates synergized to promote *de novo* lipogenesis. Increased fatty acid biosynthesis intermediates, enhanced concentration of acyl carnitines and increased dicarboxylic acid formation corroborate the presence of augmented *de novo* lipogenesis with LPON.

As evidenced by the differences in their mitochondrial respiration, fatty acids oleate or octanoate, with or without the combination of gluconeogenic substrates (lactate and pyruvate), and/or ammonia acutely modulated the TCA cycle turnover. We have shown that lactate, pyruvate, octanoate and ammonia synergized to enhance acute respiration and ROS formation to a critical point, culminating in mitochondrial impairment. Indeed, LPON-induced cellular steatosis manifests many of the key features associated with steatohepatitis such as impaired mitochondrial function, enhanced oxidative stress, increased ketogenesis and altered glucose metabolism. In stark contrast, triglyceride accumulation with oleate represents simple steatosis; mitochondrial function remained unperturbed despite the triglyceride accrued.

The focus was then to observe the events that occur as consequences of enhanced TCA activity similar to what potentially may occur with nutrient excess. Our aims were to determine (i) whether steatosis *per se* affects mitochondrial respiration and (ii) whether its effects are essentially hinged on ROS formation.

Our data have several important implications for understanding the events surrounding mitochondrial dysfunction in nutrient perturbation. First, cellular steatosis *per se* does not influence mitochondrial function. In support of this, mitochondrial function was significantly different between oleate and LPON despite their similarities in triglyceride accumulation. Enhanced respiration with LPON was not sustained; evidence of mitochondrial impairment was apparent after 72 hours as supported by decreased basal and substrate-driven respiration as well as diminished mitochondrial chain capacity. Likewise, mitochondrial function remained unaltered with LPO despite higher intracellular triglyceride accumulation than LPON. There are two potential mechanisms behind the lower triglyceride content with LPON when compared with LPO treated cells. First, impaired mitochondrial function would lead to ATP depletion, thus switching off ATP-consuming processes including *de novo* lipogenesis. Indeed, downregulation of lipogenic enzymes has been proposed to be the mechanism of decreased steatosis or 'burnt out' appearances in advanced NASH (34). Second, as discussed previously, ammonia has been shown in astrocytes to decrease the formation of triglycerides with concomitant rise in diacylglycerides further supporting the importance of triglycerides in protecting cells from the potential deleterious effect of free fatty acids (108, 121).

Importantly, reduction in intracellular triglyceride as observed with LPON in the presence of metformin, does not necessarily lead to an improvement in mitochondrial function. Mitochondrial respiration was significantly depressed with metformin despite a significant reduction in lipid accumulation. Moreover, the dose-dependent reduction

in triglyceride with metformin was paralleled by increased mitochondrial and cytosolic NADH/NAD^+ ratio suggesting decreased NADH oxidation. Such mitochondrial impairment can lead to a decline in ATP formation leading to a rise in AMP to ATP ratio. Indeed, metformin has been shown to lower triglyceride content by activating AMP-activated protein kinase (AMPK), a sensor of cellular energy activated by ATP depletion and is responsible for limiting ATP utilization (127, 128). Furthermore, significant mitochondrial impairment with metformin would lead to a decline in β-oxidation. Functioning mitochondrial respiration is a prerequisite to sustaining β-oxidation (152). Consequently, acetyl-coA formation for *de novo* lipogenesis would diminish.

ROS, not triglyceride accumulation, is a key determinant of mitochondrial function

Second, our data underline the importance of energy substrates capacity to form ROS, rather than their ability to induce triglyceride accumulation, as a key determinant of mitochondrial function. We have shown that LPON acutely enhanced ROS formation culminating in increased mitochondrial membrane potential and diminished mitochondrial respiration. The addition of antioxidant NAC reduced the mitochondrial membrane potential and prevented the decrease in basal and substrate-induced respiration seen in LPON-treated cells, thus supporting the role of ROS in modulating mitochondrial function in nutrient perturbation (43, 153). Taken together, these results indicate an inhibition of oxidative phosphorylation mediated by ROS possibly on the terminal components of mitochondrial respiratory chain, cytochrome *c* oxidase (complex IV). ROS and high fat diet have been previously shown to diminish

cytochrome *c* oxidase activity leading to an increase in $NADH/NAD^+$ and high mitochondrial membrane potential (142, 154). Therefore, it is plausible that the enhanced ROS is responsible for the ensemble of mitochondrial effects observed with LPON.

Akin to the findings in steatohepatitis, ROS formation in LPON-treated cells was not mitigated by diminished respiration (40, 59). Although the endogenous (basal) ROS formation between LPON and oleate was similar, the capacity to form ROS was higher with LPON. Indeed, there was a dramatic rise in superoxide formation with further LPON. The renewed NADH supply from the additional energy substrates are likely to burden the already strained oxidative phosphorylation leading to the rise in $NADH/NAD^+$ ratio as well as increased membrane potential (123, 155). In contrast, treatment with oleate did not affect cell respiration and maintained a relatively low mitochondrial membrane potential, resulting in a smaller amount of superoxide formation. Additionally, the intact respiration maintains constant NADH oxidation thus further minimizing the ROS formation (156).

Despite the downregulation of basal ROS formation after 72 hours, the presence of oxidative stress is apparent with LPON as evidenced by increased lipid peroxidation, enhanced dicarboxylic acid formation and elevated isoprostane levels. Furthermore, similar to that seen with FFA overload in obesity and diabetes, the formation of short and medium chain dicarboxylic acids from ω-oxidation can overwhelm β-oxidation. Additionally, dicarboxylic acids can promote mitochondrial impairment through three potential mechanisms. First, they inhibit mitochondrial respiration (133). Second, their futile recycling across the mitochondrial membrane can result in proton dissipation and

uncoupling respiration (157). Third, the ω-oxidation that leads to their formation and their oxidation by the peroxisomal β-oxidation can generate a substantial amount of ROS (158).

The potential explanation for the similarities in basal ROS formation between LPON and the untreated cells is that the mitochondrial NADH/NAD^+ ratio was comparable between the two groups. However, preserved mitochondrial function in the untreated cells, as evidenced by active respiration and low mitochondrial membrane potential, is likely to maintain steady flow of electrons along the mitochondrial chain necessary for an efficient NADH oxidation to NAD^+. The findings of lower cytosolic NADH/NAD^+ ratio in the untreated cells compared with LPON further support this notion. Therefore, it is plausible that the similarity in mitochondrial NADH/NAD^+ ratio reflects the differences in the rate of NADH formation from the TCA cycle. Specifically, the 72-hour LPON treatment may have led to the downregulation of TCA cycle and the observed mitochondrial NADH/NAD^+ ratio may have been normalized as part of the ensuing metabolic adaptations to limit ROS production.

In support of this, the concentration of malate, a TCA cycle intermediate, was found to be significantly higher with LPON than either oleate or the untreated cells. It is possible that the surge of energy substrates and the subsequent mitochondrial impairment with LPON would initially lead to a rise in NADH/NAD^+ ratio such that it favors the conversion of oxaloacetate to malate. The lowering of oxaloacetate can dampen the TCA cycle turnover, thus diminishing the NADH formation (141). In effect, such reduction in oxaloacetate decreases its availability to condense with acetyl-coA to form citrate. Indeed, citrate levels were lower with LPON compared with oleate.

Furthermore, citrate synthase activity is diminished in the presence of oxidative stress as well as in elevated NADH/NAD^+ (98, 142). Although it is conceivable that reduced basal respiration observed with LPON reflects decreased NADH availability, it is unlikely that this underpins the diminished substrate-induced respiration, particularly in the presence of DNP.

These adaptations are necessary in the presence of mitochondrial impairment. Excessive supply of NADH in the presence of electron flow disruption (for example, in ROS-induced mitochondrial injury) can promote further ROS formation. This is supported by the dramatic rise in ROS formation in LPON treated cells with further substrates. Importantly, it is likely that an ongoing surge of energy substrates can overcome the initial metabolic adaptations and their effects can be persistent. Indeed, mitochondrial NADH to NAD^+ ratio remained increased in LPON treated cells even after a further 72 hours of treatment. These conditions would favour ROS formation and thus, could potentially sustain the ROS formation leading to chronic oxidative stress.

The presence of oxidative stress with LPON is associated with several metabolic derangements. It is likely that these derangements represents adaptations to ROS mediated mitochondrial impairment. The diversion of acetyl-coA towards ketogenesis is a classic example of an acute metabolic adaptation to the reduction in the TCA cycle turnover. Indeed, steatohepatitis is characterized by enhanced ketogenesis without concomitant rise in β-oxidation (32). In the presence of decreased TCA cycle activity, acetyl-coA can also be diverted towards *de novo* lipogenesis and/or mevalonate pathways, depending on the ATP supply and cell demand. The findings of enhanced *de novo* lipogenesis with LPON and increased mevalonate pathways with oleate are likely to

reflect the discrepancy in ATP formation; mitochondrial impairment in LPON can potentially lead to decreased ATP formation. A relatively high mitochondrial membrane potential and increased uncoupled respiration observed with LPON support less ATP formation in these cells. Although *de novo* lipogenesis is an ATP consuming process, it is likely that protecting cells against the deleterious effect of free fatty acids supersedes the need for mevalonate pathways in LPON treated cells.

Increased gluconeogenesis exemplifies another appropriate response to curb further ROS formation from excessive substrate flux into the TCA cycle. In the setting of nutrient excess, increased mitochondrial superoxide production has been proposed to be the signal that drives a cellular response to induce insulin resistance as part of the antioxidant defense mechanism (159). Enhanced gluconeogenic capacity with LPON was paralleled by diminished glycolysis, increased glycogen turnover and enhanced partitioning of glycogen towards glucose formation. Taken together, these findings are consistent with decreased insulin sensitivity. In contrast, endogenous glucose formation is diminished with oleate consistent with preserved insulin sensitivity (85, 107). Importantly, the contrasting glucose metabolism between LPON and oleate highlights the discrepancy between triglyceride accumulation and glucose formation.

The finding of enhanced gluconeogenic capacity in octanoate and LPO-treated cells suggests that altered glucose metabolism occurs before the onset of mitochondrial impairment. In this respect, increased acetyl-coA formation that occurs before the onset of mitochondrial impairment is likely to contribute to enhanced glucose formation. There are two potential mechanisms that underlie the association between acetyl-coA and gluconeogenesis. First, increased acetyl-coA inhibits pyruvate dehydrogenase thus

diverting pyruvate towards gluconeogenesis. Second, acetyl-coA can be diverted towards *de novo* fatty acid synthesis resulting in long chain fatty acids formation. Incomplete long chain fatty acid oxidation yields acyl carnitine species, which have been implicated in the pathogenesis of insulin resistance.

The importance of acetyl-coA in determining glucose formation is further highlighted by the effect of NAC on glucose formation. The concomitant reduction in ketogenesis observed with NAC suggests reduced acetyl-coA accumulation, which is likely to be attributable to increased acetyl-coA flux into the TCA cycle. Indeed, NAC has been shown to improve TCA cycle metabolism by augmenting the carbon flux through PDH, independent of its ability to replenish glutathione stores (150). Importantly, the reduction in mitochondrial membrane potential with NAC can potentially decrease ROS formation and promote insulin sensitivity.

The finding that mitochondrial alterations do not precede insulin resistance is consistent with a previous study (98). However, the onset of mitochondrial impairment can sustain insulin resistance through two potential mechanisms. First, mitochondrial impairment augments ROS formation, which in turn, can alter insulin-signaling molecules (92). Second, an increase in $NADH/NAD^+$ ratio with mitochondrial impairment can lead to metabolic adaptations including a reduction in TCA cycle turnover with concomitant rise in gluconeogenesis. Such effects on glucose formation would continue until a decline in ATP formation reached a critical point culminating in the activation of AMPK pathways. AMPK reduces gluconeogenesis in an attempt to limit ATP consumption (160). In addition, the activation of AMPK-FOXO3 pathway has been shown to reduce ROS thus preserving insulin-signaling activity (161).

It is likely that the alteration in glucose metabolism driven by the excessive acetyl-coA parallels, if not precedes, any impairment in insulin signaling. In fact, altered insulin-signaling heralds the possibility of significant mitochondrial impairment and excessive ROS formation. In this respect, impaired insulin signaling can confer a protective but limited effect by reducing glucose oxidation and resultant ROS formation. Thus, the aberration of insulin signaling parallels or represents a consequence of mitochondrial impairment whereas altered glucose metabolism, as previously discussed, occurs before the onset of discernible mitochondrial impairment.

Another factor that can influence glucose formation in these cells is the differences in the surface area to volume ratio of the lipid droplets. The higher surface area with smaller lipid droplets allows complete action of lipase. Conversely, a reduction in the surface area with larger droplets can lead to partial triglyceride hydrolysis resulting in the development of diacylglycerol formation (162). The surface area to volume of lipid droplets was significantly reduced with LPON. Indeed, dietary-induced NAFLD is characterized by predominantly macrovesicular steatosis. Factors that lead to the formation of larger lipid droplets and macrovesicular steatosis remain to be elucidated.

Similar to that seen with steatohepatitis, mitochondrial impairment with LPON was associated with altered mitochondrial structure. Elongated mitochondria with indistinct cristae akin to that described in steatohepatitis were more frequently observed with LPON (64). Such morphological changes in steatohepatitis have been associated with increased hepatic oxidative stress (32, 40). Indeed, ROS have been implicated in the development of megamitochondria, which as the name implies, are characterized by enlarged mitochondria, often unusual in shape, with pale matrix and devoid of cristae

(82). However, there was a decrease in the overall cross-sectional area of the mitochondria in LPON cells. Mitochondria are dynamic organelles capable of undergoing constant fusion and fission in response to the ever-changing ROS concentration (60, 84). Smaller mitochondria are thought to represent ongoing fragmentation reported to occur transiently in the presence of ROS. Subsequent increased in fusion can result in enlarged and elongated mitochondria thereby decreasing the overall surface area to limit the release of ROS (84).

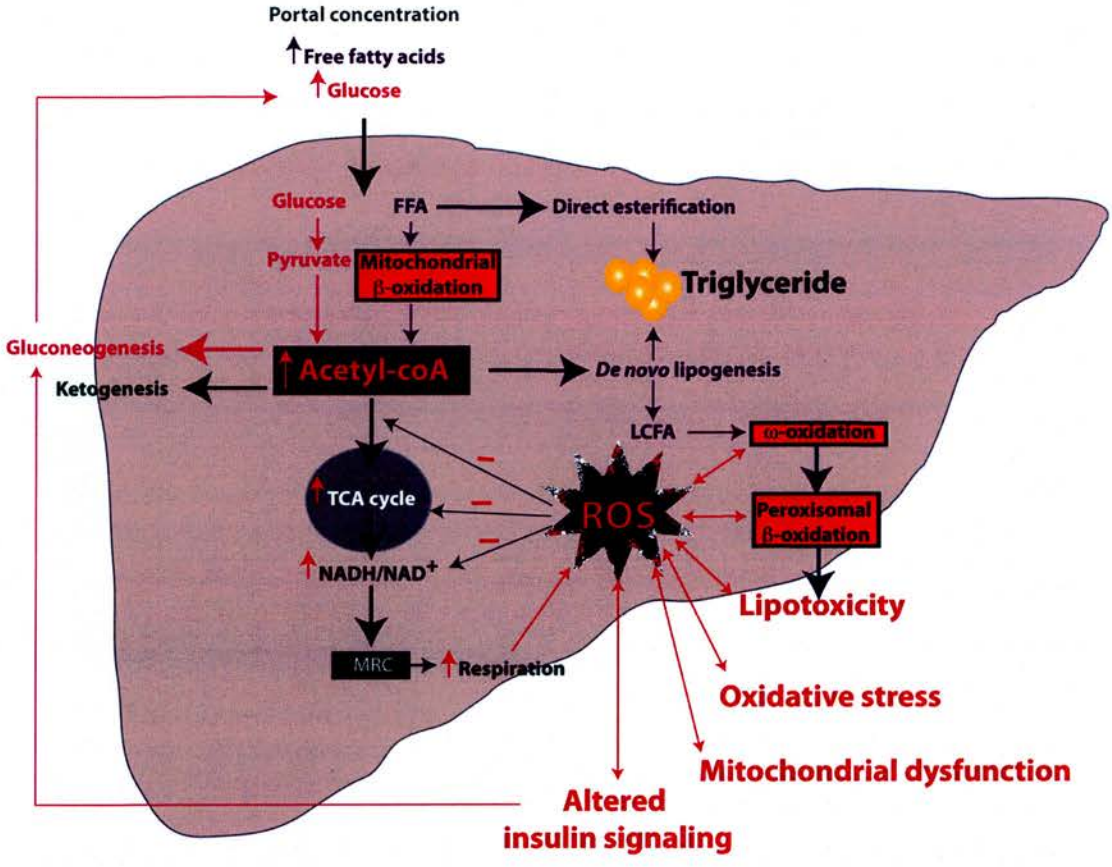

Figure 10.1. The consequences of increased energy substrates in the liver.

Schematic diagram to illustrate the sequence of events that can occur following an exposure to energy substrates. The rise in energy substrates increases respiration and enhances ROS formation. In turn, ROS lead to mitochondrial impairment. The onset of mitochondrial impairment instigates metabolic changes gearing to preserve ATP formation and to curtail further mitochondrial ROS formation (grey arrows). Such adaptations would include decreased TCA cycle activity, which can promote the partitioning of acetyl-coA to non-oxidative pathways including the *de novo* lipogenesis pathway. Increased ROS enhances lipid peroxidation producing intermediates that can overwhelm mitochondrial β-oxidation and activate alternative fatty acid oxidation pathways. These pathways generate further ROS as well as reactive lipid species thought to be responsible for lipotoxicity. MRC, mitochondrial respiratory chain; ROS, reactive oxygen species; FFA, free fatty acid; TCA, tricarboxylic acid cycle; LCFA, long chain fatty acids.

Third, our data provide a metabolic insight into the effect of NAC on hepatocytes. It is likely that the impact of NAC on metabolic alterations is underpinned by its ability to preserve basal and substrate respiration thus allowing constant NADH oxidation reducing $NADH/NAD^+$ ratio. As discussed previously, the reduction in ketogenesis and glucose formation with NAC exemplifies the importance of continuing respiration in preserving the flux of acetyl-coA into the TCA cycle. It is likely that the antioxidant effects of NAC protect the respiratory chain components from ROS injury. Furthermore, a novel finding of this study is that both NAC and the antioxidant, α-tocopherol, induced uncoupled respiration. The effect of these antioxidants on uncoupled respiration has not been previously shown. The extent of uncoupled respiration induced was modest and could not account for the entire recovery in respiration with NAC. However, increased uncoupled respiration with NAC can potentially contribute to several observations made in this present study. First, the proton leaks associated with the uncoupling process can contribute to the lower mitochondrial membrane potential. Second, it may have impeded the rise in compensatory respiration in the presence of DNP.

Although these antioxidants did not reverse the mitochondrial impairment that occurred in the presence of DNP, the role of oxidative stress in modulating cell respiration under this condition cannot be excluded for two potential reasons. First, the uncoupling process induced by these antioxidants can lead to a reduction in ROS formation. Second, neither NAC nor α-tocopherol is a mitochondrial-targeted antioxidant, which can accumulate at a higher concentration within mitochondrial matrix. NAC, a

glutathione precursor, is a powerful scavenger of hypochlorous acid (H-OCl) and hydrogen peroxide (H_2O_2), but its reaction with superoxide within the mitochondrial matrix remains unclear (163, 164).

There have been many studies that demonstrate beneficial effect of NAC in counteracting oxidative stress (126, 165, 166). However, the ability of NAC to induce uncoupling of respiration in this present study raises the question whether ATP formation would be compromised with prolonged treatment. Prolonged NAC treatment in paracetamol-induced liver necrosis has been shown to impair liver regeneration (167). We did not determine the impact of NAC on ATP homeostasis in this study.

Not all fatty acids are equal

Finally, our data highlight the differences between oleate and octanoate. The differences are largely stemmed from their disparity in β-oxidation (101, 168). The rate of β-oxidation for oleate is limited by CPT1, an enzyme responsible for its transport across the mitochondrial membrane (169). Thus, oleate is channeled towards esterification. By comparison, the ease of octanoate to diffuse into the mitochondria independent of CPT1 results in a partitioning towards oxidation rather than esterification. Enhanced lipolysis with octanoate has led to the proposal that medium chain fatty acids are beneficial in promoting weight loss and preserving insulin sensitivity (102, 103). The perceived beneficial effects however are tissue specific; despite decreased adiposity and enhanced insulin sensitivity in muscle and adipose tissue, MCFA promote steatosis and

insulin resistance in the liver (170).

LPON demonstrates the impact of octanoate on hepatocytes that are already burdened by excessive energy substrates. Efficient β-oxidation with octanoate yields higher ketogenesis hence increased acetyl-coA, which in turn, decreases glucose oxidation (despite preserved mitochondrial function), as well as promotes *de novo* lipogenesis as evidenced by increased triglyceride over the period of treatment. In the presence of increased energy substrates such as seen with LPON, these effects are augmented. Moreover, other energy substrates synergize with octanoate culminating in overwhelmed mitochondrial β-oxidation. This leads to the induction of ω- and peroxisomal β-oxidation as evidenced by increased acyl carnitines and dicarboxylic acid formation. These pathways generate a considerable amount of ROS and have been implicated in the progression from steatosis to steatohepatitis (157).

Limitations and future direction

Several limitations have to be acknowledged. These studies were focused specifically on hepatocytes *in vitro*. Therefore, the involvement of adipokines was not examined. Future *in vitro* studies should include the impact of LPON on insulin signaling, ATP homeostasis and lipid droplets dynamics. Our data have highlighted several interesting observations that can be translated into clinical research. For example, the role of incomplete fatty acid oxidation in the progression of steatohepatitis and fibrosis deserve further evaluation. The concentration of dicarboxylic acids and acyl carnitine can be measured *in vivo* as a marker of incomplete fatty acid oxidation. Similarly, the correlation

between TCA cycle activity and clinical stages of NAFLD is yet to be established. There are many studies examining mitochondrial impairment in human NAFLD. Few, however, are focused on the events leading to its development.

Conclusion

In summary, our data suggest that hepatic steatosis *per se* does not have direct impact on mitochondrial function; nor does it influence glucose metabolism. It is simply a marker of deranged metabolic milieu. In contrast, ROS is a determinant of mitochondrial function in the long term. It is likely that ROS act as energy sensor providing the impetus to metabolic adaptations gearing towards limiting further ROS production. Such adaptations would include curtailing energy substrate flux into TCA cycle, thus acetyl-coA has to be diverted towards other pathways including ketogenesis and *de novo* lipogenesis. However, a critical juncture would be reached if the surge of energy substrates were to continue. The metabolic adaptations and antioxidants would no longer able to cope with excessive ROS formation. In this milieu, further ROS formation triggers a vicious cycle including cascades of proinflammatory cytokine culminating in the onset of changes that lead to steatohepatitis and fibrosis (55). Thus, reduction in cellular steatosis is not always the desired outcome without concomitant reduction in energy substrate and ROS formation. The results of this study would support strategies focused on establishing the balance between excessive ROS production and antioxidant capacity in preventing the onset of nonalcoholic steatohepatitis.

BIBLIOGRAPHY

1. POWELL E E, COOKSLEY W G, HANSON R, SEARLE J, HALLIDAY J W, POWELL L W. The natural history of nonalcoholic steatohepatitis: a follow-up study of forty-two patients for up to 21 years. Hepatology 1990; 11(1): 74-80.

2. CONTOS M J, SANYAL A J. The clinicopathologic spectrum and management of nonalcoholic fatty liver disease. Adv Anat Pathol 2002; 9(1): 37-51.

3. ADAMS L A, SANDERSON S, LINDOR K D, ANGULO P. The histological course of nonalcoholic fatty liver disease: a longitudinal study of 103 patients with sequential liver biopsies. J Hepatol 2005; 42(1): 132-8.

4. WANLESS I R, LENTZ J S. Fatty liver hepatitis (steatohepatitis) and obesity: an autopsy study with analysis of risk factors. Hepatology 1990; 12(5): 1106-10.

5. PAGANO G, PACINI G, MUSSO G, et al. Nonalcoholic steatohepatitis, insulin resistance, and metabolic syndrome: further evidence for an etiologic association. Hepatology 2002; 35(2): 367-72.

6. CHITTURI S, ABEYGUNASEKERA S, FARRELL G C, et al. NASH and insulin resistance: Insulin hypersecretion and specific association with the insulin resistance syndrome. Hepatology 2002; 35(2): 373-9.

7. FARRELL G C, LARTER C Z. Nonalcoholic fatty liver disease: from steatosis to cirrhosis. Hepatology 2006; 43(2 Suppl 1): S99-S112.

8. WEBSTER G T. Cirrhosis of the Liver among Rats Receiving Diets Poor in Protein and Rich in Fat. The Journal of clinical investigation 1942; 21(4): 385-92.

9. CHAIKOFF I L, EICHORN K B, CONNOR C L, ENTENMAN C. The Production of Cirrhosis in the Liver of the Normal Dog by Prolonged Feeding of a High-Fat Diet. Am J Pathol 1943; 19(1): 9-21.

10. LUDWIG J, VIGGIANO T R, MCGILL D B, OH B J. Nonalcoholic steatohepatitis: Mayo Clinic experiences with a hitherto unnamed disease. Mayo Clin Proc 1980; 55(7): 434-8.

11. ONG J P, ELARINY H, COLLANTES R, et al. Predictors of nonalcoholic steatohepatitis and advanced fibrosis in morbidly obese patients. Obes Surg 2005; 15(3): 310-5.

12. ARGO C K, NORTHUP P G, AL-OSAIMI A M, CALDWELL S H. Systematic review of risk factors for fibrosis progression in non-alcoholic steatohepatitis. Journal of hepatology 2009; 51(2): 371-9.

13. STARLEY B Q, CALCAGNO C J, HARRISON S A. Nonalcoholic fatty liver disease and hepatocellular carcinoma: a weighty connection. Hepatology 2010; 51(5): 1820-32.

14. MARCHESINI G, BIANCHI G. Nonalcoholic fatty liver disease: Disease and comorbidity--effects on quality of life. Nat Rev Gastroenterol Hepatol 2009; 6(9): 504-6.

15. MARCHESINI G, BUGIANESI E, FORLANI G, et al. Nonalcoholic fatty liver, steatohepatitis, and the metabolic syndrome. Hepatology 2003; 37(4): 917-23.

16. BROWNING J D, SZCZEPANIAK L S, DOBBINS R, et al. Prevalence of hepatic steatosis in an urban population in the United States: impact of ethnicity. Hepatology 2004; 40(6): 1387-95.

17. YOUNOSSI Z M, GRAMLICH T, MATTEONI C A, BOPARAI N, MCCULLOUGH A J. Nonalcoholic fatty liver disease in patients with type 2 diabetes. Clin Gastroenterol Hepatol 2004; 2(3): 262-5.

18. BLOOMGARDEN Z T. Second World Congress on the Insulin Resistance Syndrome: insulin resistance syndrome and nonalcoholic fatty liver disease. Diabetes Care 2005; 28(6): 1518-23.

19. ANGULO P, KEACH J C, BATTS K P, LINDOR K D. Independent predictors of liver fibrosis in patients with nonalcoholic steatohepatitis. Hepatology 1999; 30(6): 1356-62.

20. ADAMS L A, SANDERSON S, LINDOR K D, ANGULO P. The histological course of nonalcoholic fatty liver disease: a longitudinal study of 103 patients with sequential liver biopsies. Journal of hepatology 2005; 42(1): 132-8.

21. ZHU L, BAKER S S, LIU W, et al. Lipid in the livers of adolescents with nonalcoholic steatohepatitis: combined effects of pathways on steatosis. Metabolism: clinical and experimental 2011; 60(7): 1001-11.

22. DONNELLY K L, SMITH C I, SCHWARZENBERG S J, JESSURUN J, BOLDT M D, PARKS E J. Sources of fatty acids stored in liver and secreted via lipoproteins in patients with nonalcoholic fatty liver disease. J Clin Invest 2005; 115(5): 1343-51.

23. BRADBURY M W. Lipid metabolism and liver inflammation. I. Hepatic fatty acid uptake: possible role in steatosis. Am J Physiol Gastrointest Liver Physiol 2006; 290(2): G194-8.

24. TOYE A A, DUMAS M E, BLANCHER C, et al. Subtle metabolic and liver gene transcriptional changes underlie diet-induced fatty liver susceptibility in insulin-resistant mice. Diabetologia 2007; 50(9): 1867-79.

25. SCHADINGER S E, BUCHER N L, SCHREIBER B M, FARMER S R. PPARgamma2 regulates lipogenesis and lipid accumulation in steatotic hepatocytes. Am J Physiol Endocrinol Metab 2005; 288(6): E1195-205.

26. SHIMOMURA I, BASHMAKOV Y, HORTON J D. Increased levels of nuclear SREBP-1c associated with fatty livers in two mouse models of diabetes mellitus. J Biol Chem 1999; 274(42): 30028-32.

27. DENTIN R, DENECHAUD P D, BENHAMED F, GIRARD J, POSTIC C. Hepatic gene regulation by glucose and polyunsaturated fatty acids: a role for ChREBP. J Nutr 2006; 136(5): 1145-9.

28. UYEDA K, REPA J J. Carbohydrate response element binding protein, ChREBP, a transcription factor coupling hepatic glucose utilization and lipid synthesis. Cell Metab 2006; 4(2): 107-10.

29. WEST J, BROUSIL J, GAZIS A, et al. Elevated serum alanine transaminase in patients with type 1 or type 2 diabetes mellitus. QJM 2006; 99(12): 871-6.

30. DIRAISON F, MOULIN P, BEYLOT M. Contribution of hepatic de novo lipogenesis and reesterification of plasma non esterified fatty acids to plasma triglyceride synthesis during non-alcoholic fatty liver disease. Diabetes Metab 2003; 29(5): 478-85.

31. FUJITA K, NOZAKI Y, WADA K, et al. Dysfunctional very-low-density lipoprotein synthesis and release is a key factor in nonalcoholic steatohepatitis pathogenesis. Hepatology 2009; 50(3): 772-80.

32. SANYAL A J, CAMPBELL-SARGENT C, MIRSHAHI F, et al. Nonalcoholic steatohepatitis: association of insulin resistance and mitochondrial abnormalities. Gastroenterology 2001; 120(5): 1183-92.

33. CALDWELL S H, LEE V D, KLEINER D E, et al. NASH and cryptogenic cirrhosis: a histological analysis. Annals of hepatology : official journal of the Mexican Association of Hepatology 2009; 8(4): 346-52.

34. NAGAYA T, TANAKA N, SUZUKI T, et al. Down-regulation of SREBP-1c is associated with the development of burned-out NASH. J Hepatol 2010; 53(4): 724-31.

35. WANLESS I R, SHIOTA K. The pathogenesis of nonalcoholic steatohepatitis and other fatty liver diseases: a four-step model including the role of lipid release and hepatic venular obstruction in the progression to cirrhosis. Semin Liver Dis 2004; 24(1): 99-106.

36. RATZIU V, GIRAL P, CHARLOTTE F, et al. Liver fibrosis in overweight patients. Gastroenterology 2000; 118(6): 1117-23.

37. RATZIU V, BONYHAY L, DI MARTINO V, et al. Survival, liver failure, and hepatocellular carcinoma in obesity-related cryptogenic cirrhosis. Hepatology 2002; 35(6): 1485-93.

38. DAY C P, JAMES O F. Steatohepatitis: a tale of two "hits"? Gastroenterology 1998; 114(4): 842-5.

39. SCHATTENBERG J M, WANG Y, SINGH R, RIGOLI R M, CZAJA M J. Hepatocyte CYP2E1 overexpression and steatohepatitis lead to impaired hepatic insulin signaling. The Journal of biological chemistry 2005; 280(11): 9887-94.

40. KOJIMA H, SAKURAI S, UEMURA M, FUKUI H, MORIMOTO H, TAMAGAWA Y. Mitochondrial abnormality and oxidative stress in nonalcoholic steatohepatitis. Alcohol Clin Exp Res 2007; 31(1 Suppl): S61-6.

41. JONES D P. Redefining oxidative stress. Antioxid Redox Signal 2006; 8(9-10): 1865-79.

42. ANDERSON E J, LUSTIG M E, BOYLE K E, et al. Mitochondrial H2O2 emission and cellular redox state link excess fat intake to insulin resistance in both rodents and humans. J Clin Invest 2009.

43. KOHLI R, PAN X, MALLADI P, WAINWRIGHT M S, WHITINGTON P F. Mitochondrial reactive oxygen species signal hepatocyte steatosis by regulating the phosphatidylinositol 3-kinase cell survival pathway. J Biol Chem 2007; 282(29): 21327-36.

44. DROGE W. Free radicals in the physiological control of cell function. Physiol Rev 2002; 82(1): 47-95.

45. MURPHY M P. How mitochondria produce reactive oxygen species. The Biochemical journal 2009; 417(1): 1-13.

46. PESSAYRE D, FROMENTY B, MANSOURI A. Mitochondrial injury in steatohepatitis. Eur J Gastroenterol Hepatol 2004; 16(11): 1095-105.

47. YOON Y S, LEE J H, HWANG S C, CHOI K S, YOON G. TGF beta1 induces prolonged mitochondrial ROS generation through decreased complex IV activity with senescent arrest in Mv1Lu cells. Oncogene 2005; 24(11): 1895-903.

48. KAMATA H, HONDA S, MAEDA S, CHANG L, HIRATA H, KARIN M. Reactive oxygen species promote TNFalpha-induced death and sustained JNK activation by inhibiting MAP kinase phosphatases. Cell 2005; 120(5): 649-61.

49. SCHATTENBERG J M, WANG Y, SINGH R, RIGOLI R M, CZAJA M J. Hepatocyte CYP2E1 overexpression and steatohepatitis lead to impaired hepatic insulin signaling. J Biol Chem 2005; 280(11): 9887-94.

50. VIDELA L A, RODRIGO R, ORELLANA M, et al. Oxidative stress-related parameters in the liver of non-alcoholic fatty liver disease patients. Clinical science 2004; 106(3): 261-8.

51. SEKI S, KITADA T, SAKAGUCHI H. Clinicopathological significance of oxidative cellular damage in non-alcoholic fatty liver diseases. Hepatol Res 2005; 33(2): 132-4.

52. CHALASANI N, DEEG M A, CRABB D W. Systemic levels of lipid peroxidation and its metabolic and dietary correlates in patients with nonalcoholic steatohepatitis. The American journal of gastroenterology 2004; 99(8): 1497-502.

53. SCHATTENBERG J M, SINGH R, WANG Y, et al. JNK1 but not JNK2 promotes the development of steatohepatitis in mice. Hepatology 2006; 43(1): 163-72.

54. LECLERCQ I A, FARRELL G C, SEMPOUX C, DELA PENA A, HORSMANS Y. Curcumin inhibits NF-kappaB activation and reduces the severity of experimental steatohepatitis in mice. Journal of hepatology 2004; 41(6): 926-34.

55. ABIRU S, MIGITA K, MAEDA Y, et al. Serum cytokine and soluble cytokine receptor levels in patients with non-alcoholic steatohepatitis. Liver international : official journal of the International Association for the Study of the Liver 2006; 26(1): 39-45.

56. PONIACHIK J, CSENDES A, DIAZ J C, et al. Increased production of IL-1alpha and TNF-alpha in lipopolysaccharide-stimulated blood from obese patients with non-alcoholic fatty liver disease. Cytokine 2006; 33(5): 252-7.

57. YOUNOSSI Z M, BARANOVA A, ZIEGLER K, et al. A genomic and proteomic study of the spectrum of nonalcoholic fatty liver disease. Hepatology 2005; 42(3): 665-74.

58. YONEDA M, ENDO H, MAWATARI H, et al. Gene expression profiling of non-alcoholic steatohepatitis using gene set enrichment analysis. Hepatol Res 2008; 38(12): 1204-12.

59. VENDEMIALE G, GRATTAGLIANO I, CARACENI P, et al. Mitochondrial oxidative injury and energy metabolism alteration in rat fatty liver: effect of the nutritional status. Hepatology 2001; 33(4): 808-15.

60. YU T, SHEU S S, ROBOTHAM J L, YOON Y. Mitochondrial fission mediates high glucose-induced cell death through elevated production of reactive oxygen species. Cardiovasc Res 2008; 79(2): 341-51.

61. GRAY M W, BURGER G, LANG B F. Mitochondrial evolution. Science 1999; 283(5407): 1476-81.

62. PEREZ-CARRERAS M, DEL HOYO P, MARTIN M A, et al. Defective hepatic mitochondrial respiratory chain in patients with nonalcoholic steatohepatitis. Hepatology 2003; 38(4): 999-1007.

63. CORTEZ-PINTO H, CHATHAM J, CHACKO V P, ARNOLD C, RASHID A, DIEHL A M. Alterations in liver ATP homeostasis in human nonalcoholic steatohepatitis: a pilot study. JAMA 1999; 282(17): 1659-64.

64. CALDWELL S H, SWERDLOW R H, KHAN E M, et al. Mitochondrial abnormalities in non-alcoholic steatohepatitis. J Hepatol 1999; 31(3): 430-4.

65. MITCHELL P. Coupling of phosphorylation to electron and hydrogen transfer by a chemi-osmotic type of mechanism. Nature 1961; 191: 144-8.

66. SERVIDDIO G, BELLANTI F, TAMBORRA R, et al. Alterations of hepatic ATP homeostasis and respiratory chain during development of non-alcoholic steatohepatitis in a rodent model. Eur J Clin Invest 2008; 38(4): 245-52.

67. GARCIA-RUIZ I, FERNANDEZ-MOREIRA D, SOLIS-MUNOZ P, et al. Mitochondrial complex I subunits are decreased in murine nonalcoholic fatty liver disease: implication of peroxynitrite. J Proteome Res 2010; 9(5): 2450-9.

68. GREEN K, BRAND M D, MURPHY M P. Prevention of mitochondrial oxidative damage as a therapeutic strategy in diabetes. Diabetes 2004; 53 Suppl 1: S110-8.

69. DIVAKARUNI A S, BRAND M D. The regulation and physiology of mitochondrial proton leak. Physiology (Bethesda) 2011; 26(3): 192-205.

70. ECHTAY K S, ROUSSEL D, ST-PIERRE J, et al. Superoxide activates mitochondrial uncoupling proteins. Nature 2002; 415(6867): 96-9.

71. ECHTAY K S, MURPHY M P, SMITH R A, TALBOT D A, BRAND M D. Superoxide activates mitochondrial uncoupling protein 2 from the matrix side. Studies using targeted antioxidants. J Biol Chem 2002; 277(49): 47129-35.

72. CORTEZ-PINTO H, ZHI LIN H, QI YANG S, ODWIN DA COSTA S, DIEHL A M. Lipids up-regulate uncoupling protein 2 expression in rat hepatocytes. Gastroenterology 1999; 116(5): 1184-93.

73. MURPHY M P, ECHTAY K S, BLAIKIE F H, et al. Superoxide activates uncoupling proteins by generating carbon-centered radicals and initiating lipid peroxidation: studies using a mitochondria-targeted spin trap derived from alpha-phenyl-N-tert-butylnitrone. The Journal of biological chemistry 2003; 278(49): 48534-45.

74. CHAVIN K D, YANG S, LIN H Z, et al. Obesity induces expression of uncoupling protein-2 in hepatocytes and promotes liver ATP depletion. The Journal of biological chemistry 1999; 274(9): 5692-700.

75. YANG S, ZHU H, LI Y, et al. Mitochondrial adaptations to obesity-related oxidant stress. Archives of biochemistry and biophysics 2000; 378(2): 259-68.

76. SERVIDDIO G, BELLANTI F, TAMBORRA R, et al. Uncoupling protein-2 (UCP2) induces mitochondrial proton leak and increases susceptibility of non-alcoholic steatohepatitis (NASH) liver to ischaemia-reperfusion injury. Gut 2008; 57(7): 957-65.

77. CALDWELL S H, SWERDLOW R H, KHAN E M, et al. Mitochondrial abnormalities in non-alcoholic steatohepatitis. Journal of hepatology 1999; 31(3): 430-4.

78. CALDWELL S H, DE FREITAS L A, PARK S H, et al. Intramitochondrial crystalline inclusions in nonalcoholic steatohepatitis. Hepatology 2009; 49(6): 1888-95.

79. DIANZANI M U, BAHR G F. Electron microscope investigation of mitochondria isolated from normal and steatotic livers by differential centrifugation. Acta Pathol Microbiol Scand 1954; 35(1): 25-38.

80. LE T H, CALDWELL S H, REDICK J A, et al. The zonal distribution of megamitochondria with crystalline inclusions in nonalcoholic steatohepatitis. Hepatology 2004; 39(5): 1423-9.

81. MATSUHASHI T, LIU X, KARBOWSKI M, WOZNIAK M, ANTOSIEWICZ J, WAKABAYASHI T. Role of free radicals in the mechanism of the hydrazine-induced formation of megamitochondria. Free radical biology & medicine 1997; 23(2): 285-93.

82. KARBOWSKI M, KURONO C, WOZNIAK M, et al. Free radical-induced megamitochondria formation and apoptosis. Free Radic Biol Med 1999; 26(3-4): 396-409.

83. PALMER C S, OSELLAME L D, STOJANOVSKI D, RYAN M T. The regulation of mitochondrial morphology: intricate mechanisms and dynamic machinery. Cell Signal 2011; 23(10): 1534-45.

84. YU T, ROBOTHAM J L, YOON Y. Increased production of reactive oxygen species in hyperglycemic conditions requires dynamic change of mitochondrial morphology. Proc Natl Acad Sci U S A 2006; 103(8): 2653-8.

85. NAKAMURA S, TAKAMURA T, MATSUZAWA-NAGATA N, et al. Palmitate induces insulin resistance in H4IIEC3 hepatocytes through reactive oxygen species produced by mitochondria. J Biol Chem 2009; 284(22): 14809-18.

86. CHEN X, IQBAL N, BODEN G. The effects of free fatty acids on gluconeogenesis and glycogenolysis in normal subjects. J Clin Invest 1999; 103(3): 365-72.

87. RUDDOCK M W, STEIN A, LANDAKER E, et al. Saturated fatty acids inhibit hepatic insulin action by modulating insulin receptor expression and post-receptor signalling. J Biochem 2008; 144(5): 599-607.

88. KUMASHIRO N, ERION D M, ZHANG D, et al. Cellular mechanism of insulin resistance in nonalcoholic fatty liver disease. Proceedings of the National Academy of Sciences of the United States of America 2011; 108(39): 16381-5.

89. SAVAGE D B, CHOI C S, SAMUEL V T, et al. Reversal of diet-induced hepatic steatosis and hepatic insulin resistance by antisense oligonucleotide inhibitors of acetyl-CoA carboxylases 1 and 2. J Clin Invest 2006; 116(3): 817-24.

90. SAMUEL V T, LIU Z X, QU X, et al. Mechanism of hepatic insulin resistance in non-alcoholic fatty liver disease. J Biol Chem 2004; 279(31): 32345-53.

91. SEMPLE R K, SLEIGH A, MURGATROYD P R, et al. Postreceptor insulin resistance contributes to human dyslipidemia and hepatic steatosis. J Clin Invest 2009; 119(2): 315-22.

92. HOUSTIS N, ROSEN E D, LANDER E S. Reactive oxygen species have a causal role in multiple forms of insulin resistance. Nature 2006; 440(7086): 944-8.

93. TILG H, MOSCHEN A R. Inflammatory mechanisms in the regulation of insulin resistance. Mol Med 2008; 14(3-4): 222-31.

94. IWAKAMI S, MISU H, TAKEDA T, et al. Concentration-dependent Dual Effects of Hydrogen Peroxide on Insulin Signal Transduction in H4IIEC Hepatocytes. PLoS One 2011; 6(11): e27401.

95. LOH K, DENG H, FUKUSHIMA A, et al. Reactive oxygen species enhance insulin sensitivity. Cell metabolism 2009; 10(4): 260-72.

96. HOEHN K L, SALMON A B, HOHNEN-BEHRENS C, et al. Insulin resistance is a cellular antioxidant defense mechanism. Proc Natl Acad Sci U S A 2009; 106(42): 17787-92.

97. YAMAGUCHI K, YANG L, MCCALL S, et al. Inhibiting triglyceride synthesis improves hepatic steatosis but exacerbates liver damage and fibrosis in obese mice with nonalcoholic steatohepatitis. Hepatology 2007; 45(6): 1366-74.

98. BONNARD C, DURAND A, PEYROL S, et al. Mitochondrial dysfunction results from oxidative stress in the skeletal muscle of diet-induced insulin-resistant mice. J Clin Invest 2008; 118(2): 789-800.

99. WANG T, SI Y, SHIRIHAI O S, et al. Respiration in Adipocytes is Inhibited by Reactive Oxygen Species. Obesity (Silver Spring) 2009.

100. KUMAR S, SITASAWAD S L. N-acetylcysteine prevents glucose/glucose oxidase-induced oxidative stress, mitochondrial damage and apoptosis in H9c2 cells. Life Sci 2009; 84(11-12): 328-36.

101. GUO W, CHOI J K, KIRKLAND J L, CORKEY B E, HAMILTON J A. Esterification of free fatty acids in adipocytes: a comparison between octanoate and oleate. Biochem J 2000; 349(Pt 2): 463-71.

102. ECKEL R H, HANSON A S, CHEN A Y, BERMAN J N, YOST T J, BRASS E P. Dietary substitution of medium-chain triglycerides improves insulin-mediated glucose metabolism in NIDDM subjects. Diabetes 1992; 41(5): 641-7.

103. WEIN S, WOLFFRAM S, SCHREZENMEIR J, GASPERIKOVA D, KLIMES I, SEBOKOVA E. Medium-chain fatty acids ameliorate insulin resistance caused by high-fat diets in rats. Diabetes Metab Res Rev 2009; 25(2): 185-94.

104. LARTER C Z, YEH M M. Animal models of NASH: getting both pathology and metabolic context right. J Gastroenterol Hepatol 2008; 23(11): 1635-48.

105. PURI P, WIEST M M, CHEUNG O, et al. The plasma lipidomic signature of nonalcoholic steatohepatitis. Hepatology 2009; 50(6): 1827-38.

106. PURI P, BAILLIE R A, WIEST M M, et al. A lipidomic analysis of nonalcoholic fatty liver disease. Hepatology 2007; 46(4): 1081-90.

107. DE GOTTARDI A, VINCIGUERRA M, SGROI A, et al. Microarray analyses and molecular profiling of steatosis induction in immortalized human hepatocytes. Lab Invest 2007; 87(8): 792-806.

108. LISTENBERGER L L, HAN X, LEWIS S E, et al. Triglyceride accumulation protects against fatty acid-induced lipotoxicity. Proceedings of the National Academy of Sciences of the United States of America 2003; 100(6): 3077-82.

109. KAISER S, GEROK W, HAUSSINGER D. Ammonia and glutamine metabolism in human liver slices: new aspects on the pathogenesis of hyperammonaemia in chronic liver disease. Eur J Clin Invest 1988; 18(5): 535-42.

110. CHOI Y S, LEE D Y, KIM I Y, et al. Ammonia removal using hepatoma cells in mammalian cell cultures. Biotechnol Prog 2000; 16(5): 760-8.

111. SUSSMAN N L, GISLASON G T, CONLIN C A, KELLY J H. The Hepatix extracorporeal liver assist device: initial clinical experience. Artif Organs 1994; 18(5): 390-6.

112. FILIPPI C, KEATCH S A, RANGAR D, NELSON L J, HAYES P C, PLEVRIS J N. Improvement of C3A cell metabolism for usage in bioartificial liver support systems. J Hepatol 2004; 41(4): 599-605.

113. GARCIA M C, AMANKWA-SAKYI M, FLYNN T J. Cellular glutathione in fatty liver in vitro models. Toxicol In Vitro 2011; 25(7): 1501-6.

114. WILLARD R R, SHAPPELL N W, MEEKIN J H, TALBOT N C, CAPERNA T J. Cytochrome P450 expression profile of the PICM-19H pig liver cell line: potential application to rapid liver toxicity assays. In Vitro Cell Dev Biol Anim 2010; 46(1): 11-9.

115. ELKAYAM T, AMITAY-SHAPRUT S, DVIR-GINZBERG M, HAREL T, COHEN S. Enhancing the drug metabolism activities of C3A--a human hepatocyte cell line--by tissue engineering within alginate scaffolds. Tissue Eng 2006; 12(5): 1357-68.

116. CLARKE C, BAGHDADI H, HOWIE A F, MASON J I, WALKER S W, BECKETT G J. Selenium supplementation attenuates procollagen-1 and interleukin-8 production in fat-loaded human C3A hepatoblastoma cells treated with TGFbeta1. Biochim Biophys Acta 2010; 1800(6): 611-8.

117. GAY R J, MCCOMB R B, BOWERS G N, JR. Optimum reaction conditions for human lactate dehydrogenase isoenzymes as they affect total lactate dehydrogenase activity. Clin Chem 1968; 14(8): 740-53.

118. LISTENBERGER L L, BROWN D A. Lipid droplets. Curr Biol 2008; 18(6): R237-8.

119. GREEN H, KEHINDE O. An established preadipose cell line and its differentiation in culture. II. Factors affecting the adipose conversion. Cell 1975; 5(1): 19-27.

120. ONTKO J A. Metabolism of free fatty acids in isolated liver cells. Factors affecting the partition between esterification and oxidation. J Biol Chem 1972; 247(6): 1788-800.

121. GOTTSCHALK S, ZWINGMANN C. Altered fatty acid metabolism and composition in cultured astrocytes under hyperammonemic conditions. J Neurochem 2009; 109 Suppl 1: 258-64.

122. NICHOLLS D G, WARD M W. Mitochondrial membrane potential and neuronal glutamate excitotoxicity: mortality and millivolts. Trends Neurosci 2000; 23(4): 166-74.

123. SKULACHEV V P. Role of uncoupled and non-coupled oxidations in maintenance of safely low levels of oxygen and its one-electron reductants. Q Rev Biophys 1996; 29(2): 169-202.

124. RAFFAELLA C, FRANCESCA B, ITALIA F, MARINA P, GIOVANNA L, SUSANNA I. Alterations in hepatic mitochondrial compartment in a model of obesity and insulin resistance. Obesity (Silver Spring) 2008; 16(5): 958-64.

125. BAUMGARDNER J N, SHANKAR K, HENNINGS L, ALBANO E, BADGER T M, RONIS M J. N-acetylcysteine attenuates progression of liver pathology in a rat model of nonalcoholic steatohepatitis. The Journal of nutrition 2008; 138(10): 1872-9.

126. GALICIA-MORENO M, RODRIGUEZ-RIVERA A, REYES-GORDILLO K, et al. N-acetylcysteine prevents carbon tetrachloride-induced liver cirrhosis: role of liver transforming growth factor-beta and oxidative stress. European journal of gastroenterology & hepatology 2009; 21(8): 908-14.

127. ZHOU G, MYERS R, LI Y, et al. Role of AMP-activated protein kinase in mechanism of metformin action. J Clin Invest 2001; 108(8): 1167-74.

128. ZANG M, ZUCCOLLO A, HOU X, et al. AMP-activated protein kinase is required for the lipid-lowering effect of metformin in insulin-resistant human HepG2 cells. J Biol Chem 2004; 279(46): 47898-905.

129. BERGMEYER H. Methods of enzymatic analysis Academic Press, London 1974.

130. HOWARD B V, HOWARD W J, KEFALIDES N A. Regulation of lipid synthesis from acetate in diploid fibroblast cultures -- variation with passage level and stage of cell growth. Journal of cellular physiology 1976; 89(2): 325-36.

131. PASSI S, PICARDO M, DE LUCA C, NAZZARO-PORRO M, ROSSI L, ROTILIO G. Saturated dicarboxylic acids as products of unsaturated fatty acid oxidation. Biochim Biophys Acta 1993; 1168(2): 190-8.

132. INOUYE M, MIO T, SUMINO K. Dicarboxylic acids as markers of fatty acid peroxidation in diabetes. Atherosclerosis 2000; 148(1): 197-202.

133. PASSI S, PICARDO M, NAZZARO-PORRO M, BREATHNACH A, CONFALONI A M, SERLUPI-CRESCENZI G. Antimitochondrial effect of saturated medium chain length (C8-C13) dicarboxylic acids. Biochem Pharmacol 1984; 33(1): 103-8.

134. REDDY J K, RAO M S. Lipid metabolism and liver inflammation. II. Fatty liver disease and fatty acid oxidation. Am J Physiol Gastrointest Liver Physiol 2006; 290(5): G852-8.

135. MORROW J D, ROBERTS L J. The isoprostanes: unique bioactive products of lipid peroxidation. Prog Lipid Res 1997; 36(1): 1-21.

136. MONTUSCHI P, BARNES P J, ROBERTS L J, 2ND. Isoprostanes: markers and mediators of oxidative stress. The FASEB journal : official publication of the Federation of American Societies for Experimental Biology 2004; 18(15): 1791-800.

137. COMPORTI M, SIGNORINI C, AREZZINI B, VECCHIO D, MONACO B, GARDI C. Isoprostanes and hepatic fibrosis. Mol Aspects Med 2008; 29(1-2): 43-9.

138. SUNNY N E, PARKS E J, BROWNING J D, BURGESS S C. Excessive Hepatic Mitochondrial TCA Cycle and Gluconeogenesis in Humans with Nonalcoholic Fatty Liver Disease. Cell metabolism 2011; 14(6): 804-10.

139. MAILLOUX R J, BERIAULT R, LEMIRE J, et al. The tricarboxylic acid cycle, an ancient metabolic network with a novel twist. PLoS One 2007; 2(1): e690.

140. POWELL C S, JACKSON R M. Mitochondrial complex I, aconitase, and succinate dehydrogenase during hypoxia-reoxygenation: modulation of enzyme activities by MnSOD. Am J Physiol Lung Cell Mol Physiol 2003; 285(1): L189-98.

141. WANG Q, YU L, YU C A. Cross-talk between mitochondrial malate dehydrogenase and the cytochrome bc1 complex. The Journal of biological chemistry 2010; 285(14): 10408-14.

142. VIAL G, DUBOUCHAUD H, COUTURIER K, et al. Effects of a high-fat diet on energy metabolism and ROS production in rat liver. Journal of hepatology 2011; 54(2): 348-56.

143. PETERSEN K F, DUFOUR S, BEFROY D, LEHRKE M, HENDLER R E, SHULMAN G I. Reversal of nonalcoholic hepatic steatosis, hepatic insulin resistance, and hyperglycemia by moderate weight reduction in patients with type 2 diabetes. Diabetes 2005; 54(3): 603-8.

144. VILJANEN A P, IOZZO P, BORRA R, et al. Effect of weight loss on liver free fatty acid uptake and hepatic insulin resistance. J Clin Endocrinol Metab 2009; 94(1): 50-5.

145. PETERSEN K F, ORAL E A, DUFOUR S, et al. Leptin reverses insulin resistance and hepatic steatosis in patients with severe lipodystrophy. J Clin Invest 2002; 109(10): 1345-50.

146. BELL M, WANG H, CHEN H, et al. Consequences of lipid droplet coat protein downregulation in liver cells: abnormal lipid droplet metabolism and induction of insulin resistance. Diabetes 2008; 57(8): 2037-45.

147. MIHALIK S J, GOODPASTER B H, KELLEY D E, et al. Increased levels of plasma acylcarnitines in obesity and type 2 diabetes and identification of a marker of glucolipotoxicity. Obesity 2010; 18(9): 1695-700.

148. KOVES T R, USSHER J R, NOLAND R C, et al. Mitochondrial overload and incomplete fatty acid oxidation contribute to skeletal muscle insulin resistance. Cell metabolism 2008; 7(1): 45-56.

149. ADAMS S H, HOPPEL C L, LOK K H, et al. Plasma acylcarnitine profiles suggest incomplete long-chain fatty acid beta-oxidation and altered tricarboxylic acid cycle activity in type 2 diabetic African-American women. The Journal of nutrition 2009; 139(6): 1073-81.

150. ZWINGMANN C, BILODEAU M. Metabolic insights into the hepatoprotective role of N-acetylcysteine in mouse liver. Hepatology 2006; 43(3): 454-63.

151. JORNAYVAZ F R, BIRKENFELD A L, JURCZAK M J, et al. Hepatic insulin resistance in mice with hepatic overexpression of diacylglycerol acyltransferase 2. Proceedings of the National Academy of Sciences of the United States of America 2011; 108(14): 5748-52.

152. LEVERVE X M. Mitochondrial function and substrate availability. Crit Care Med 2007; 35(9 Suppl): S454-60.

153. NULTON-PERSSON A C, SZWEDA L I. Modulation of mitochondrial function by hydrogen peroxide. J Biol Chem 2001; 276(26): 23357-61.

154. PARADIES G, PETROSILLO G, PISTOLESE M, RUGGIERO F M. The effect of reactive oxygen species generated from the mitochondrial electron transport chain on the cytochrome c oxidase activity and on the cardiolipin content in bovine heart submitochondrial particles. FEBS Lett 2000; 466(2-3): 323-6.

155. VOTYAKOVA T V, REYNOLDS I J. DeltaPsi(m)-Dependent and -independent production of reactive oxygen species by rat brain mitochondria. Journal of neurochemistry 2001; 79(2): 266-77.

156. SEO B B, MARELLA M, YAGI T, MATSUNO-YAGI A. The single subunit NADH dehydrogenase reduces generation of reactive oxygen species from complex I. FEBS Lett 2006; 580(26): 6105-8.

157. REDDY J K. Nonalcoholic steatosis and steatohepatitis. III. Peroxisomal beta-oxidation, PPAR alpha, and steatohepatitis. Am J Physiol Gastrointest Liver Physiol 2001; 281(6): G1333-9.

158. REDDY J K, HASHIMOTO T. Peroxisomal beta-oxidation and peroxisome proliferator-activated receptor alpha: an adaptive metabolic system. Annu Rev Nutr 2001; 21: 193-230.

159. HOEHN K L, SALMON A B, HOHNEN-BEHRENS C, et al. Insulin resistance is a cellular antioxidant defense mechanism. Proceedings of the National Academy of Sciences of the United States of America 2009; 106(42): 17787-92.

160. TOWLER M C, HARDIE D G. AMP-activated protein kinase in metabolic control and insulin signaling. Circ Res 2007; 100(3): 328-41.

161. HOU X, SONG J, LI X N, et al. Metformin reduces intracellular reactive oxygen species levels by upregulating expression of the antioxidant thioredoxin via the AMPK-FOXO3 pathway. Biochemical and biophysical research communications 2010; 396(2): 199-205.

162. HALL A M, BRUNT E M, CHEN Z, et al. Dynamic and differential regulation of proteins that coat lipid droplets in fatty liver dystrophic mice. J Lipid Res 2010; 51(3): 554-63.

163. ARUOMA O I, HALLIWELL B, HOEY B M, BUTLER J. The antioxidant action of N-acetylcysteine: its reaction with hydrogen peroxide, hydroxyl radical, superoxide, and hypochlorous acid. Free Radic Biol Med 1989; 6(6): 593-7.

164. TANG C, HAN P, OPRESCU A I, et al. Evidence for a role of superoxide generation in glucose-induced beta-cell dysfunction in vivo. Diabetes 2007; 56(11): 2722-31.

165. SAMUHASANEETO S, THONG-NGAM D, KULAPUTANA O, PATUMRAJ S, KLAIKEAW N. Effects of N-acetylcysteine on oxidative stress in rats with non-alcoholic steatohepatitis. J Med Assoc Thai 2007; 90(4): 788-97.

166. RONIS M J, BUTURA A, SAMPEY B P, et al. Effects of N-acetylcysteine on ethanol-induced hepatotoxicity in rats fed via total enteral nutrition. Free radical biology & medicine 2005; 39(5): 619-30.

167. YANG R, MIKI K, HE X, KILLEEN M E, FINK M P. Prolonged treatment with N-acetylcystine delays liver recovery from acetaminophen hepatotoxicity. Crit Care 2009; 13(2): R55.

168. CROZIER G L. Medium-chain triglyceride feeding over the long term: the metabolic fate of [14C]octanoate and [14C]oleate in isolated rat hepatocytes. J Nutr 1988; 118(3): 297-304.

169. TOL V A. Aspects of long-chain acyl-COA metabolism. Molecular and cellular biochemistry 1975; 7(1): 19-31.

170. TURNER N, HARIHARAN K, TIDANG J, et al. Enhancement of muscle mitochondrial oxidative capacity and alterations in insulin action are lipid species dependent: potent tissue-specific effects of medium-chain fatty acids. Diabetes 2009; 58(11): 2547-54.

PUBLISHED PAPER

Oxidative stress rather than triglyceride accumulation is a determinant of mitochondrial dysfunction in in vitro models of hepatic cellular steatosis.

Lockman KA, Baren JP, Pemberton CJ, Baghdadi H, Burgess KE, Plevris-Papaioannou N, Lee P, Howie F, Beckett G, Pryde A, Jaap AJ, Hayes PC, Filippi C, Plevris JN.

Liver Int. 2012 Mar 19. doi: 10.1111/j.1478-3231.2012.02775.x.

PMID: 22429485

http://www.ncbi.nlm.nih.gov/pubmed/22429485

APPENDICES

Supplementary data 1: Confirming the presence of insulin receptor in C3A cells

S1.1. Introduction

Our aim was to confirm that insulin receptors are present in treated C3A cells.

S1.2. Methods

S1.2.1. Immunohistochemistry

Immunohistochemistry was performed to confirm the presence of insulin receptors on C3A cells. C3A and HepG2 cells (positive control) were grown in chamber slides until 70% confluence. Slides were fixed using 4% paraformaldehyde and rinsed in PBS before 5-minute incubation in hydrogen peroxide. Insulin receptor antibody (120µl at the following concentrations: 1:25, 1:50, 1:100) was added to the designated chamber and was allowed to incubate overnight at $4^{O}C$. A separate slide was incubated with IgG as negative control. Slides were then rinsed and incubated with labeled polymer-HRP anti mouse as the secondary antibody for 40 minutes. DAB chromogen solution (200µl) was then applied to each slide for 5 minutes. Slides were then washed, counterstained with haematoxylin, dehydrated using alcohols (from 50 to 100%) and mounted. The slides were viewed under light microscopy and photographed. The stained area was quantified using ImageJ. Briefly, the images were set to a threshold to highlight stained area and analysed using 'analyze particle' function of the ImageJ.

S1.3. Results

S1.3.1. Insulin receptors are present in C3A cells

Figure S1.3.1 shows representative images of slides from the immunohistochemistry studies. The dark brown staining of insulin receptors was present in C3A cells and appeared to be comparable to that seen with HepG2 cells (positive control).

Next, we examined whether insulin receptors remained present in C3A cells after a 72-hour treatment with LPON. Figure S1.3.2 Panel A and B are representative images of LPON treated cells following incubation with anti-β subunit of insulin receptor (dilution 1:100). Insulin receptors remained detectable after LPON treatment.

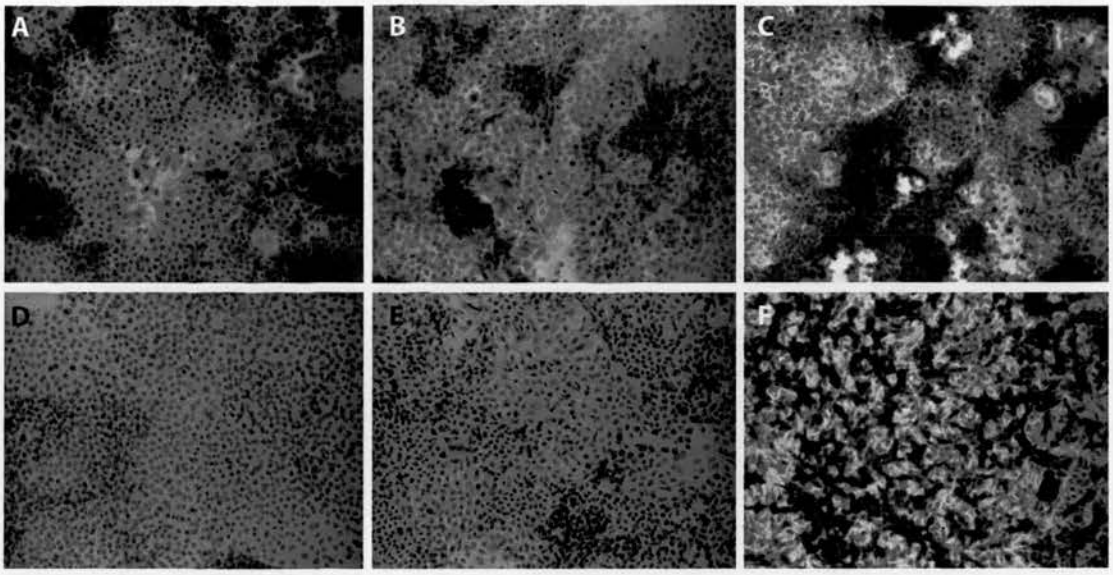

Figure S1.3.1. Insulin receptors are present in C3A cells.

C3A cells were grown in two-chamber slides until 70% confluent. Cells were not treated with energy substrates but were grown for further 72 hours. Anti-β subunit of insulin receptor was used as the primary antibody (described in section 1.2.1). Insulin receptors were stained dark brown in the presence of anti-β subunit of insulin receptor antibody. A, C3A cells with 1:25 primary antibody; B, C3A cells with 1:50 primary antibody; C, C3A cells with 1:100; D, C3A cells without primary antibody; E, C3A cells with IgG (negative control); F, HepG2 (positive control).

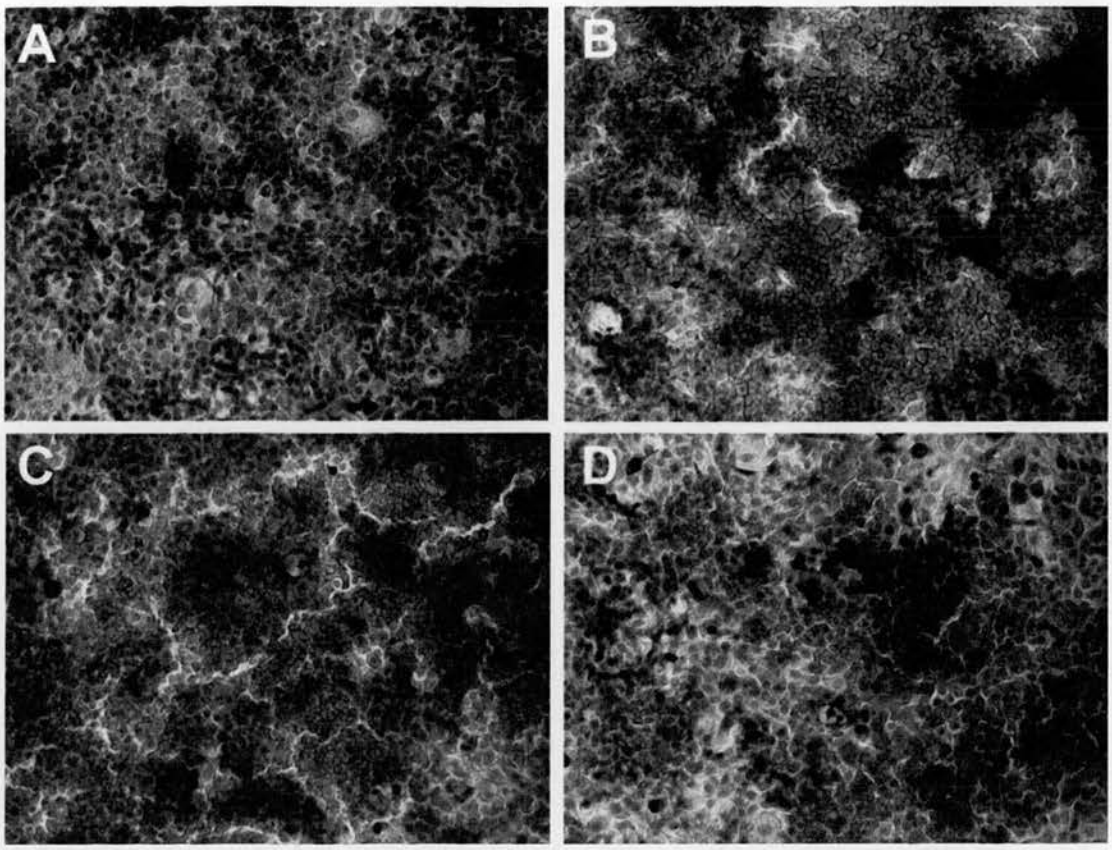

Figure S1.3.2. Insulin receptors in C3A cells treated with LPON.

C3A cells were grown and treated in two chamber slides until 70% confluent for 72 hours before immunohistochemistry using anti-β subunit of insulin receptor (diluted to 1:100) as the primary antibody. A, Untreated; B, LPON; C, LP; D, Octanoate. Magnification x20.

Supplementary data 2: Determining the optimal concentration of insulin

S2.1. Introduction

Dose response curve using insulin concentration (0-75nM) was performed to determine the optimal concentration of insulin for subsequent experiments.

S2.2. Methods

S2.2.1. Insulin dose response curve

Cells were grown and treated with LPON in 6-well plate as previously described in section 2.1.1. FBS was removed 24 hour prior to experimentation. MEME (without FBS) was then aspirated; cells were then rinsed before a 4-hour incubation with insulin at the specified concentrations. Glucose flux in the incubation medium was determined using the method described in section 9.2.2 of the main text.

S2.3. Results

S2.3.1. Insulin dose response curve to determine optimal insulin concentration

As demonstrated in Figure S2.3.1, maximal reduction of endogenous glucose flux formation was attained at 10nM of insulin. Interestingly, there was a dose dependent increase in glucose with subsequent concentrations of insulin. Indeed, a dramatic rise in glucose was observed with 75nM of insulin.

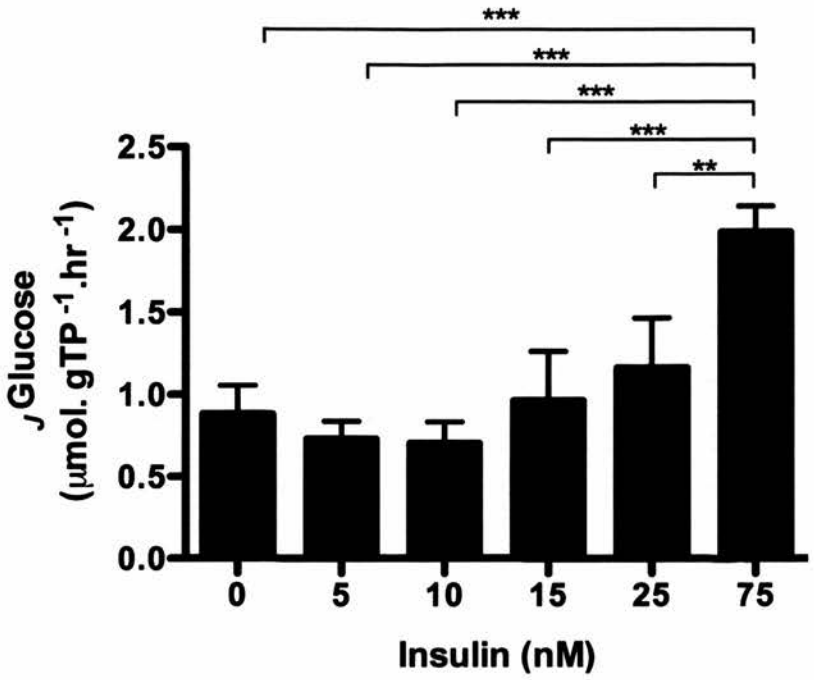

Figure S2.3.1. Dose response curve with insulin (0-75nM).

Untreated C3A cells were grown in MEME with FBS until 70% confluent. Cells were incubated for further 72 hours. FBS were then removed and cells were left in MEME culture medium for another 72 hours. Cells were rinsed before a 4-hour incubation of insulin without exogenous glucose. Data are presented as mean ± SEM; $P<0.0001$, $^{*}P<0.05$.